2

NASA CR-108571

R-8411

FINAL REPORT

NONCIRCULAR ORIFICE HOLES AND ADVANCED FABRICATION TECHNIQUES FOR LIQUID ROCKET INJECTORS

PHASE II: ANALYTICAL AND EXPERIMENTAL STUDY OF NONCIRCULAR INJECTOR ORIFICES, AND ELEMENTS FOR GAS/LIQUID INJECTORS

NAS9-9528

By

R. M. McHale

Rocketdyne
A Division of North American Rockwell Corporation

Prepared for

NASA MANNED SPACECRAFT CENTER

NASA CR-108571
R-8411

FINAL REPORT

NONCIRCULAR ORIFICE HOLES AND ADVANCED FABRICATION TECHNIQUES FOR LIQUID ROCKET INJECTORS

PHASE II: ANALYTICAL AND EXPERIMENTAL STUDY OF NONCIRCULAR INJECTOR ORIFICES, AND ELEMENTS FOR GAS/LIQUID INJECTORS

NAS9-9528

By

R. M. McHale

Rocketdyne
A Division of North American Rockwell Corporation

Prepared for

NASA MANNED SPACECRAFT CENTER

FOREWORD

This report was prepared for NASA Manned Spacecraft Center, Houston, Texas by Rocketdyne, a Division of North American Rockwell Corporation. The study was conducted in accordance with Contract NAS9-9528, G.O. 09206. Mr. M. F. Lausten of the Manned Spacecraft Center served as NASA Technical Manager.

This technology program was performed within the Advanced Programs Organization of Rocketdyne headed by Mr. S. F. Iacobellis.

The Technical effort was conducted within the Propulsion Technology Unit managed by Dr. D. T. Campbell. This unit is a part of the Science and Engineering Technology Group under the direction of Mr. S. D. Clapp, who also served as the program manager for this contract.

ABSTRACT

This report contains the results of the Phase II effort of the subject program, Noncircular Orifice Holes and Advanced Fabrication Techniques for Liquid Rocket Injectors. The Phase II portion of the program was comprised of an analytical and experimental study of injector elements incorporating noncircular orifices for application with gas/liquid propellant combinations. Based upon the results of a preliminary analysis and evaluation of several candidate injector elements, a rectangular concentric tube element was selected for further evaluation. Cold flow tests and subsequent analytical combustion modeling conducted with this element, and a standard, circular concentric tube, demonstrated that the rectangular concentric tube element concept was superior, in many ways, to conventional injector concepts, especially in the area of propellant atomization.

ACKNOWLEDGMENT

The author wishes to express his personal thanks to the following individuals for their contributions to the overall program effort. It is unfortunate that their names must be presented in list format dictated by limitations of space. Several pages could be written about each individual and still not satisfactorily describe the true value of their assistance.

A. Okuda
D. Zwald
S. Clapp
D. Campbell
J. Sabol
R. Burick
N. Bachman
R. Bright
W. Bose
P. Lowe
R. Guilliams

CONTENTS

ILLUSTRATIONS

TABLES

1.0 SUMMARY

The Noncircular Orifice Holes and Advanced Fabrication Techniques for L/R Injectors Program, Phase II, was conducted at the Rocketdyne, Santa Susana Field Laboratory, near Canoga Park, California. Work was performed during the period April to October, 1970.

The program objective was to extend the technology of injector elements incorporating noncircular orifices to gas/liquid propellant applications. This was accomplished with a preliminary analysis and evaluation of several candidate injector element types followed by the selection of one element for cold flow experimental evaluation and theoretical combustion model performance analysis. Throughout the program, the cold flow and predicted performance characteristics of the candidate noncircular injector element were compared with those same characteristics of a standard circular concentric tube injector element which served as a reference.

Several injector element types were selected for evaluation in the Preliminary Analysis task. Among these were: a rectangular concentric tube element; doublet impinging jet and four-on-one impinging jet elements incorporating rectangular and triangular orifices; and doublet, triplet and four-on-one elements composed of rectangular gas orifices and spray fan (self atomizing) liquid orifices.

The analysis of these elements was organized under three subtasks:

1. Development of Analytical Methods, wherein analytical techniques were prepared which enabled the design geometries of the various noncircular elements (as well as the circular concentric tube) to be related to performance parameters; specifically mixing uniformity as typified by E_m and quality of atomization as measured by the mass median droplet diameter, $\overline{D}$.

2. Preliminary Design of Element Types, wherein the analytical tools which had been developed were employed in the design of specific configurations for each element type. Preliminary design guidelines were dictated by a conceptual configuration of the Orbit Maneuvering System Engine (OMS) in the Space Shuttle System Complex. The envisioned OMS engine is an 8000 lb_f thruster which is designed to operate at the 800 psia chamber pressure level with LOX/GH_2 at a mixture ratio of 6:1. The elements were designed for this injector concept at the 200 lb_f thrust per element level (40 elements for the injector).

3. Preliminary Design Summary and Evaluation wherein the predicted performance parameters of the various candidate elements were compared, one with another and with those of the reference circular concentric tube to evaluate the relative merits of each element. As a result of this evaluation, based upon its superior predicted atomization, mixing and throttling characteristics, the noncircular (rectangular) concentric tube element

was selected for further evaluation in the experimental phase of the program along with the standard, circular concentric tube element.

The Cold Flow Experimentation portion of the program was comprised of Design of Experimental Hardware and Cold Flow Testing. One cold flow model was designed and fabricated for each of the two elements under consideration (i.e., the rectangular and circular concentric tube types). These models were designed to produce, respectively, equal fuel and oxidizer injection velocities at equivalent operating conditions. The rectangular element design incorporated a liquid injection port with a length-to-width ratio of 6:1 (i.e., aspect ratio).

Both mixing uniformity and atomization quality experiments were conducted with each element.

The mixing uniformity tests were conducted with gaseous nitrogen and water as the fuel and oxidizer simulants, respectively. Two phase impact probe measurements were employed to determine the spacial distributions of oxidizer and fuel simulants and these data were employed to determine the mixing uniformity parameter E_m.

The quality, or degree of atomization was determined with the molten wax method and was expressed in terms of the mass median droplet diameter, $\overline{D}$. Gaseous (hot) nitrogen and molten wax were employed as fuel and oxidizer simulants, respectively.

Experiments were conducted at several total flow rates at mixture ratios of 3:1 and 6:1 (liquid to gas) with both elements. The mixing uniformity values obtained (E_m) varied between 95% and 65%. The lowest values were obtained with the circular element at the higher mixture ratio and higher flow rate levels. In general, E_m dropped off with increasing mixture ratio for both element types. Although E_m values dropped off with increased flow rate for both elements, the noncircular element showed much less sensitivity to flowrate level. At a mixture ratio of 6:1 and a gas velocity of 800 ft/sec, the value of E_m for the noncircular and circular elements are 78% and 72% respectively. In general, the mixing levels of the two elements are comparable.

An examination of the mass flux and mixture ratio distributions produced by the two elements showed that the noncircular element produced flow patterns quite different from those of the circular orifice design. Instead of retaining a relatively high mixture ratio core centered on the axis of the liquid orifice, the liquid was drawn outward by the gas, resulting in a relatively low mixture ratio "core". This apparently results from the large gas/liquid contact perimeter with this aspect ratio of 6 rectangular element. An obvious inference is that at intermediate aspect ratios further improvement could readily be obtained with rectangular concentric tube elements, resulting in mixing efficiency levels substantially higher than those of the conventional circular concentric tube injectors.

Atomization results showed the noncircular element to be far superior to its circular counterpart, especially at the higher mixture ratios. At a mixture ratio of 6:1, the droplet sizes produced by the noncircular element were 100 to 200 microns smaller than those produced by the circular element. In general, dropsizes were smallest at the higher flow rate per element levels.

Following the cold flow experimentation, a performance analysis was conducted wherein the cold flow results were employed as input to theoretical mixing-limited and vaporization-rate-limited combustion models to estimate the C* efficiency value that could be expected for the two elements. A chamber pressure of 200 psia was selected for the combustion modeling proposed because the density of the hydrogen at these conditions would be equal to that of the nitrogen simulant at the cold flow conditions. The parametric performance analysis was conducted for a range of mixture ratio (3:1 to 6:1) and chamber length (3 to 9 inches). The C* efficiencies predicted for the noncircular element were typically 2 to 10 percentage points higher than those for the circular element over the range of variables investigated. The greatest performance advantages were found in the higher mixture ratio, shorter chamber regions.

It was concluded from the results of the program that the noncircular concentric tube element will provide many advantages for injector design technology in the areas of performance and design flexibility.

Specifically, greatly enhanced atomization has been demonstrated and the potential for similar improvements in gas/liquid propellant mixing is indicated. The demonstrated ability to control the shape of the flow field with noncircular orifice elements also provides the designer with a means for enhancing injector/chamber compatibility. It was further concluded that the overall technical approach to the selection and characterization of this element was sound. This approach had been selected, in lieu of a "cut and try" hot fire approach, so that the various individual aspects of the candidate element could be characterized. In other words, the results of this program included parametric characterization of mixing and atomization characteristics and estimates of element flow patterns. These independent contributions to overall performance and potential chamber compatibility would not be available from the results of a traditional hot fire investigation.

2.0 INTRODUCTION

This report contains the results of Phase II of an applied research program of analysis, design, and experimentation to evaluate the potential performance advantages of injector elements incorporating noncircular orifices for application with gas/liquid propellant combinations. The program objective was to compare the mixing uniformity and atomization characteristics of a candidate noncircular orifice injector element with those of a conventional circular orifice element and to evaluate this element in the light of these comparisons.

2.1 BACKGROUND

Rocketdyne (Ref. 1), in the Phase I effort of the subject program has extended the scope of injector design technology to include injector elements incorporating noncircular orifices. The investigation was directed toward applications with liquid/liquid propellant combinations, such as NTO/50-50.

In the present state of development of rocket engine technology, the liquid oxygen/gaseous hydrogen propellant combination is receiving a great deal of attention. The popularity of these propellants is prompted by their high energy potential and their relative low cost and ready availability. These propellants, along with other high energy combinations, have stimulated research and development in the area of gas/liquid rocket engine injector technology. Phase II of the subject program

provides a logical extension of the work of Phase I into the realm of gas/liquid injector technology for noncircular orifices.

2.2 TECHNICAL APPROACH

There is an apparent dichotomy which has developed in present day technology. On the one hand, there is an increasing demand for excellence, while on the other hand, there is a demand to lower costs. This is especially true of the technology associated with the aerospace industry. It is becoming more and more obvious that yesterdays techniques and approaches to research and development efforts are not suited to the accomplishment of both these primary objectives.

In this program, the objective was to evaluate and characterize new and different rocket engine injector elements to broaden the foundation of injector design. The requirements for these new elements include such considerations as ultra-high performance, reduced fabrication costs, and increased design flexibility. If the original development technique of cut and try with full-scale hardware were selected to meet this objective, the time and money expenditures required would prove to be intolerable.

At Rocketdyne, a new and advanced approach to rocket engine injector characterization has been developed. The major objectives of this new approach are to reduce overall costs and to provide, at the same time, greater insight into the actual mechanisms which affect injector performance.

Rather than attempting to analyze a complete injector on a hot fire basis, study is initiated with single injector elements on a cold flow basis using non-reactive propellant simulants. Furthermore, the overall performance limiting processes associated with combustion in a rocket chamber are grouped into two major classes: (1) mixing processes, and (2) atomization processes.

These processes are investigated independently with cold flow modeling techniques which have been developed for each. Mixing characteristics are defined by the direct measurement of mass and mixture ratio distribution profiles employing appropriate propellant simulants to model the injection parameters. These profiles are characterized by a mixing uniformity parameter, E_m, and also by $\eta_{c^*_{mix}}$ obtained by combustion model analysis of the mass and mixture ratio profile data. The atomization process is investigated with the frozen wax technique wherein molten wax is injected through the element and the frozen particles collected to determine the mass median droplet diameter as well as the drop size distribution about the median size. A vaporization rate limited combustion model is employed to estimate the contribution of the vaporization process to the overall performance in the form of the vaporization limited C* efficiency $\eta_{c^*_{vap}}$. The two independent limited performance estimates are then combined to estimate the overall efficiency through the first order approximation of their product, $\eta_{c^*_{pred}} = \eta_{c^*_{mix}} \times \eta_{c^*_{vap}}$. This method produces design and analysis information pertaining to the performance of many different elements and modifications of these elements at a cost far less than that incurred in hot firing.

Following single element cold flow analysis, the usual program plan includes single element hot firing studies of those elements and their various configurations which were shown to be of interest by the cold flow tests. Single element hot fire tests provide additional information about the mixing and atomization mechanisms at a cost which is also substantially below full scale injector firings.

The final step in the research investigation is usually the design of a full scale or multi-element injector whose design has been dictated by the information obtained in the single element cold flow and hot fire programs. The full scale injector design dictated by this approach is usually quite close to the final configuration and will not require costly major redesign. The overall cost of the development program is well below that of the cut and try approach with the added advantage that detailed information is available concerning the role of operating and design variables in the performance of the injector. In other words, the injector will be high performing and the investigators will know why it is and will be able to extend their knowledge to the design of related hardware without the necessity of starting from scratch.

Information pertaining to chamber compatibility is also made available in the results of a program which contains single element cold flow studies. The mass and mixture ratio profiles offer a direct picture of the flow field which can be expected from a given element. Superposition of these pictures and the geometry of the chamber wall yields an estimate of the interaction of zones of defined temperature and the wall surface. Without

cold flow results, information of this nature must be obtained through direct hot fire testing.

The validity of this overall approach has been documented in the past by many programs. Two such programs of particular interest are the space storable propellant injector study, NAS3-12051, and the gas augmented injector study, NAS3-12001. In these programs, excellent agreement was obtained between hot fire test results and cold flow estimates of these results.

2.3 PROGRAM OUTLINE

The subject program was designed to follow the guidelines of approach to injector characterization just described. The work which is reported in this document follows a typical development through the stages of single element cold flow and combustion model analysis. No hot fire work has been attempted to date. A logic diagram of the program is shown in Fig. A.

The program was initiated by selection of a number of candidate noncircular elements. A preliminary analysis of these elements was performed in order to evaluate their relative merits and to intelligently design the cold flow experiments which would be required to characterize their performance trends.

PROGRAM LOGIC DIAGRAM

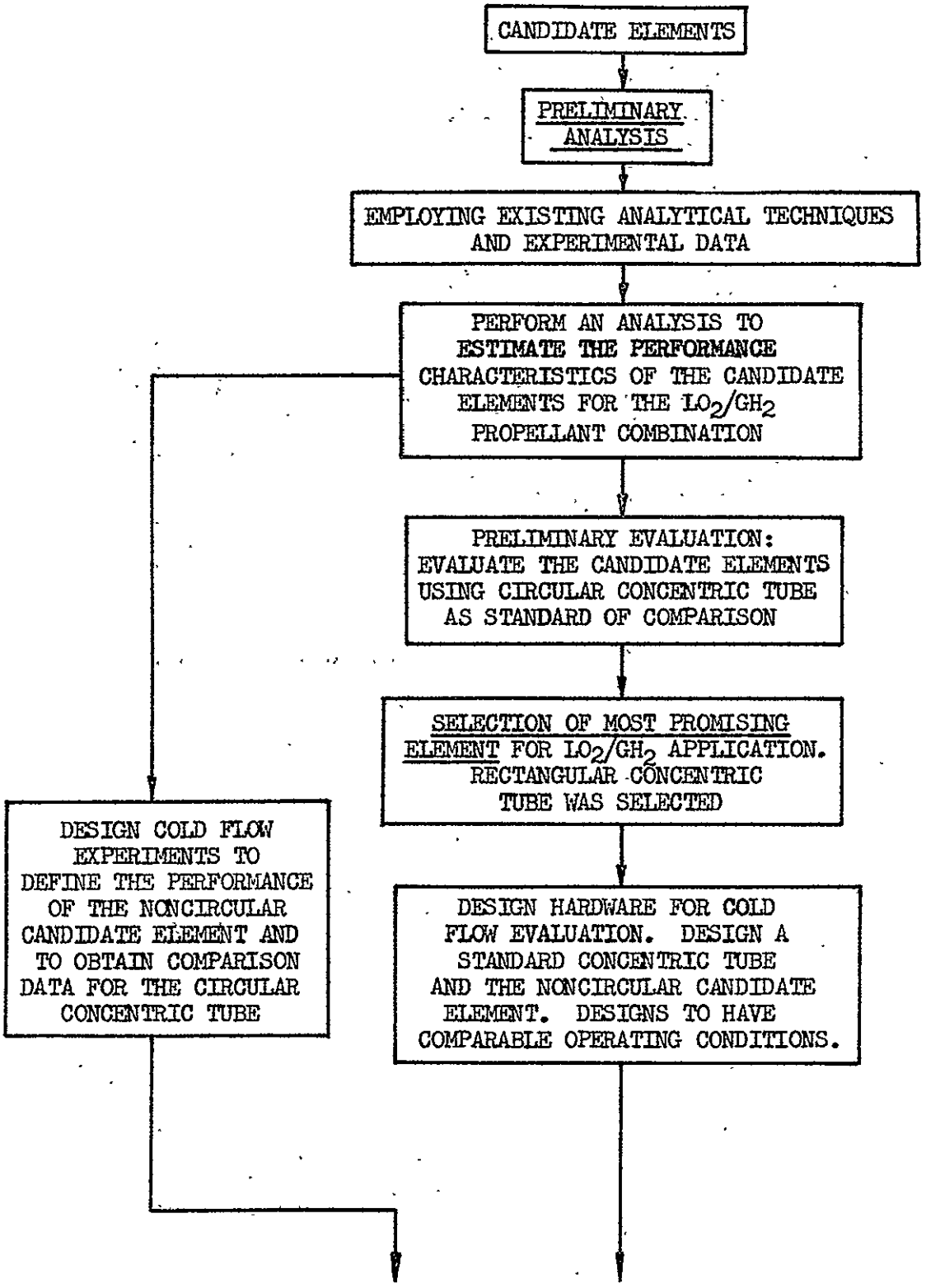

Figure A. Program Logic Diagram

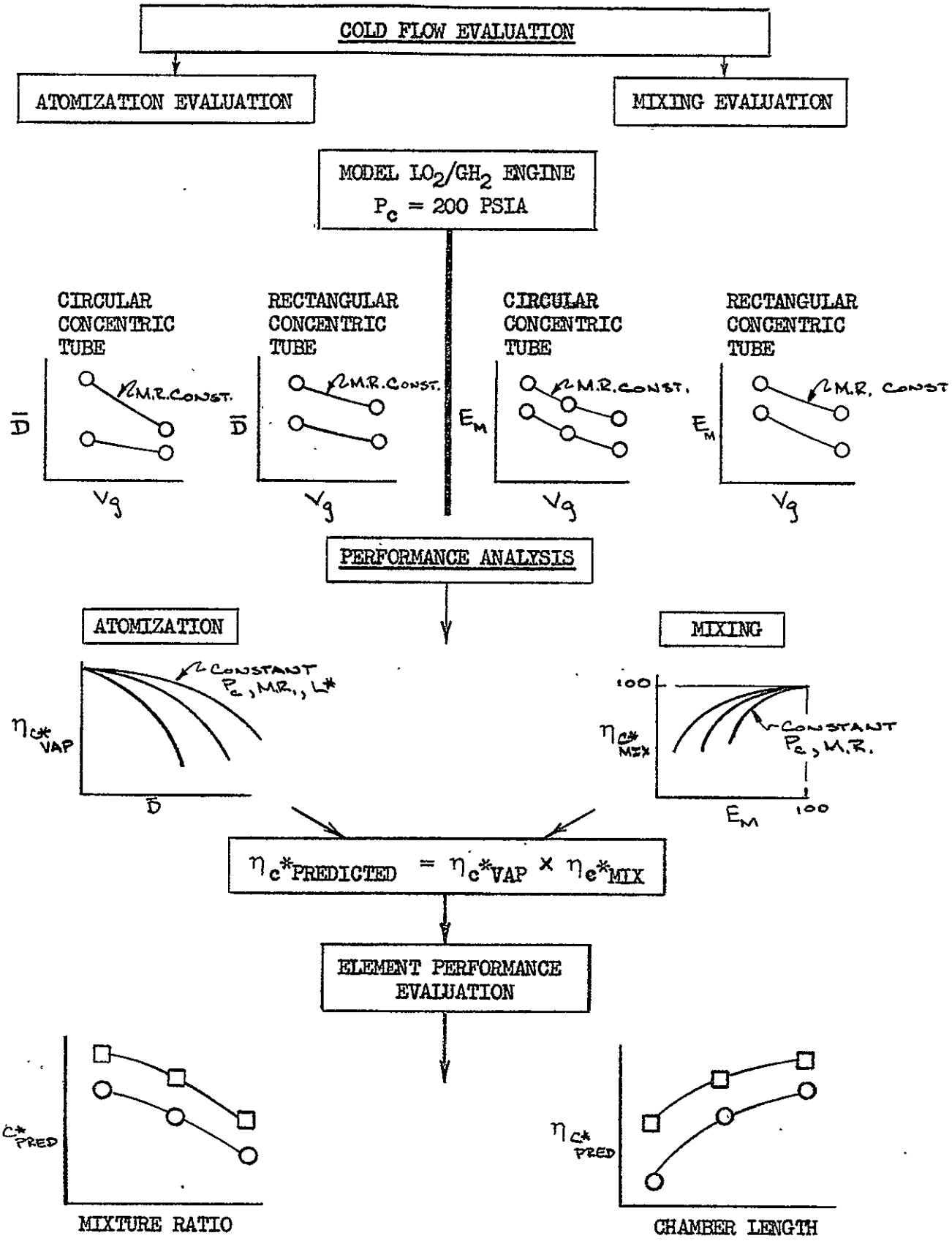

Figure A. (Concluded)

Based upon the results of the preliminary analysis, a rectangular concentric tube element was selected as the noncircular candidate for further analysis. A circular and a rectangular concentric element were designed and fabricated in the form of cold flow model hardware. (The circular concentric tube element was to be carried through all stages of the program to provide a basis of comparison for the noncircular elements.) Mixing and atomization cold flow tests were performed to obtain estimates of the mixing uniformity and the median drop sizes produced by the two elements over ranges of appropriate operating conditions.

The mixing and atomization data were analyzed with the aid of combustion models and the overall levels of performance were estimated. Finally, these estimates of performance were employed to evaluate the merits of the noncircular concentric tube element by comparison to its circular counterpart.

3.0 PRELIMINARY ANALYSIS

Essentially, the preliminary analysis was an analytical feasibility study of several candidate injector elements incorporating noncircular orifices. Employing existing analytical techniques and experimental data, several element configurations were designed for application to a conceptual Orbit Maneuvering System Engine (O.M.S.) of the Space Shuttle Mission. The operational characteristics of the O.M.S. engine, as currently envisioned, are summarized below.

ENVISIONED OPERATIONAL CHARACTERISTICS OF THE ORBIT MANEUVERING SYSTEM ENGINE

Propellants	LOX/GH_2
Thrust	8000 lbf
Chamber Pressure	800 psia
Mixture Ratio	6:1
Expansion Ratio	200:1

The mission of the engine system is to assist the space shuttle vehicle in inter-orbit transfer following injection into primary orbit status.

The objective of this analysis was to provide quantitative data upon which to base an evaluation of the elements, with respect to a standard circular concentric tube element, for the purpose of selecting one, noncircular element for experimental evaluation in the latter phases of the program.

The circular concentric tube element was selected as a basis of comparison because of its general and wide spread acceptance as an excellent element for application with the LOX/GH_2 propellant combination.

Noncircular element configurations selected for preliminary analysis and evaluation are shown schematically in Table I along with the standard, circular concentric tube element. Three basic element types are represented in Table I; concentric tube elements, impinging type elements incorporating spray fan orifices, and impinging jet type elements. These element types were selected primarily because they represent applications of noncircular orifice concepts to present state-of-the-art elements. Incorporated in both spray fan and jet orifice type element selections are doublets, triplets, and four-on-one concepts.

High mass and mixture ratio uniformity, as indexed by the Rupe (Ref. 2) mixing parameter E_m, and small droplet diameters produced by the gas-liquid atomization process were the basic targets employed in the design of element geometry. The most difficult task of the preliminary analysis was to relate mixing and atomization characteristics to geometry and operating conditions. In some cases, it was not possible to obtain a direct relationship between element design variables and performance parameters. In these instances, relationships had to be inferred through the similarity of certain noncircular design concepts with circular designs for which performance characteristics were available. This was the case, for example, with the noncircular concentric tube element for which operational characteristics were estimated through analogy with the circular concentric tube element.

TABLE I

CANDIDATE ELEMENT CONCEPTS FOR GAS/LIQUID APPLICATIONS

	BASIC CONCEPT TYPE		
	Concentric Tube	Impinging Spray Fans	Impinging Jets
Shaded Areas Indicate Liquid Injection Orifices	 Standard Circular Concentric Tube	 Triplet Self-Atomizing Nozzles Injecting into a Gas Showerhead	 Unlike Doublet Gas Showerhead. Vary Apsect Ratio.
	 Noncircular Concentric Tube Increased Surface Area	 Unlike Doublet One Spray Nozzle on Gas Showerhead	 4-on-one Gas Showerhead
		 4 Spray Nozzles on One Gas Showerhead	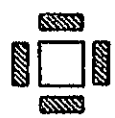 4-on-one Gas Showerhead. Increased Surface Areas
Source of Data or Analysis Techniques	1) Gas-Aug. Data 2) Space Store-Prog.	1) Present Atomiz. Data on Spray Fans 2) Individual Drop Ballistic Routing.	1) X_p/D_g -Dickerson & Burick 2) Jet Ballistic 3) Gas-Aug.

The following material which describes the "Preliminary Analysis" task, is organized under three primary subsections:

- Development of Analytical Methods and "Design Criteria", wherein the analytical tools are developed which are required to logically design and evaluate each of the various candidate element configurations.

- Preliminary Design, wherein the analytical tools which have been developed are applied to the design of the elements.

- Preliminary Design Summary and Evaluation, wherein the elements designed are compared to the circular concentric tube element and evaluated as to their individual merits.

3.1 DEVELOPMENT OF ANALYTICAL METHODS

3.1.1 Analysis of Concentric Tube Elements

Circular Concentric Tube Elements. Preliminary analysis of circular concentric tube elements consisted of an attempt to correlate existing atomization and mixing data with element geometry and various physical parameters. Data which were used in the analysis were taken under Contract No. NAS3-12001 (Ref. 3) entitled "Investigation of Gas Augmented Injectors". This program was conducted under the auspices of the NASA Lewis Research Center, Cleveland, Ohio.

The approach to correlation of these data consisted of first listing those parameters which were considered to be most important for coaxial stream atomization and mixing, then grouping these parameters into a single parameter and subsequently into an overall model which would describe the physical trends observed in the data. The results of atomization tests were expressed in terms of $\bar{D}$, the mass median droplet diameter obtained with the frozen wax technique. The results of mixing tests were expressed in terms of a mass and mixture ratio uniformity parameter, E_m (Appendix C).

Mixing Analysis. Those parameters which were initially selected to describe mixing are listed below:

1. The relative gas momentum which is available to break up and mix the liquid mass

   $$\dot{w}_g(V_g - V_L)$$

   For the preliminary analysis, the gas velocities were computed using the annulus area between the liquid jet and the outer body. In the final analysis, the area between the center post outside diameter and the outer body was used for reasons which will be discussed in later sections.

2. The amount of liquid which must be mixed with the gas

   $$\dot{w}_L$$

3. The surface area of the liquid through which the gas can attack the liquid per unit volume of the liquid

$$\frac{\pi D_L V_L}{\frac{\pi D_L^2}{4} V_L} = \frac{4}{D_L}$$

These parameters were combined into a "performance factor", P_F, in such a manner that an increase in the value of this parameter would be expected to produce an increase in the mixing efficiency, E_m. The form of the performance factor selected is presented as Eq. (1)

$$P_F = \dot{w}_g(V_g - V_L) \frac{1}{\dot{w}_L} \frac{4}{D_L} \tag{1}$$

Equation (1) can be rearranged in terms of total mixture ratio as follows:

$$P_F = \frac{4}{D_L} \frac{\Delta V}{MR} \tag{2}$$

where

D_L = inside diameter of the oxidizer post

$\Delta V \doteq V_{gas} - V_{liquid}$

MR = weight flow mixture ratio $\frac{\dot{w}_L}{\dot{w}_g}$

This parameter suggests that high performance should be associated with high relative gas velocity, small elements, and low mixture ratios.

It is evident from Eq. (2) that the performance factor cannot be directly related to E_m because the value of E_m has an upper limit of 100% while the value of P_F has no upper bound. In order to correlate E_m with P_F,

a qualitative relationship between the two was assumed. The relationship is shown graphically in Fig. 1.

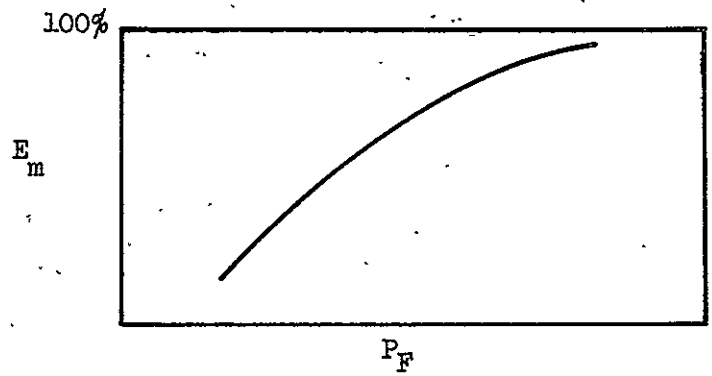

Figure 1. Qualitative Relationship Between E_m and P_F

A mathematical function, Eq. (3), was selected which provides the desired properties represented in Fig. 1.

$$E_m = 100\left[1 - \frac{1}{e^{AP_F}}\right] \tag{3}$$

where E_m = mixing uniformity parameter, % (see Appendix C)

P_F = performance factor

A = Arbitrary constant

To check the validity of the model represented by Eqs. (2) and (3) and to solve for the value of the constant "A", the experimental data which have been mentioned were employed. These data consist of mass and mixture ratio surveys from two circular, concentric tube elements, each of different size. These data are summarized in Table II. Most of these data were obtained with the oxidizer post of the elements recessed one liquid post diameter ($R/D_L = 1$).

TABLE II

GAS AUGMENTED PROGRAM MIXING RESULTS

Test No.	D_L	R/D_L	$\dot{w}_g$	$\dot{w}_L$	MR	V_g	V_L	E_m	$P_F \times 10^{-4}$
13	0.22	1	0.0337	0.202	5.99	783	13.5	78.0	2.93
14	0.22	1	0.0253	0.140	5.53	607	9.3	71.4	2.47
16	0.22	1	0.0334	0.342	10.24	793	22.8	54.6	1.72
43	0.43	1	0.1078	0.680	6.31	768	10.8	50.5	1.34
21	0.22	0	0.0235	0.136	5.79	613	9.07	53.2	2.24

A least squares analysis of these data employing the model represented by Eq. (3) produced a value of 48.2×10^{-6}(sec) for the constant "A" in Eq. (3). One other data point was available for center post recess of zero (i.e., flush post). This data point is also shown in Table II. This point gave a value of 34.2×10^{-6} (sec) for the constant "A" for flush posts. Values of "A" are summarized in Table III.

TABLE III
VALUES OF THE CONSTANT "A" FOR EQ. (3)

Recess R/D_L	A
0	34.2×10^{-6}
1	48.2×10^{-6}

These data points from Table II are plotted on Fig. 2 along with the curves generated using Eq. (3) for both zero and one liquid post inside diameter recess. Results presented in Fig. 2 suggested that the parameter and the model selected provided an acceptable description of this limited number of data points.

Based on the preceding analysis, the parameter $4\Delta V/D_L MR$ was selected as preliminary design criterion for circular concentric tube elements for achievement of high mixing efficiency.

Atomization Analysis. Following the guidelines of the mixing uniformity analysis, which has been presented, a method was devised to estimate the dropsizes for circular concentric tube elements.

$$E_m = 100 \left(1 - \frac{1}{e^{AP_F}}\right)$$

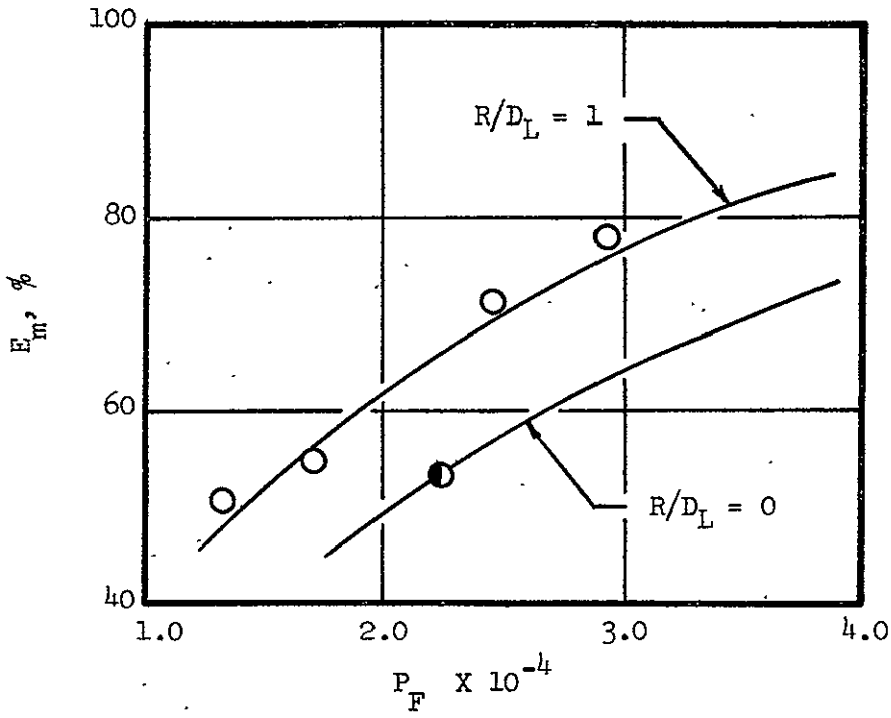

Figure 2. Correlation of Circular Concentric Tube Element Mixing Data in Terms of the Mixing Uniformity Parameter, E_m and the Performance Factor, P_F. (Data taken under NASA Contract NAS3-12001, Gas Augmented Injector Study.)

It was postulated that dropsize, as mixing, is a function of three primary variables:

1. Relative momentum of the gas, $\dot{w}_g\ (V_g - V_L)$
2. Amount of liquid to be atomized,
3. Size of the liquid port, D_L

Further, it was assumed that droplet size would approach, asymmptotically, a size equal to some fraction of the diameter of the liquid injection port as the gas flow rate through the outer annulus was reduced uniformly to zero. These postulates are expressed functionally in Eq. (4).

$$\frac{\bar{D}}{K\,D_L} = f\left(\frac{\dot{w}_g\,(V_g - V_L)}{\dot{w}_L}\right) = f\left(\frac{\Delta V}{MR}\right) \qquad (4)$$

where $\bar{D}$ = Mass median droplet diameter (microns)

D_L = Liquid post inside diameter (microns)

K = Fraction of D_L such that $\bar{D}$ approaches $(K\,D_L)$ as $\dot{w}_g \rightarrow 0$

The term $\Delta V/MR$ is similar to the "performance factor" for mixing. As $\Delta V/MR$ increases, it is expected that $\bar{D}$ should decrease.

To determine the form of the function "f", its limits were investigated. These limits were assumed to be:

$$\frac{\Delta V}{MR} \xrightarrow{\text{Lim}\ \rightarrow \infty} \frac{\bar{D}}{K\,D_L} = 0$$

$$\frac{\Delta V}{MR} \xrightarrow{\text{Lim}\ \rightarrow 0} \frac{\bar{D}}{K\,D_L} = 1$$

A simple function having these properties is represented by Eq. (5).

$$\frac{\bar{D}}{K\,D_L} = \frac{1}{e^{B(\Delta V/MR)}} \tag{5}$$

where

B = arbitrary constant

Equation (5) may be rearranged to produce the final correlating expression.

$$\frac{\bar{D}}{D_L} = \frac{K}{e^{B(\Delta V/MR)}} \tag{6}$$

It was assumed that the constant K was universal and not a function of element size, recess or flow rate. It is more than likely a function of liquid velocity; however, for this preliminary study, it was assumed constant. It was further assumed that the constant "B" was a function of liquid center post recess only.

Experimental (cold flow) data generated under Contract NAS3-12001 (Gas Augment Injectors) was again employed to estimate the constants K and B. Data from elements of three different sizes with three recess dimensions were employed. The value of K was found to be 0.354 for these circular concentric tube elements. Values of "B" for various post recess values are presented in Table IV.

TABLE IV
VALUES OF "B" FOR DIFFERENT POST RECESS

R/D_L	B
0	0.0142
1	0.0161
2	0.0257

Correlation of Eq. (6) with the pertinent atomization data is presented in Fig. 3 for circular concentric tube elements with post recess, $R/D_L = 1.0$. Relative droplet mass median diameters are plotted versus $\Delta V/MR$. The solid line in Fig. 3 was generated using Eq. (6) and may be compared with existing cold flow experimental data points.

Since high combustion efficiency is associated with small droplets, it is evident that the same parameters are required for high efficiency from both a mixing and atomization standpoint. Both Eq. (3) and (6) suggest that high efficiency should be obtained with high relative gas velocity, low liquid to gas mixture ratios, and small elements.

Equations (3) and (6) provided tools with which to relate concentric tube design parameters to specific engine operating conditions. The application of these equations to the Orbit Maneuvering Engine Concept is presented in the Element Preliminary Design Section.

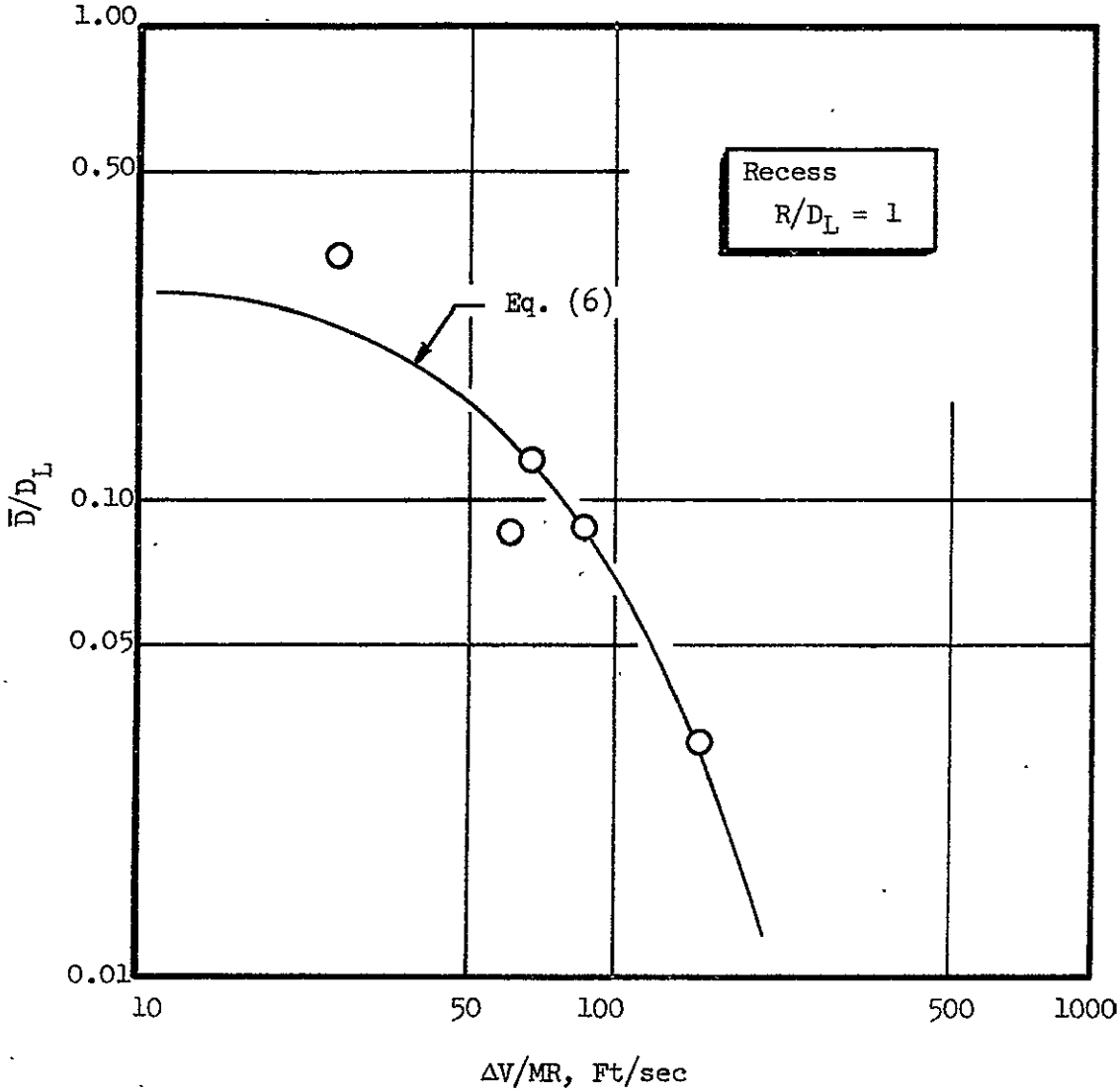

Figure 3. Correlation of Dropsize Data in Terms of $\bar{D}/D_L$ and $\Delta V/MR$ (data taken under NASA Contract NAS3-12001, Gas Augmented Injector Study)

Noncircular Concentric Tube Elements. The analysis techniques which have been discussed for circular concentric tube elements were extended by way of analogy to the analysis of noncircular (rectangular) concentric tube elements.

Mixing Analysis. A sketch of a noncircular (in this case rectangular) concentric tube element is shown in Fig. 4.

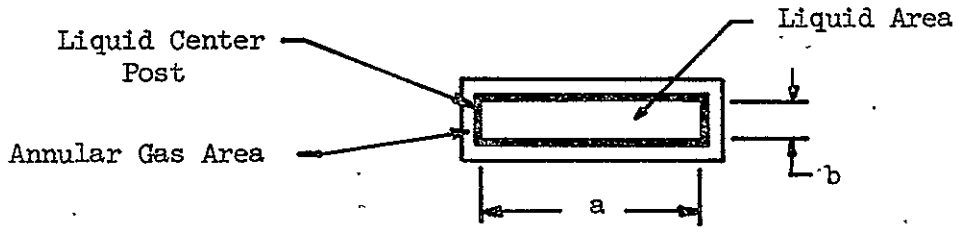

Figure 4. Noncircular Concentric Tube

Initially it was assumed that the same parameters which were important for circular concentric tube mixing were also important for noncircular concentric tube element mixing. The expressions for relative gas momentum and total liquid flow rate are identical for both circular and noncircular elements. However, the expression for the ratio of the gas/liquid contact surface area to the volume flux of liquid is a function not only of size but also of orifice aspect ratio for the noncircular element. The aspect ratio of the liquid port (Fig. 4) is defined by Eq. (7).

$$AR = \frac{a}{b} \tag{7}$$

For the noncircular element, the liquid surface area to volume flux ratio may be written as follows:

$$\frac{\text{surface flux}}{\text{volume flux}} = \frac{2(a+b)V_L}{ab\ V_L} \tag{8}$$

Combining Eqs. (7) and (8) and simplifying the surface to volume flux ratio becomes:

$$\frac{\text{surface flux}}{\text{volume flux}} = \frac{2(1+AR)}{a} \tag{9}$$

A "performance factor", analogous to that for the circular element was defined which is a combination of the three parameters selected:

$$P_{F_{NC}} = \left[\dot{w}_g(V_g - V_L)\right]\left[\frac{1}{\dot{w}_L}\right]\left[\frac{2(1+AR)}{a}\right] \tag{10}$$

relative gas momentum

total liquid flow

surface to volume flux ratio

Equation (10) may be rearranged to yield the final form of the performance factor:

$$P_{F_{NC}} = \frac{2(1+AR)}{a}\,\frac{\Delta V}{MR} \tag{11}$$

Equation (11) is comparable to Eq. (2) for the circular element.

In order to relate the mixing characteristics of circular and noncircular concentric tube elements, the supposition was made that if the performance

factors for the two elements were equal, they would produce the same quality of mixing.

If a circular and noncircular element were designed such that their respective liquid and gas injection areas were equal, then the values of ΔV and MR would be identical for the two at equivalent operating conditions. The ratio of Eq. (11) to Eq. (2) gives the ratio of performance factors for comparison of the two elements,

$$\frac{P_{F_{NC}}}{P_{F_C}} = \frac{\frac{2(1+AR)}{a}\ \frac{\Delta V}{MR}}{\frac{4}{D_L}\ \frac{\Delta V}{MR}} \tag{12}$$

If the liquid and gas areas are the same for each, then the following relationship between the geometric variables must hold true:

$$\frac{\pi D_L^2}{4} = ab \tag{13}$$

Introducing Eq. (7), it may also be shown that:

$$ab = \frac{a^2}{AR} \tag{14}$$

Equations (13) and (14) may be combined to show that:

$$\frac{D_L}{a} = 2\sqrt{\frac{1}{\pi AR}} \tag{15}$$

Therefore:

$$\frac{P_{F_{NC}}}{P_{F_C}} = \frac{(1+AR)}{\sqrt{\pi\, AR}} = \frac{1}{\sqrt{\pi}}\left[\sqrt{AR} + \frac{1}{\sqrt{AR}}\right] \tag{16}$$

To further compare circular and noncircular elements on the basis of E_m, the performance factor for the noncircular element was cast into a mixing model equation identical to Eq. (3). As with the circular element model, the constant "A" was taken to be a function of recess only. The measure of recess for the noncircular element was arbitrarily assumed to be the recess depth divided by the shorter length of the liquid port, "b". For the purpose of comparison, the constant "A" for both elements was assumed to be the same for equivalent recess.

Equation (3) was formulated such that a ratio between the mixing efficiency of the two elements could be taken:

$$1 - E_m = \frac{1}{e^{AP_F}} \tag{17}$$

where

E_m = mixing uniformity efficiency, decimal fraction

The term $1 - E_m$ is an expression of the deviation from perfect mass and mixture ratio distribution. The ratio of this term for noncircular to circular configuration is given in Eq. (18).

$$\frac{(1-E_m)_{NC}}{(1-E_m)_C} = e^{A(P_{F_C} - P_{F_{NC}})} \tag{18}$$

Equation (18) may be rewritten in terms of the ratio of performance factors:

$$\frac{(1-E_m)_{NC}}{(1-E_m)_C} = e^{AP_{F_C}\left(1 - \frac{P_{F_{NC}}}{P_{F_C}}\right)} \tag{19}$$

For a liquid port aspect ratio of 6.0, Eq. (19) reduces to the following:

$$\frac{(1-E_m)_{NC}}{(1-E_m)_C} = e^{AP_{F_C}(-0.61)} \tag{20}$$

For a recess of R/D = R/b = 0:

$$\frac{(1-E_m)_{NC}}{(1-E_m)_C} = e^{-20.9 \times 10^{-6} P_{F_C}} \tag{21}$$

This function is plotted in Fig. 5, with P_F as a nonapparent parameter. The term $(1-E_m)_C$ was computed from Eq. (3). A "break even" line $(E_{m_{NC}} - E_{m_C})$ is also plotted on Fig. 5 for reference.

It may be concluded from the mixing analysis that the noncircular element is expected, on a preliminary basis, to provide an advantage for mixing over the circular element and that this advantage is expected to increase, monotonically, with the aspect ratio of the liquid center post (Eq.(16)). From the preliminary analysis, an optimum for aspect ratio was not indicated. Therefore, the upper bound for aspect ratio would be established by structural and other practical design limitations.

Atomization Analysis. To estimate the droplet diameters produced by noncircular, concentric tube elements, a model identical to Eq. (6) for circular elements was chosen. The constants "K" and "B" were taken to be the same for both circular and noncircular elements. The one difference between the two models is the characteristic length, D_L in

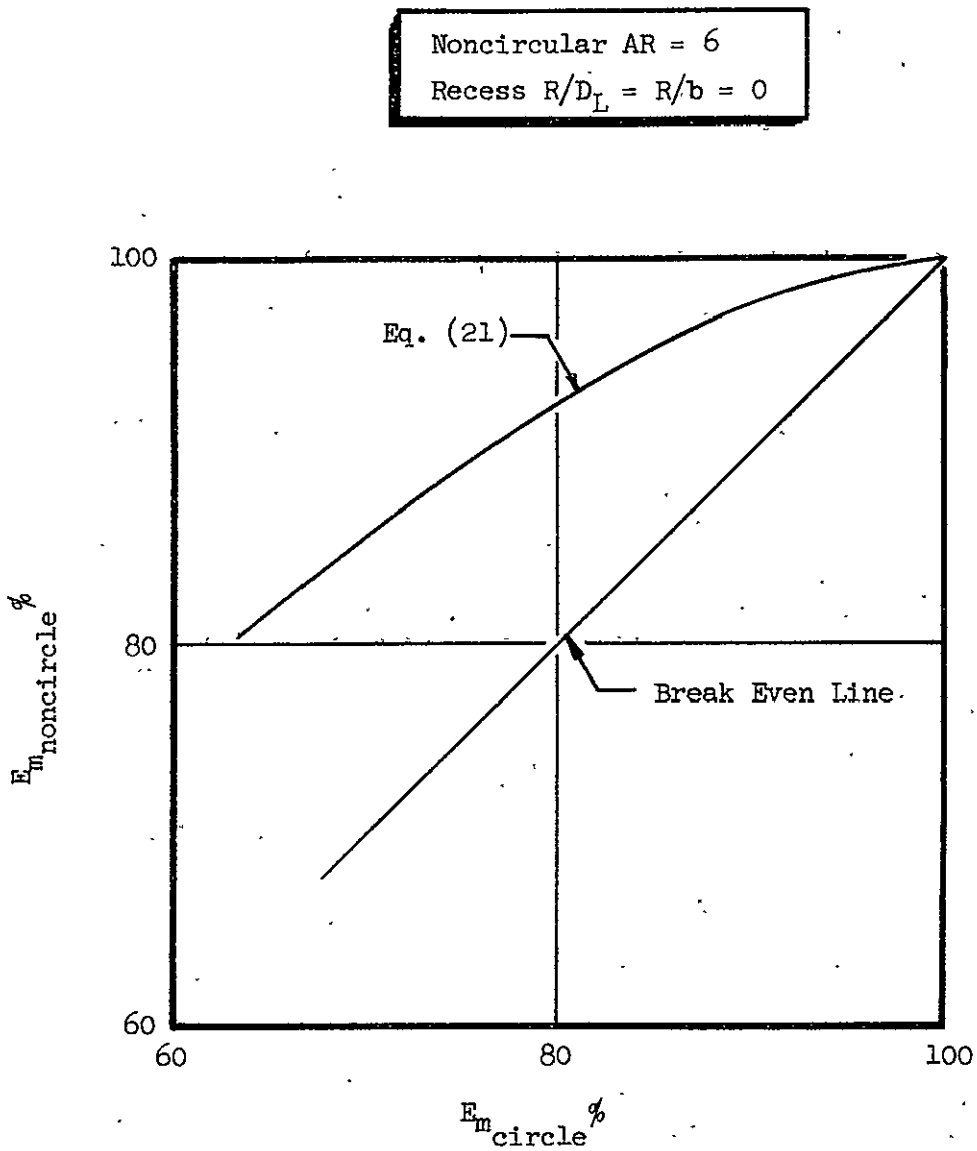

Figure 5. Comparison of Estimated Mixing Uniformity for the Circular and Noncircular Concentric Tube Elements

Eq. (6). For the noncircular configuration, the smaller dimension of the liquid center port, b, was chosen for this length. The atomization model for the noncircular element is presented as Eq. (22):

$$\frac{\bar{D}_{NC}}{b} = \frac{K}{e^{B(\Delta V/MR)}} \tag{22}$$

where

$\bar{D}_{NC}$ = Mass median droplet diameter for noncircular concentric tube

b = Height of liquid port

K = Constant equal to that for Eq. (6) = 0.354

B = Constant for given recess (see Table IV)

$\Delta V = V_{gas} - V_{liquid}$

$MR = \dot{w}_L/\dot{w}_g$

To compare the droplet sizes produced by similar circular and noncircular elements at equivalent operating conditions, Eq. (22) may be divided by Eq. (6):

$$\frac{\bar{D}_{NC}/b}{\bar{D}_C/D_L} = \frac{K/e^{B(\Delta V/MR)}}{K/e^{B(\Delta V/MR)}} = 1 \tag{23}$$

Thus, the droplet diameter ratio is reduced to a function of relative characteristic length:

$$\frac{\bar{D}_{NC}}{\bar{D}_C} = \frac{b}{D_L} \tag{24}$$

If the liquid port areas are equal for the two elements, then:

$$\frac{\pi D_L^2}{4} = ab = b^2 AR \tag{25}$$

Therefore:

$$\frac{b}{\bar{D}_L} = \frac{\sqrt{\pi/AR}}{2} \tag{26}$$

Substitution of Eq. (26) into Eq. (24) produces:

$$\frac{\bar{D}_{NC}}{\bar{D}_C} = \frac{\sqrt{\pi/AR}}{2} \tag{27}$$

For an aspect ratio 6.0:

$$\frac{\bar{D}_{NC}}{\bar{D}_C} = 0.362 \tag{28}$$

The relationship expressed by Eq.(28) is plotted in Fig. 6 along with a "break even line" for comparison (i.e., $\bar{D}_{NC} = \bar{D}_C$).

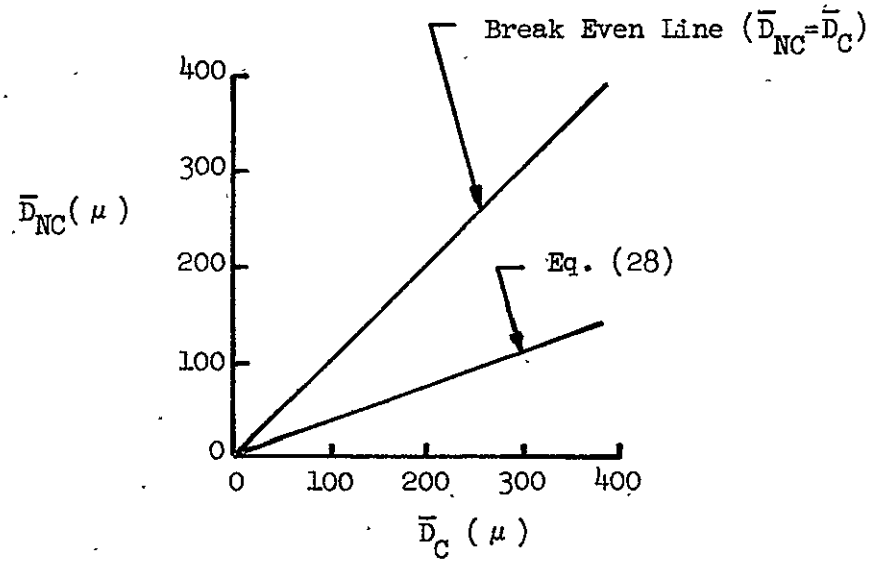

Figure 6. Estimated Relationship Between Droplet Diameters Produced by Circular and Noncircular Concentric Tube Elements

Again, as with mixing, the preliminary analysis points to a distinct advantage of the noncircular element for atomization. From Eq. (28), a noncircular element with orifice aspect ratio of six would be expected to produce droplets which are approximately 1/3 the diameter of those produced by a circular element at any equivalent operating condition.

In summary, the concentric tube element types have been tentatively characterized through the generalization of correlations of available cold flow data. The characterization of the noncircular concentric tube element was developed through analogy with the circular concentric tube element. Expressions were developed which may be used to estimate the mixing uniformity and mass median droplet sizes produced by these elements under various operating conditions and design configurations. These expressions provide the analytical tools required to produce preliminary designs for these elements and evaluate these designs on a relative basis along with other element types.

3.1.2 Analysis of Spray Fan Elements

A general spray fan type element is composed of one or more spray nozzle orifices which produce thin sheets of liquid droplets that are injected into a gas stream produced by a slot-shaped orifice.

The Spray Nozzle Orifice. The basic form of the spray nozzle orifice is depicted in Fig. 7.

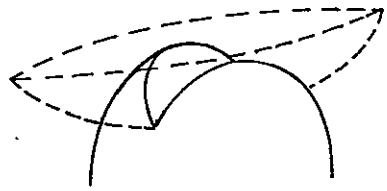

Figure 7. Basic Geometry of a Spray Nozzle Orifice

This orifice geometry is generated by drilling a blind hole from the "backside" of an injector such that the end of the orifice hole is just below the face of the injector. The end of the orifice hole is shaped into a spherical dome configuration. Finally, a thin, wedge-shaped cut is made from the face of the injector which slices through the spherical dome of the orifice below the injector face.

When fluid flows through this configuration, it is forced into a fan-shaped, separated jet. This jet is subsequently broken into small droplets by internal hydrodynamic wavelets and turbulence as well as external aerodynamic forces.

Approach to Spray Fan Element Analysis. Processes of interest occurring in the spray fan element flow field potentially include primary liquid atomization, secondary atomization, and gas/liquid mixing. A typical flow field is shown schematically in two views, in Fig. 8, for a doublet

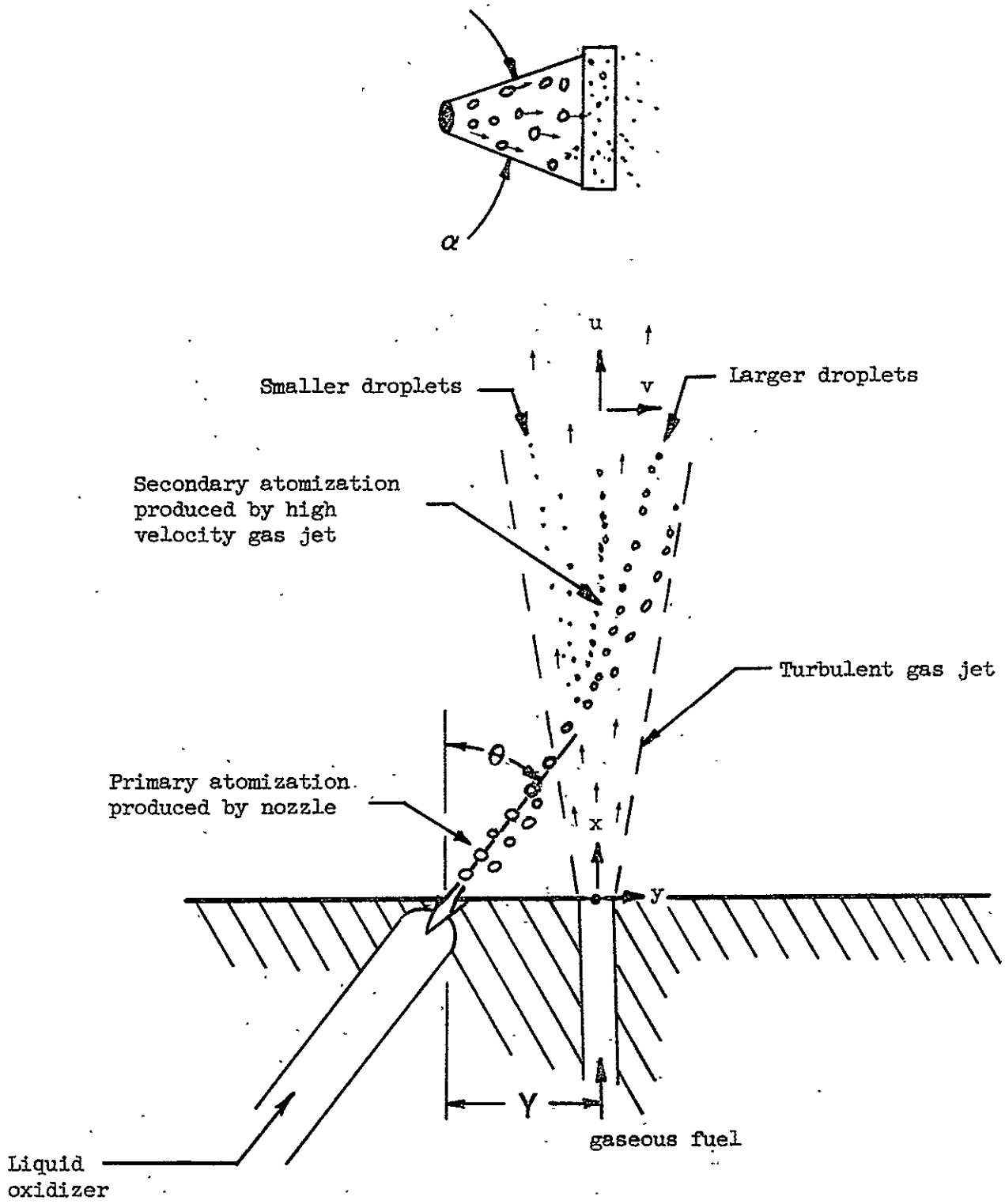

Figure 8. Spray Fan Element Flow Field Schematic

fan element. Those variables which must be considered in the analysis of this flow field are listed in Table V.

TABLE V
VARIABLES OF THE SPRAY FAN ELEMENT FLOW FIELD

Variable Symbol	Variable Name
$\dot{w}_L$	Liquid Flow Rate
$\dot{w}_g$	Gas Flow Rate
D_L	Spray Nozzle Size
A_G	Gas Orifice Area
AR	Gas Orifice Aspect Ratio
V_L	Liquid Injection Velocity
V_g	Gas Injection Velocity
α	Spray Nozzle Spread Angle
θ	Spray Nozzle Impingement Angle
$\bar{D}_1$	Primary Droplet Median Size
$\bar{D}_2$	Secondary Droplet Median Size
Y	Orifice Spacing
P_c	Chamber Pressure

The first step in the spray fan element preliminary analysis was to develop an analytical tool for selection of those combinations of the design and operating variables listed in Table V which will yield flow fields containing small droplet diameters and uniform mixture ratio distribution (i.e., high values of E_m). What follows is a description

of the development of the model used to estimate the atomization and mixing characteristics of the spray fan element.

To describe the flow field generated by the gas jet, the simplified, two-dimensional, turbulent jet description given by Goertler and outlined by Schlichting in Ref. 4 was employed. The equations which describe the velocity components within the jet are:

$$u = \frac{\sqrt{3}}{2} \sqrt{\frac{k\sigma}{x}} \left(1 - \tanh^2 \eta\right) \tag{29}$$

$$v = \frac{\sqrt{3}}{4} \sqrt{\frac{k}{x\sigma}} \left(2\eta \left[\, 1 - \tanh^2 \eta \,\right] - \tanh \eta\right) \tag{30}$$

$$\eta = \sigma \frac{y}{x} \tag{31}$$

where

u = velocity component in x-direction

v = velocity component in y-direction

η = similarity parameter

σ = spreading parameter equal to 7.67 for incompressible jets

k = kinematic jet momentum = $\int_{-\infty}^{\infty} u^2 \, dy$ (x = const)

x,y = coordinates defined in Fig. 8.

Equations (29) through (31) do not account for the presence of droplets in the flow field. To approximate the interaction of the gas jet and droplets, the kinematic momentum of the jet, "k", was reduced in the flow field by the amount of momentum which was imparted to the droplets. Thus, "k" was made a function of x.

The trajectories of the various droplets were computed by numerical integration of simplified x- and y-momentum equations for single particles. These equations are reproduced below:

x-Momentum

$$\frac{1}{2}\ \rho_g\ |\vec{V} - \vec{V}_d|\ (u - V_{dx})\ C_D\ \frac{\pi D^2}{4} - \frac{\pi D^3}{6}\ \frac{\partial p}{\partial x}$$

$$= \frac{D^3}{6}\ \rho_L \left(V_{dx}\ \frac{\partial V_{dx}}{\partial x} + V_{dy}\ \frac{\partial V_{dx}}{\partial y}\right) \qquad (32)$$

y-Momentum

$$\frac{1}{2}\ \rho_g\ |\vec{V} - \vec{V}_d|\ (v - V_{dy})\ C_D\ \frac{\pi D^2}{4} - \frac{\pi D^3}{6}\ \frac{\partial p}{\partial y}$$

$$= \frac{\pi D^3}{6}\ \rho_L \left(V_{dy}\ \frac{\partial V_{dy}}{\partial y} + V_{dx}\ \frac{\partial V_{dy}}{\partial x}\right) \qquad (33)$$

where

$\vec{V}$ = total gas velocity vector $\sqrt{u^2 + v^2}$

$\vec{V}_d$ = total drop velocity vector $\sqrt{V_{dx}^2 + V_{dy}^2}$

ρ_g = gas density

ρ_L = liquid density

C_D = drag coefficient for droplets

D = droplet diameter

p = local static pressure

For the purpose of a preliminary analysis, it was concluded that the solution of Eqs. (32) and (33) in their complete form was not justified and that a greatly simplified set of equations would be required.

The first simplification selected was the elimination of the "buoyancy" terms, that is, terms involving pressure gradients. This was justified under the assumption that the buoyancy forces on a droplet would be quite small compared to the drag forces in almost any gas flow field. With the elimination of these terms, however, Eqs. (32) and (33) were still partial differential in form. It was decided that one of the cross differential terms in each equation must also be eliminated in order to produce ordinary differential equations. In Eq. (32), the term $V_{dy} \frac{\partial V_{dx}}{\partial y}$ was eliminated and in Eq. (33) the term $V_{dy} \frac{\partial V_{dy}}{\partial y}$ was eliminated. Elimination cannot be justified on the grounds that they are small compared to the others. As a matter of fact, they are more than likely equal to their respective cross terms in magnitude. If it is assumed that they are indeed everywhere equal to their cross terms, then a multiplier can be applied to the other term to account for the absence of these terms. This multiplier can then be divided out and included in the magnitude of the drag coefficient which appears on the left side of the equations. The uncertainty involved in the determination of and the functional variation of the drag coefficient, itself, more than likely overshadows the uncertainty in the droplet trajectory caused by equating the cross differential terms.

The equations which resulted from this gross simplification of Eqs. (32) and (33) are:

x-Momentum

$$V_{dx} \frac{dV_{dx}}{dx} = \frac{3}{4} \frac{\rho_g}{\rho_L} \frac{C_D}{D} \left| \vec{V} - \vec{V}_d \right| (u - V_{dx}) \qquad (34)$$

y-Momentum

$$V_{dx} \frac{dV_{dy}}{dx} = \frac{3}{4} \frac{\rho_G}{\rho_L} \frac{C_D}{D} \left| \vec{V} - \vec{V}_d \right| (v - V_{dy}) \tag{35}$$

Equations (34) and (35) can be solved numerically by finite difference techniques with the additional assumption that the drag coefficient, C_D, is constant.

A computer program was written which solves Eq. (29), (30), (31), (34), and (35) given a gas jet geometry and initial momentum, and a spray droplet size distribution, initial angle, θ, and initial droplet velocity. An artificial collection matrix was positioned downstream in the flow field normal to the x-axis (Fig. 8). The final positions of injected gas and liquid in the various elements of the collection matrix were used to compute the mixture ratio uniformity parameter E_m.

In addition to computing the spacial trajectories of all the droplets in the spray field, an assumed secondary breakup of each droplet was computed. The secondary droplet breakup initiation criterion selected is that reported by Dickerson (Ref. 5) which states that breakup should begin when

$$\frac{W_E}{\sqrt{R_e}} \geq 1.0 \tag{36}$$

where

W_E = relative Weber No. of droplet = $\rho_G \frac{|\vec{V} - \vec{V}_d|^2 D}{\sigma_L}$

R_E = relative Reynolds No. of droplet = $\frac{\rho_G |\vec{V} - \vec{V}_d| D}{\mu_G}$

σ_L = surface tension of liquid

μ_G = viscosity of gas

ρ_L = gas density

D = droplet diameter

$|\vec{V} - \vec{V}_d|$ = relative gas velocity

Following initiation of breakup, a time lag is required prior to final breakup. The magnitude of the time lag is also reported in Ref. 5:

$$t_b = \frac{D}{|\vec{V} - \vec{V}_d|} \left[\frac{\rho_L}{\rho_g}\right]^{1/2} \tag{37}$$

where

t_b = time to breakup

Initial droplet size and distribution data as a function of spray nozzle size and pressure drop required for the analysis was obtained from the data taken under Phase I of this program, Ref. 1. These data are reproduced in Fig. 9 for reference.

The droplet diameters produced through secondary atomization were computed using a modified Wolfe and Anderson equation which was also reported by Dickerson in Ref. 5.

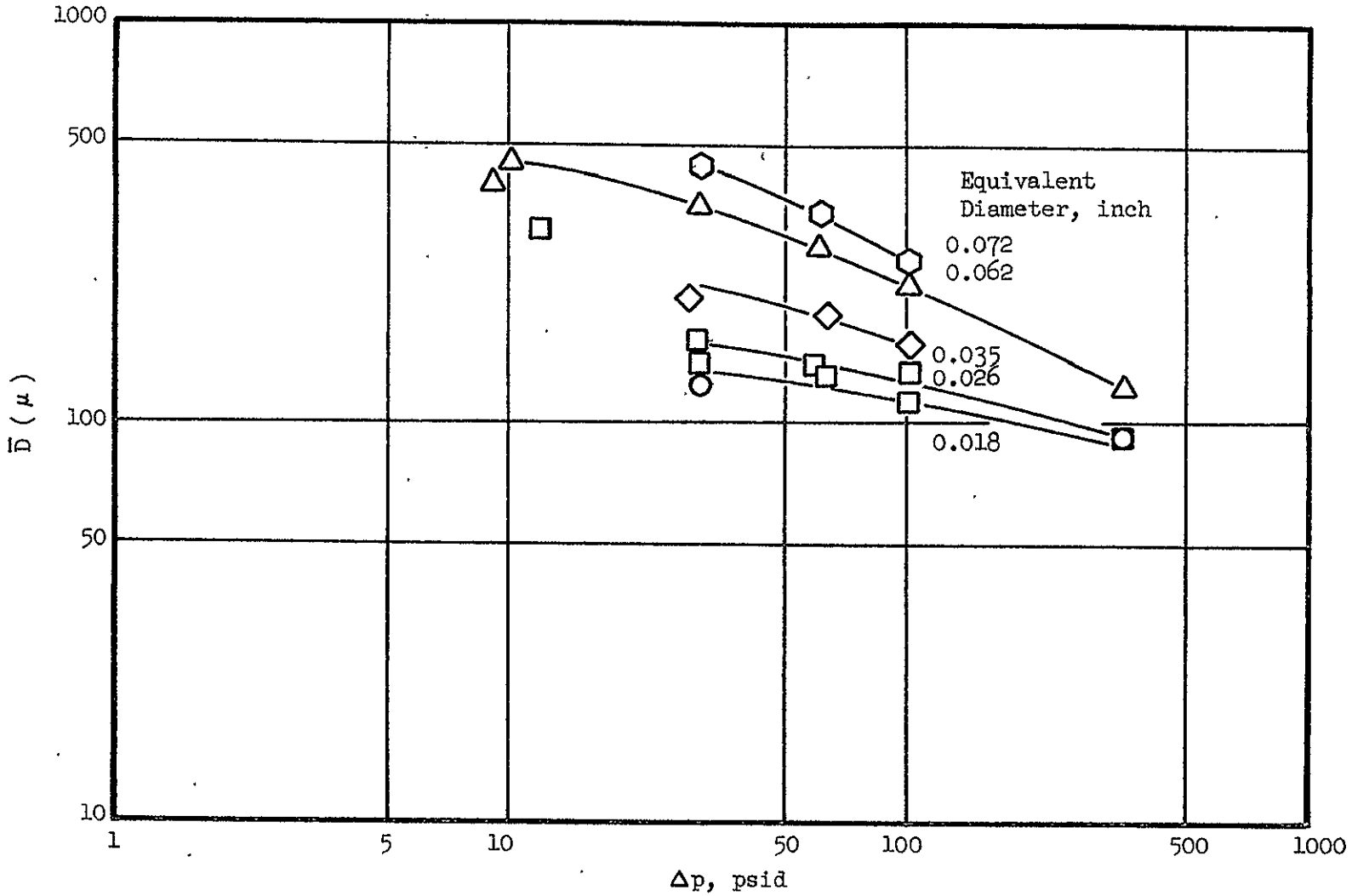

Figure 9. Mass Median Droplet Diameters for Various Spray Fan Nozzles as a Function of Pressure Drop (Data taken under Phase I of subject Contract NAS9-9528)

$$\bar{D}_2 = \lambda \left[\frac{136\, \mu_L\, \dot{\sigma}_L^{3/2}\, D_{L_1}^{1/2}}{\rho_L^{1/2}\, \rho_g^{2}\, \Delta V^{4}} \right]^{1/3} \tag{38}$$

where

λ = a constant

μ_L = liquid viscosity (absolute)

σ_L = liquid surface tension

D_{L_1} = primary droplet diameter

ρ_L = liquid density

ρ_g = gas density

$\Delta V = \left| \vec{V}_{gas} - \vec{V}_{drop} \right|$

The arbitrary constant, λ, was introduced to increase the droplet diameters computed by Eq. (38) to diameters produced in typical gas liquid atomization processes involving clouds of droplets. The absolute magnitude of the droplet diameters computed with the original Wolfe-Anderson model (Ref. 6) are unrealistically small. The Wolfe-Anderson model was developed as a result of studies involving the breakup of single droplets in a relatively large gas flow field.* Although the absolute value of the original model was changed, the functional relationship of the variables was not altered.

*No experimental data were found describing droplet shattering in dense, two-phase flow fields typical of a rocket engine. Lacking such information, the approach described here was applied as a best estimate, and as such, may be subject to appreciable inaccuracy.

The secondary breakup model was employed to determine the secondary sizes of the droplets produced by the breakup of several size groups in a given flow field.

In the model, 10 size groups were employed to describe the original droplet distribution. Ten additional droplet size groups were employed to describe the secondary droplet size distribution for each of the primary groups. Thus, following completion of secondary atomization, a total of 100 droplet size groups were employed to describe the spray droplet distribution.

One final point concerning the analysis should be mentioned. At the position of the artificial collector, the gas flow field is composed of both primary injectant (i.e., fuel) and gas which has been ingested during the flight from the injector face to the collector. The fuel concentration of the gas collected at each point was computed using the similarity equation postulated by Abramovich (Ref. 7):

$$\frac{\Delta C}{\Delta C_m} = \sqrt{\frac{u}{u_m}} \tag{39}$$

where

ΔC = concentration of injectant at a given point

ΔC_m = concentration of injectant on the center line of the jet in the same axial plane

u = velocity at the arbitrary point

u_m = center line velocity in the same plane

To summarize, the interaction of a gas jet produced by a slot shaped orifice and a droplet spray field produced by a spray fan orifice has been described by an analytical computer model. The model computes the spacial distribution of liquid and gas and the primary and secondary droplet sizes of the liquid species. These results are employed to compute the mixing uniformity parameter, E_m, and the secondary mass median droplet diameter, $\bar{D}$, for elements incorporating spray fan orifices.

It must be emphasized that the model which has been described is strictly tentative in nature and highly simplified. It is intended that this model be used only for the purposes of generating preliminary design data and correlating preliminary results. The nature of the secondary breakup of droplet clouds is extremely complex, and it is not presumed that this model describes this process fully.

The model was employed in the Preliminary Design section to estimate the performance of spray fan doublet, triplet, and four-on-one elements.

3.1.3 Analysis of Impinging Jet Elements

An impinging jet-type element is one which is composed of fuel and oxidizer orifices designed to produce separate and independent jets which subsequently impinge some distance downstream from the injector face. Primary atomization of any liquid species and mixing of propellant is produced by the direct interaction of these free jets. These characteristics distinguish the jet impinging-type element from the spray fan

element which injects a liquid spray rather than a coherent jet and from the concentric tube element which produces mixing and atomization through interpropellant shear forces.

Analysis of impinging type elements was accomplished with the aid of a jet penetration model proposed by Dickerson (Ref. 5). For the purpose of explaining this model and the variables involved, a sketch of an unlike, gas/liquid doublet element is shown in Fig. 10.

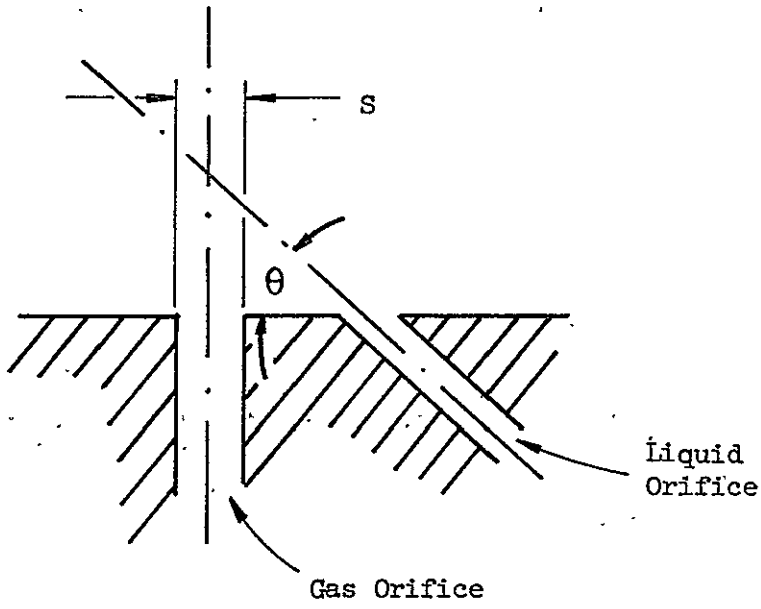

Figure 10. Unlike Doublet - Impinging Jet

In Fig. 10, a liquid orifice is depicted which will produce a jet impinging on a jet from a gas orifice at an angle, θ, measured from a plane normal to the gas jet. The width of the gas orifice is denoted by the symbol "S". Dickerson's criterion estimates the fractional penetration distance of the liquid jet across the gas jet "S":

$$\frac{X_p}{S} = 2.5 \sqrt{\frac{\rho_L V_L^2}{\rho_g V_g^2}} \quad \text{Cos } \theta \tag{40}$$

where

$\frac{X_p}{S}$ = fraction of the distance "S" penetrated by the liquid jet

ρ_L = liquid density

ρ_g = gas density

V_L = liquid velocity

V_g = gas velocity

θ = impingment angle of the liquid jet on the gas jet measured from a plane normal to the gas jet.

Equation (40) was developed for unlike impinging jet elements incorporating circular orifices, however, it is likely that the same variables which govern circular jet mixing are important for mixing of noncircular jets.

In physical terms, the right-hand side of Eq. (40) represents the ratio of the liquid jet moment flux normal to the gas jet to the momentum flux of the gas jet. Thus, the penetration criteria expresses the relative strength of the jet being penetrated. The form of the equation and the magnitude of the constant were determined by curve fitting experimental data.

The usual application of Eq. (40) involves the design of an injector element. Depending on the particular element configuration (i.e., doublet,

triplet, etc.), a value of the penetration distance X_p/S is selected. For a fixed value of X_p/S, Eq. (40) provides a functional relationship between the propellant momentum ratio and the impingement angle of the various streams.

A specific atomization study was not conducted for the impinging jet element types. There are limited data available (Ref. 5), however, which indicate that the values of $\bar{D}$ for these elements should be smaller than 40 microns in the operating range of interest. For oxygen/hydrogen propellants, droplets smaller than 40 μ, $\bar{D}$, will normally yield vaporization c* efficiencies very nearly equal to 100%. Based on these limited data, it was concluded that the unlike-impinging jet elements would be mixing limited in their performance characteristics, and, therefore, no further atomization analysis was attempted.

3.2 PRELIMINARY DESIGN OF ELEMENT TYPES

The Preliminary Design section consists of a direct application of the analysis tools which were developed in the previous section to the design of elements for a conceptual Orbit Maneuvering Engine for the Space Shuttle System. Ground rules used in the design study are summarized in Table VI. For this study, the Orbit Maneuvering System Engine (OMS) was assumed to be an 8000 lb_f thrustor which operates at a chamber pressure of 800 psia. The propellants are gaseous hydrogen and liquid oxygen.

Element types which were configured for this conceptual mission are those which were presented previously in Table I. Designs of these element types

TABLE VI.
TENTATIVE DESIGN GUIDELINES FOR THE
ORBIT MANEUVERING SYSTEM ENGINE

Propellants - LOX/GH_2

Chamber Pressure = 800 psia

Thrust = 8000 lb_f

Total Flow rate = 17.3 lbm/sec

Mixture Ratio = 6:1

Expansion Ratio = 200:1

Hydrogen Injection Temperature = 490°R

Oxygen Injection Temperature = 180°R

Throat Area = 5.1 $in.^2$

Maximum Fuel Pressure Drop = 130 psid

Minimum Oxidizer Pressure Drop = 11 psid (not including artificial hydraulic resistances added to the system)

are discussed in the same order as their respective analysis techniques, followed by a summary of element designs.

All elements were designed at the 200 lb_f thrust per element level or 40 elements for the OMS injector. In addition, 130 lb_f thrust elements (61 elements) were designed for both the circular and noncircular concentric tube element types.

3.2.1 Design of Concentric Tube Elements

Circular Concentric Tube Element. Equations (2), (3), and (6) along with the ground rules presented in Table VI were employed in the design of the circular concentric tube element. These equations are reproduced below for convenience:

Mixing

$$P_F = \frac{4}{D_L} \frac{\Delta V}{MR} \tag{2}$$

$$E_m = 100 \left(1 - \frac{1}{A_e P_F}\right)$$

Atomization

$$\frac{\bar{D}}{D_L} = \frac{K}{e^{B(\Delta V/MR)}} \tag{6}$$

It is evident from these equations that the velocity difference, ΔV, should be made as large as possible for a given element within the restrictions imposed by overall system design. This, of course, dictates that the maximum allowable gas velocity and the minimum allowable liquid velocity be employed in the design. These velocity limits for the OMS engine are reflected indirectly in the allowable pressure drop figures presented in Table VI.

For purposes of converting pressure drop limitations to velocity criteria, orifice coefficients were selected based upon analysis of the fuel and oxidizer flow passages of typical concentric tube elements. An orifice coefficient of 1.0 was selected for the oxidizer orifice and

a coefficient of 0.74 was selected for the fuel annulus. These figures translate to a maximum fuel injection velocity of 1500 ft/sec and a minimum oxidizer injection velocity of 38 ft/sec.

Two different thrust level elements were designed for the concentric tube element types; 200 lb_f and 130 lb_f thrust per element. The first requires 40 elements and the second requires 61 elements. Total fuel and oxidizer flow requirements are listed in Table VI and the various single element flowrates are presented in Table VII for the two thrust levels.

TABLE VII
SINGLE ELEMENT FLOW RATE SUMMARY

Thrust per Element (lb_f)	Oxidizer Flow per Element (lb_m/sec)	Fuel Flow per Element (lb_m/sec)
130	0.2435	0.040
200	0.371	0.0619

With the flow rates and velocities defined, the element injection areas were computed through the continuity equation:

$$A = \frac{\dot{w}}{\rho V} \tag{41}$$

The results of this calculation are presented in Table VIII for the two element thrust levels. The element design nomenclature is defined in Fig. 11.

TABLE VIII
CIRCULAR CONCENTRIC TUBE DESIGN SUMMARY

Thrust per Element (lb_f)	D_L (in.)	D_p (in.)	D_g (in.)	R/D_L	A_{ox}	A_F
130	0.129	0.169	0.2065	0.0	0.0131	0.0131
200	0.160	0.200	0.256	0.0	0.0201	0.0201

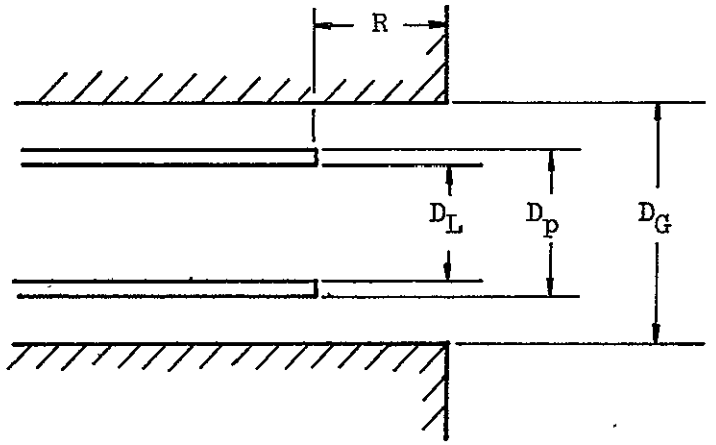

Figure 11. Circular Concentric Tube Nomenclature

At this point, all of the design and operational variables were known and Eqs. (2), (3), and (6) were employed to estimate the mixing and atomization characteristics of these elements. A summary of these results is presented in Table IX for elements with flush center posts ($R/D_L = 0$).

TABLE IX

PREDICTED MIXING AND ATOMIZATION CHARACTERISTICS FOR THE CIRCULAR CONCENTRIC TUBE ELEMENTS

Thrust per Element	Performance Factor, P_F	Predicted E_m (%)	Predicted $\bar{D}$ (μ)
130	90,600	95.5	37
200	73,200	91.8	45

Details of the relationship between E_m, $\bar{D}$ and predicted C* efficiency are discussed later in this report. However, a comment should be made at this time concerning the significance of the results in Table IX with respect to η_{c*}. As a typical example, in a combustion chamber with a length of 6 to 8 inches and contraction ratio between 2 and 3, the vaporization of 37 to 45 micron droplets would be expected to be completed by the throat section, thereby producing a vaporization limited efficiency of 100%. In the same example, with hydrogen/oxygen at a mixture ratio of 6.0, mixing uniformities of the order of 91 to 95.5 would be expected to produce mixing limited efficiencies in excess of 99%. Thus, the overall C* efficiency associated with the elements described in Table IX should be in excess of 98.5% with the higher efficiency associated with the smaller element.

It should be pointed out at this time that the vaporization rate limited efficiency is a sensitive function of chamber length. The performance values quoted here are for chambers which are 6 to 7 inches in length. The efficiency would be expected to fall as chamber length is reduced.

In short chambers, therefore, the droplet sizes will have to be smaller than those indicated in Table IX to achieve 100% vaporization limited efficiency values. If a noncircular element can be designed to deliver smaller droplets, then it will have an advantage over the circular element in short chamber applications. Short chambers offer weight savings and packaging advantages.

Noncircular Concentric Tube Element. In the analysis section devoted to the noncircular concentric tube, it was postulated that the same operational parameters which would produce high efficiencies for circular concentric elements would also produce high efficiencies for noncircular elements. Thus, based on the ground rules stated in Table VI and the computations for the circular element in the preceding section, the fuel and oxidizer areas for the noncircular elements must be made equal to the fuel and oxidizer areas of their circular counterparts (see Table VIII). The areas, however, do not constitute the complete design for the noncircular elements. It is apparent from examination of Eqs. (21) and (22) that one additional variable is required and that is the aspect ratio of the oxidizer port in the element (see Fig. 4).

An aspect ratio of 6.0 was selected for preliminary design purposes. The equations indicated that performance would increase in a monotonic fashion with element aspect ratio. Thus, one would like to have aspect ratios as large as possible. However, fabrication and structural design factors limit the aspect ratio that can actually be employed. The aspect

ratio of 6.0 was selected as a reasonable compromise between performance and structural considerations.

With respective areas of the circular and noncircular elements being equal and with the selection of an aspect ratio of 6.0, the predicted mixing and atomization characteristics of the noncircular element were obtained from Figs. 5 and 6 as functions of the characteristics of the circular elements which have been presented in Table IX. The predicted performance parameters for the noncircular elements are presented in Table X for both thrust levels.

TABLE X
PREDICTED MIXING AND ATOMIZATION CHARACTERISTICS
FOR NONCIRCULAR CONCENTRIC TUBE ELEMENTS

Thrust per Element	Performance Factor, P_F	Predicted E_m (%)	Predicted $\bar{D}$ (μ)
130	146,000	99.3	14
200	118,000	98.3	16

It would be expected that E_m and $\bar{D}$ values such as those listed in Table X would produce overall c* efficiencies very nearly equal to 100% for the hydrogen/oxygen propellant combination with 6 to 8-inch chamber lengths with contraction ratio of 2 to 3. Even with shorter chambers (e.g., 2 to 4 inches), overall C* efficiency would be expected to remain high (e.g., $\geq$ 98%).

Parametric Study of Concentric Tube Elements. Both the circular and noncircular concentric tube elements have been designed and performance estimates have been made for one specific chamber operating condition (see Table VI). It would be of interest to determine the effect of mixture ratio and chamber pressure excursions upon the performance parameters, E_m and $\bar{D}$, for these elements. An estimate of these effects, was obtained through the use of a simplified engine operating model, to determine the changes of the various physical parameters with P_c and mixture ratio, along with the correlating parameters to determine the influence of the changes in the physical parameters upon E_m and $\bar{D}$. Two engine models were required, one for chamber pressure variation at constant mixture ratio and one for mixture ratio variation at constant chamber pressure.

Throttling. The following assumptions were made for the case of chamber pressure variation at constant mixture ratio:

$C^* = \text{constant}$

$V_g = \text{constant}$

$V_L = K P_c$: ($K = \text{constant}$)

The effect of throttling on mixing uniformity was estimated through the formulation of the performance factor, P_F, in terms of the operating conditions dictated by the engine model. The performance factor for the circular concentric tube is defined in Eq. (2). This expression may be rewritten in the following form for constant mixture ratio throttling:

$$P_F = K_1 (V_g - K_2 P_c) \tag{42}$$

where

K_1 and K_2 = constants

V_g = constant

Values of K_1 and K_2 were obtained by introducing the nominal operating values into Eqs. (42) and (2). The resulting equation for P_F for the circular concentric tube element at the 200 lb thrust per element level is shown below.

$$P_F = 50 (1500 - 0.045 P_c) \tag{43}$$

It is evident from Eq. (43) that the estimated influence of P_c on P_F is slight. The estimated variation of E_m with P_c was obtained from simultaneous solution of Eqs. (3) and (43).

The effect of throttling on dropsize was estimated by the incorporation of the engine modeling assumptions into the expression for dropsize, Eq. (6). Results of this formulation are summarized in Eq. (44):

$$\frac{\bar{D}}{D_L} = \frac{K_1}{e^{B(V_g - K_2 P_c)/MR}} \tag{44}$$

Analysis of Eq. (44) suggested that the variation of estimated dropsize with P_c was negligible, and it was assumed that the $\bar{D}/D_L$ is approximately constant over a reasonable chamber pressure range.

Variation of E_m and D with chamber pressure for the noncircular concentric tube element was estimated from the variations for the circular element with the aid of Figs. 5 and 6.

The results of the analysis of the throttling effect on E_m and $\bar{D}$ for both the circular and noncircular concentric tube elements are presented in Figs. 12 and 13, respectively. For all practical purposes, mixing uniformity and dropsize were estimated to remain constant with chamber pressure.

Mixture Ratio Variation. The engine operating model for mixture ratio variation at constant chamber pressure was based upon the following assumptions:

$$C^* = \text{constant}$$

$$\dot{w}_T = \text{constant}$$

$$P_c = \text{constant}$$

$$V_I/V_g = \text{constant}$$

Under these assumptions, the parameter $\Delta V/MR$ (which appears in both the performance factor and the droplet size model) may be written in the following form:

$$\frac{\Delta V}{MR} = \frac{K_2 (1 - K_1 MR)}{MR (1 + MR)} \tag{45}$$

where K_1 and $K_2 \equiv$ constants

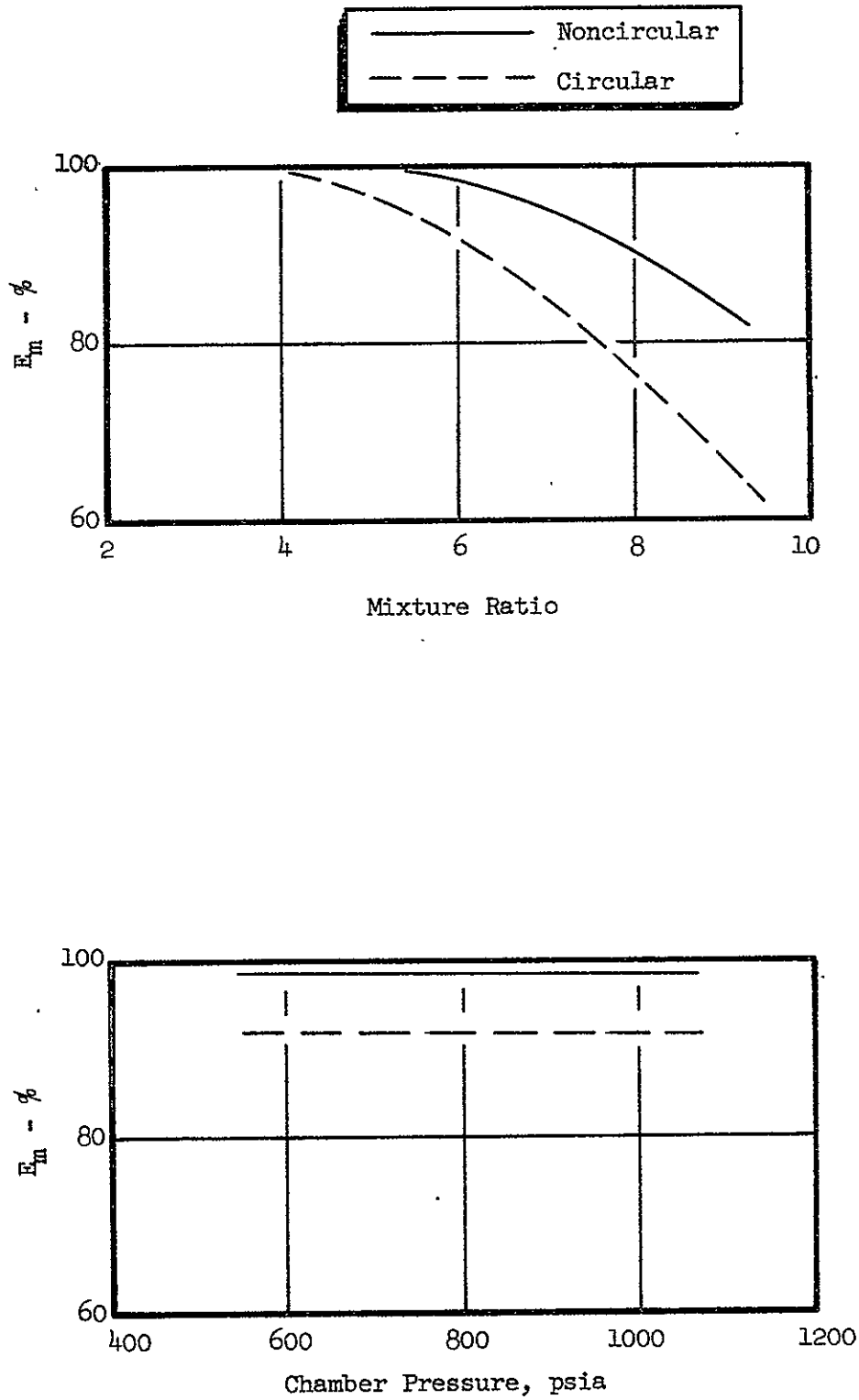

Figure 12. Estimated Mixing Uniformity, E_m, for the Circular and Noncircular Concentric Tube Elements as a Function of Mixture Ratio and Chamber Pressure

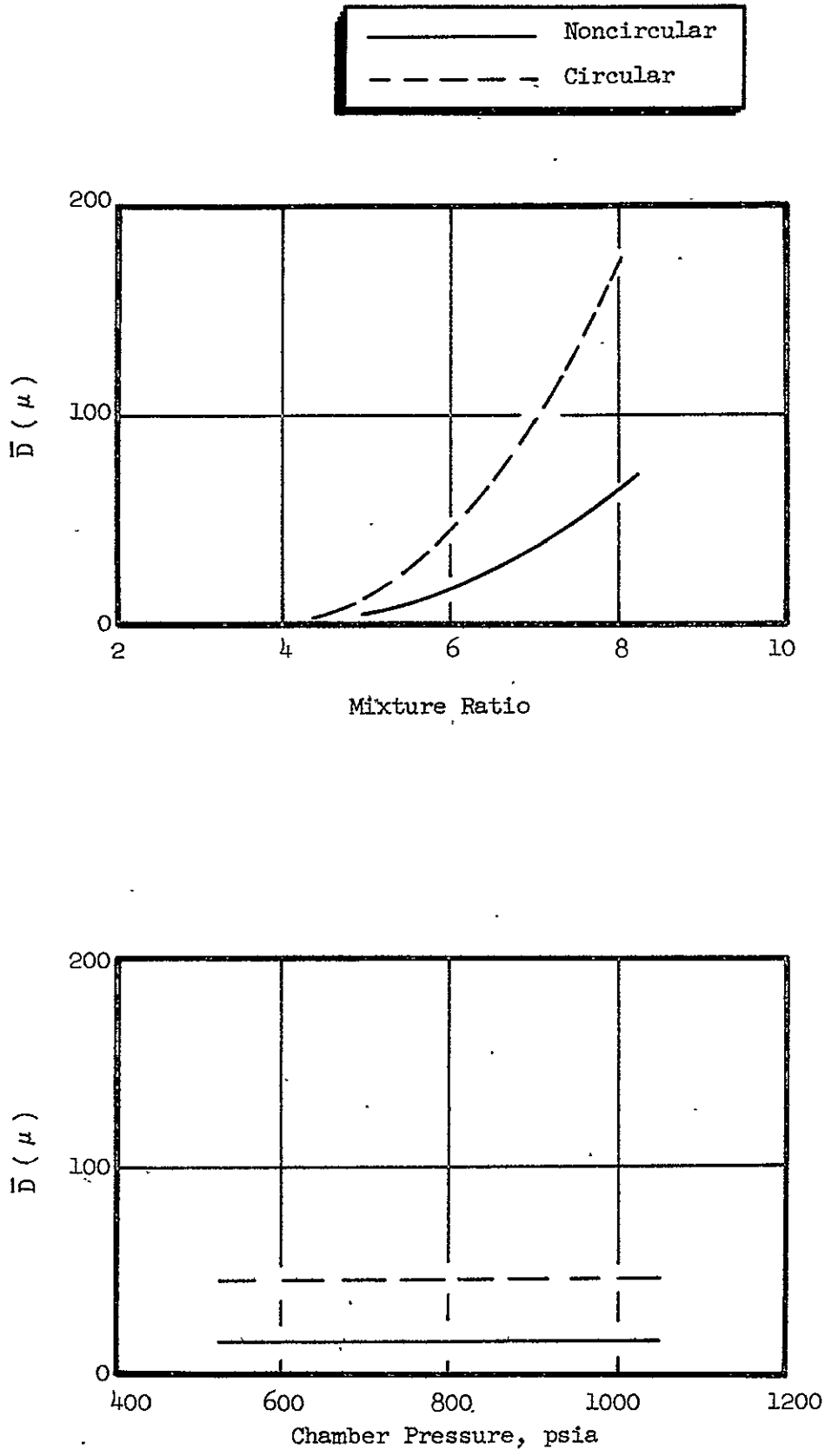

Figure 13. Estimated Mass Median Droplet Diameters, $\bar{D}$, for the Circular and Noncircular Concentric Tube Elements as a Function of Mixture Ratio and Chamber Pressure

The values of K_1 and K_2 were determined by substitution of the known nominal point values into Eq. (45). With these constants known, Eq. (45) appears in the form shown as Eq. (46) below:

$$\frac{\Delta V}{MR} = \frac{10,500\ (1 - 0.004\ MR)}{MR\ (1 + MR)} \tag{46}$$

The effects of mixture ratio variation upon mixing and atomization for the circular concentric tube element were estimated by simultaneous solution of Eqs. (46), (2), (3), and (6). This analysis was extended to the noncircular element with the aid of Figs. 5 and 6.

Results of this analysis are presented in Figs. 12 and 13 for E_m and $\bar{D}$ respectively. In contrast to the negligible variations of E_m and $\bar{D}$ with chamber pressure, these parameters vary widely with mixture ratio. In Fig. 12, the mixing uniformity is observed to decrease with increasing mixture ratio. Droplet diameter, Fig. 13, increases with increasing mixture ratio. From a performance standpoint, both of these trends are indicative of decreasing C* efficiency with increasing mixture ratio.

3.2.2 Design of Spray Fan Elements

Based upon the design guidelines presented in Table VI, three different configurations of the impinging spray fan element were investigated; (1) doublet (see Fig. 8), (2) triplet, and (4) four-on-one. The variables which were considered in the design are those listed in Table V.

For the type of spray nozzle used, the spread angle, α, (see Fig. 8) is approximately 80°. This variable was held constant throughout the entire analysis. The liquid and gas flow rates as well as chamber pressure are prescribed in Table VI. All of the spray fan element types were designed for the 200 lb_f thrust per element level. Thus, the fuel and oxidizer flow rates per element are the same as those prescribed for the concentric tube elements shown in Table VII at the 200 lb_f thrust level.

Each of the element configurations under consideration has but one fuel orifice. For the purpose of analysis, this orifice was assumed to be rectangular in shape. The first assumption which was made to begin the design process was that the fuel velocity be made as high as possible to assure efficient secondary atomization. It was assumed that the discharge coefficient of the fuel orifice was 0.74. With the maximum fuel side pressure drop of 130 psid defined in Table VI, the fuel velocity was fixed at 1500 ft/sec. Thus, the fuel orifice area for all three element configurations was defined by the continuity equation, Eq. (41).

$$A_g = 0.0201 \text{ in.}^2 \tag{47}$$

The fuel orifice aspect ratio, AR, was not defined and remained a free variable in the design analysis. Those independent variables from Table V which were as yet undefined are summarized below in Table XI.

TABLE XI
REMAINING INDEPENDENT DESIGN VARIABLES
FOR SPRAY FAN ELEMENTS

Symbol	Name
D_L	Spray Nozzle Size
AR	Gas Orifice Aspect Ratio
V_L	Liquid Injection Velocity
θ	Spray Nozzle Impingement Angle
Y	Orifice Spacing

The primary droplet diameter for the liquid side, $\bar{D}_1$, is a dependent function of D_L and V_L (see Fig. 9) and the secondary droplet diameter, $\bar{D}_2$, is a dependent function of the overall model (see Table V). The functional relationship between the pressure drop across a given spray nozzle and the liquid injection velocity, V_L, is presented below:

$$V_L = \sqrt{\frac{2g\,\Delta P_L}{\rho_L}} \tag{48}$$

Since the spray nozzle effectively produces a separated jet or fan, it was assumed that the pressure drop is totally converted to velocity head.

Spray Fan Doublet. The distinction between the doublet, triplet, and four-on-one element configurations is the number of spray nozzles in each and the aspect ratio of the fuel orifice. The simplest element is the unlike doublet; one spray nozzle impinging on one gas jet.

Due to the spreading angle of the spray fans, α, there is a geometrical dependence between the orifice spacing, Y, and the impingement angle, θ. (see Fig. 8). A design restriction was introduced which required the width of the spray to equal the length of the gas orifice at the point of contact. This situation is illustrated in the two views shown in Fig. 8. With the area of the gas orifice fixed, there is then a unique relationship of the form expressed below in Eq. (49).

$$AR = f(Y, \theta) \tag{49}$$

Solutions to Eq. (49) are presented in Fig. 14 wherein the aspect ratio of the fuel (gas) orifice is shown as a function of the impingement angle, θ, for various orifice spacings. The area of the gas orifice is constant and equal to 0.0201 $in.^2$.

At this point, a parametric study of the effect of spacing, impingement angle, and nozzle pressure drop was conducted using the computer model described in the spray fan analysis section. Results of this study are presented in Figs. 15 and 16.

First, to study the effect of impingement angle and spacing, a pressure drop of 100 psid was imposed on the spray nozzle and Y and θ were varied. Spacing was varied between 0.1 and 0.2 inch and impingement angle was varied between 20° and 50°. The results are shown in Fig. 15. Curves are presented for spacings of 0.10, 0.15, and 0.20 inch. The mixing uniformity parameter, E_m*, is plotted as a function of θ.

*See Appendix C.

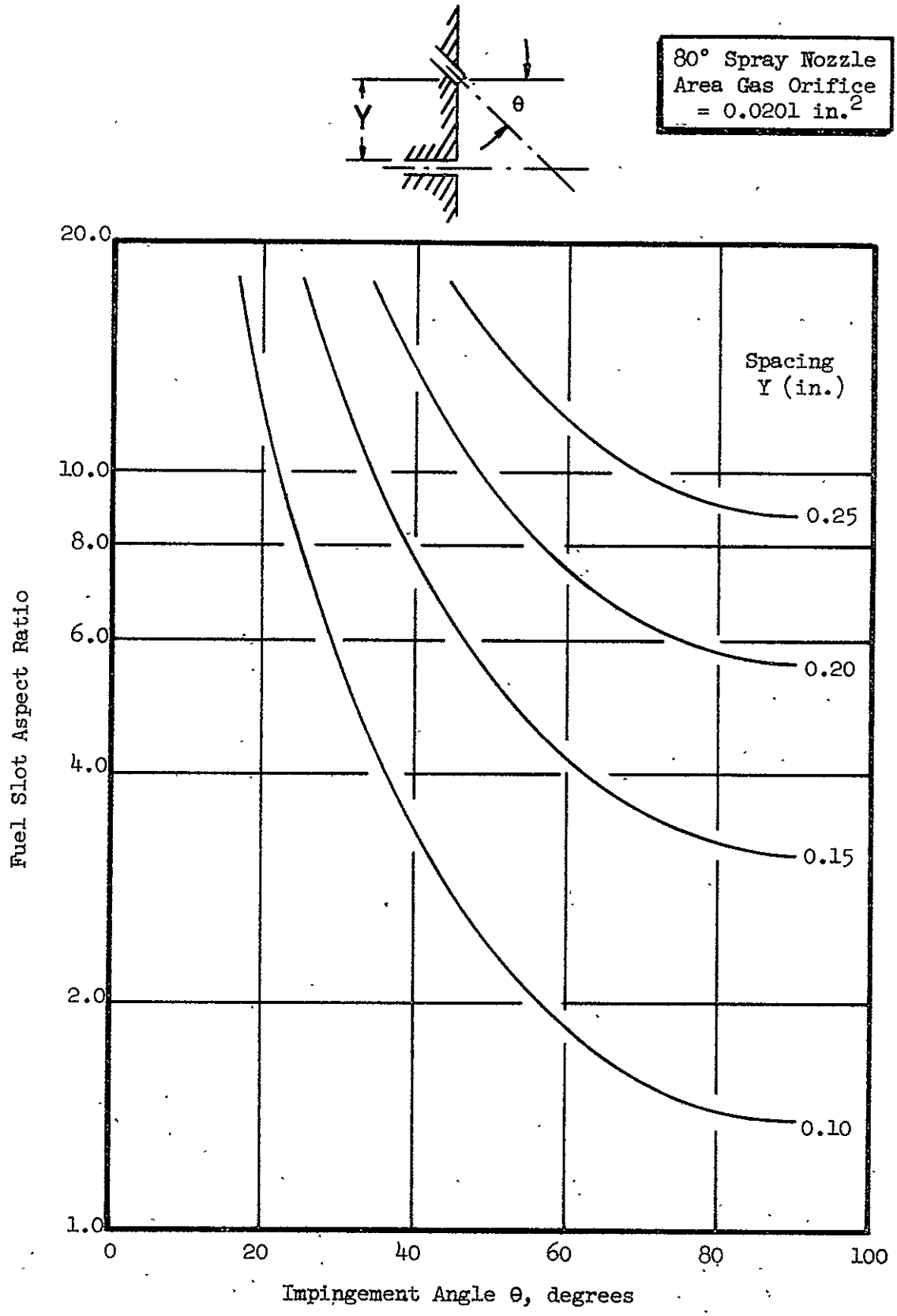

Figure 14. Fuel Slot Aspect Ratio for the Spray Fan Unlike Doublet as a Function of Spacing and Impingment Angle

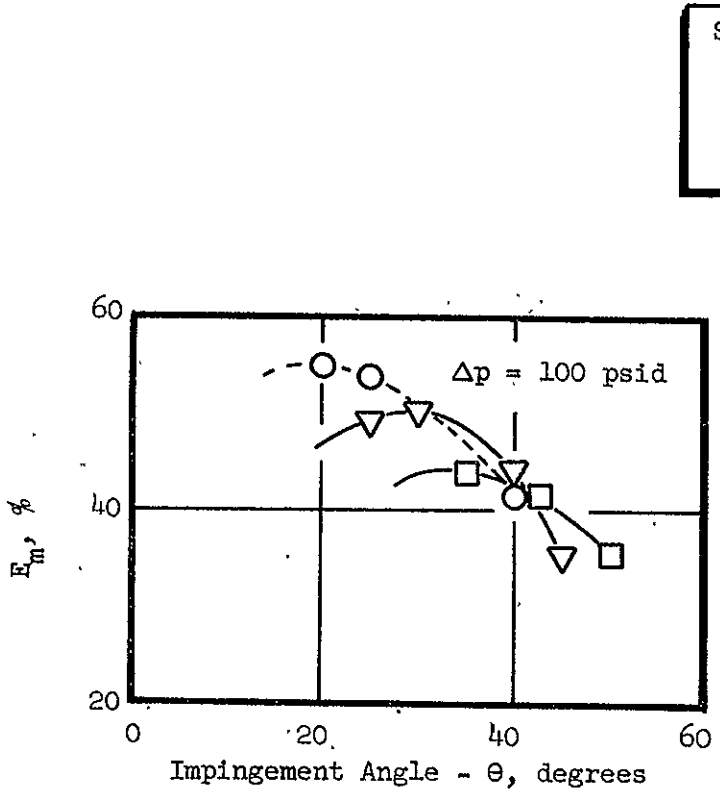

Figure 15. Mixing Uniformity, E_m, for the Spray Fan Doublet as a Function of Orifice Spacing and Impingement Angle

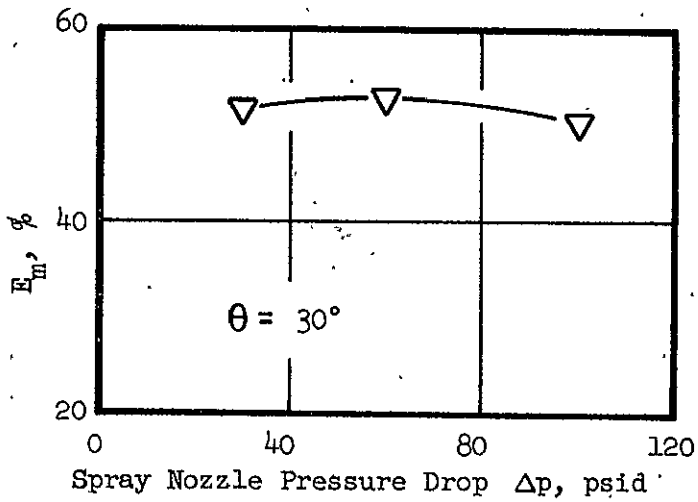

Figure 16. Mixing Uniformity, E_m, for the Fan Doublet as a Function of Spray Nozzle Pressure Drop

Conclusions which can be drawn from Fig. 15 are that E_m reaches a maximum value at a specific value of θ for fixed spacing and that these maximum values of E_m drop off with increased spacing.

It may be noted that the level of mixing uniformity is low for these elements even at the relative maximum points. This low level can be explained, on a physical basis, in the following way. The spray fans which are produced by the spray nozzles are composed of a very thin sheet of droplets of widely differing size. These droplets are all traveling with equal velocities. As they enter the gas jet, they are subjected to the aerodynamic forces which turn the droplets and subject them to secondary breakup. The larger droplets, due to their greater mass, travel farther into the gas jet than the smaller droplets. As a result, the large droplets over penetrate while the smaller droplets do not penetrate far enough. The ideal situation would be one in which the individual velocities of the various droplet size groups could be adjusted to produce exactly the penetration desired for each group. This, of course, is impossible, so the average penetration is adjusted to produce the relative optimum designs shown in Fig. 15.

Next, to investigate the effect of nozzle Δp or V_L on mixing, the spacing of Y = 0.15 inch was selected and Δp was varied from 30 to 100 psid. Results of this study are shown in Fig. 16. The effect of Δp is not pronounced. However, E_m does appear to maximize at a pressure drop very nearly equal to 60 psid. The spacing of 0.15 inch was selected rather than 0.10 inch due to the fact that small angles,

i.e., $\theta \leq 30°$ are required for the latter spacing. This, coupled with the spacing itself, would produce undesirable crowding of the manifolding and feed passages for the liquid and gas orifices.

Estimated secondary atomization results corresponding to the various possible design points represented in Figs. 15 and 16 indicated secondary, mass median droplet diameters between 10 and 20 microns. It would be expected, that for the hydrogen/oxygen propellant combination, the vaporization limited C* efficiencies would be 100% for all conditions. For this reason, detailed atomization results are not presented.

The mixing uniformity parameter, E_m, predicted for the doublet ($Y = 0.15$, $\theta = 30°$, $\Delta p = 60$ psid) is 52.7%, Fig. 16. A mixing limited C* efficiency between 80% and 85% would be expected for an E_m of this magnitude. Thus, the overall C* efficiency would be expected to fall between 80% and 85%. The relationship between E_m and η_{C*} is discussed in some detail in Appendix C.

Spray Fan Triplet. In order to reduce the scope of the analytical effort and to make the results of the analysis for the various configurations comparable, it was decided to limit the study of the triplet and four-on-one configurations to those with orifice spacing of 0.15 inch and nozzle pressure drop of 60 psid. Therefore, the only remaining design variable was the impingement angle, θ. Since the area of the fuel orifice is the

same as that for the doublet element, the relationship between the impingement angle, θ, and the fuel orifice aspect ratio is the same as that shown in Fig. 14.

The computer model was employed to generate the parametric study of E_m versus θ. These results are shown in Fig. 17. It may be noted that the maximum value of E_m of 88% is significantly higher than that for the doublet element which was near 50%. The maximum E_m occurs at approximately $\theta = 30°$ which is similar to the doublet curve. It is also evident from examination of Fig. 17 that the spray fan triplet element performance is highly sensitive to the value of θ.

For the hydrogen/oxygen combination, E_m values of 88% would produce C* efficiencies in excess of 98% (see Appendix C).

As was the case with the doublet element, the spray fan triplet produced predicted droplet diameters less than 20 μ suggesting that the performance of the element would be totally mixing limited.

Four-on-One Spray Fan. The same design limitations which were placed on the triplet element were also placed upon the four-on-one element, i.e., $\Delta p = 60$ psig, spacing Y = 0.15 inch, and the area of the fuel orifice equal to that of the spray fan doublet. The only difference between the triplet and four-on-one is that there are twice as many spray nozzles in the four-on-one, 2 on each side of the fuel orifice. Therefore, the

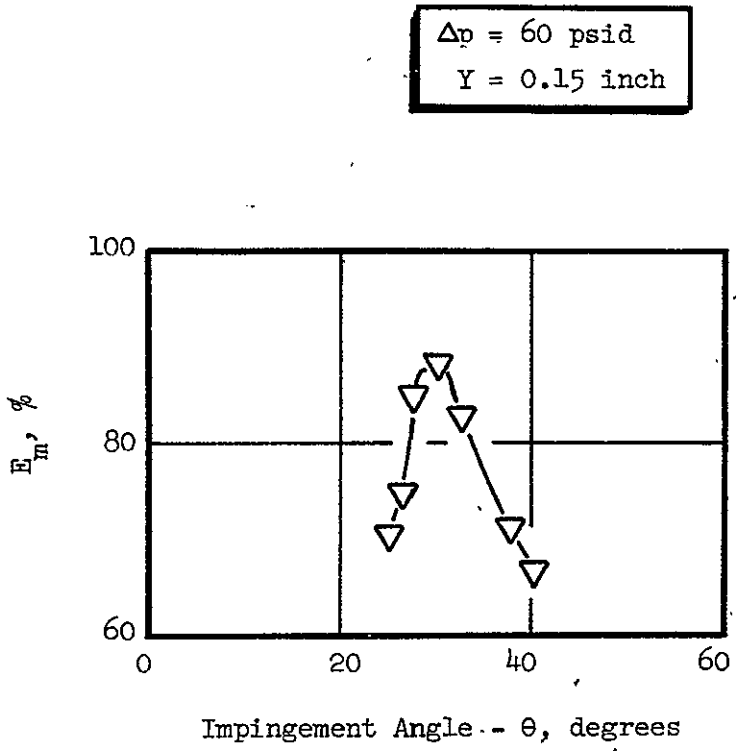

Figure 17. Mixing Uniformity, E_m, for the Spray Fan Triplet as a Function of Impingement Angle

relationship between the impingement angle and the fuel orifice aspect ratio is the same as that shown in Fig. 14 if the aspect ratio scale is multiplied by 2 (i.e., 2 triplets, side by side, with 1/2 the fuel area each).

Computer model results for the four-on-one element are shown in Fig. 18. Here, E_m is shown as a function of the impingement angle θ. The maximum value of E_m is approximately 86% and occurs at $\theta = 34°$. These results are similar to those of the triplet element ($E_m = 88\%$, $\theta = 30°$).

Droplet sizes for the four-on-one were similar to those of the doublet and triplet elements, indicating vaporization limited efficiencies of 100%.

Parametric Study of the Spray Fan Triplet. Evaluation of the results of the design analysis of spray fan elements points to the spray fan triplet as the outstanding representative for this class of elements. The triplet out-performs the doublet by a large margin and is far less complicated than the four-on-one, which it also out-performs. This element was, therefore, selected as a candidate for a parametric study of its mixing characteristics over ranges of chamber pressure and mixture ratio.

Before proceeding to the results of the parametric analysis, a typical output of the computer model for this selected triplet element will be shown as a matter of interest. Gas and liquid flow rate profiles and a

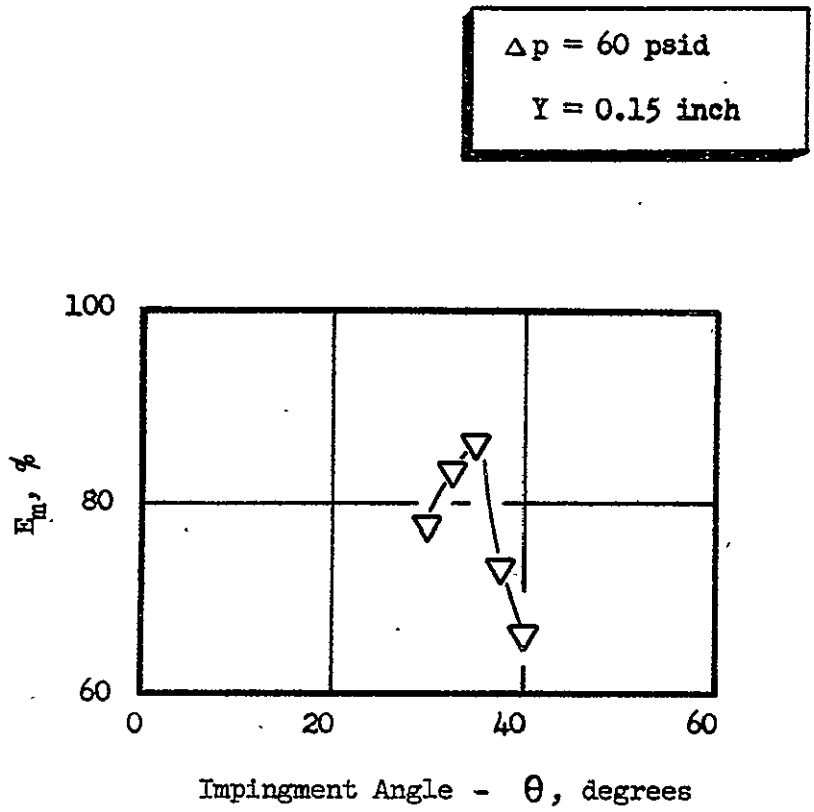

Figure 18. Mixing Uniformity, E_m, for the 4-on-1 Spray Fan Element as a Function of Impingment Angle

mixture ratio profile as produced by the computer model are shown in Fig. 19 for the triplet operating at the following conditions (P_c = 800 psia, MR = 6, Δp_{ox} = 60 psid, θ = 30°, and Y = 0.15 inch). It can be seen that the mixture ratio is low in the center and on the outer boundaries and goes through maximum values at intermediate distances. These results correspond to the relative maximum value of E_m of 88%. The highest mixture ratio is approximately 10 and the lowest is 4.

The parametric study was conducted over a range of mixture ratio values from 4 to 9 and chamber pressure values from 600 to 1000. Results of the analysis are shown in Fig. 20.

For both mixture ratio and chamber pressure variations, it is evident that the maximum value of E_m is achieved at the nominal conditions (i.e., P_c = 800 psia and MR = 6.0). For the mixture ratio survey, the total flow rate was fixed at 0.433 lbm/sec while for the chamber pressure survey, total flowrate was computed as a linear function of chamber pressure ($\dot{w}_T = KP_c$).

A parametric study of the dropsize characteristics of the spray fan elements was not included due to the fact that the estimated droplet diameters are expected to be small enough over practical operating ranges to produce vaporization limited efficiencies approaching 100%.

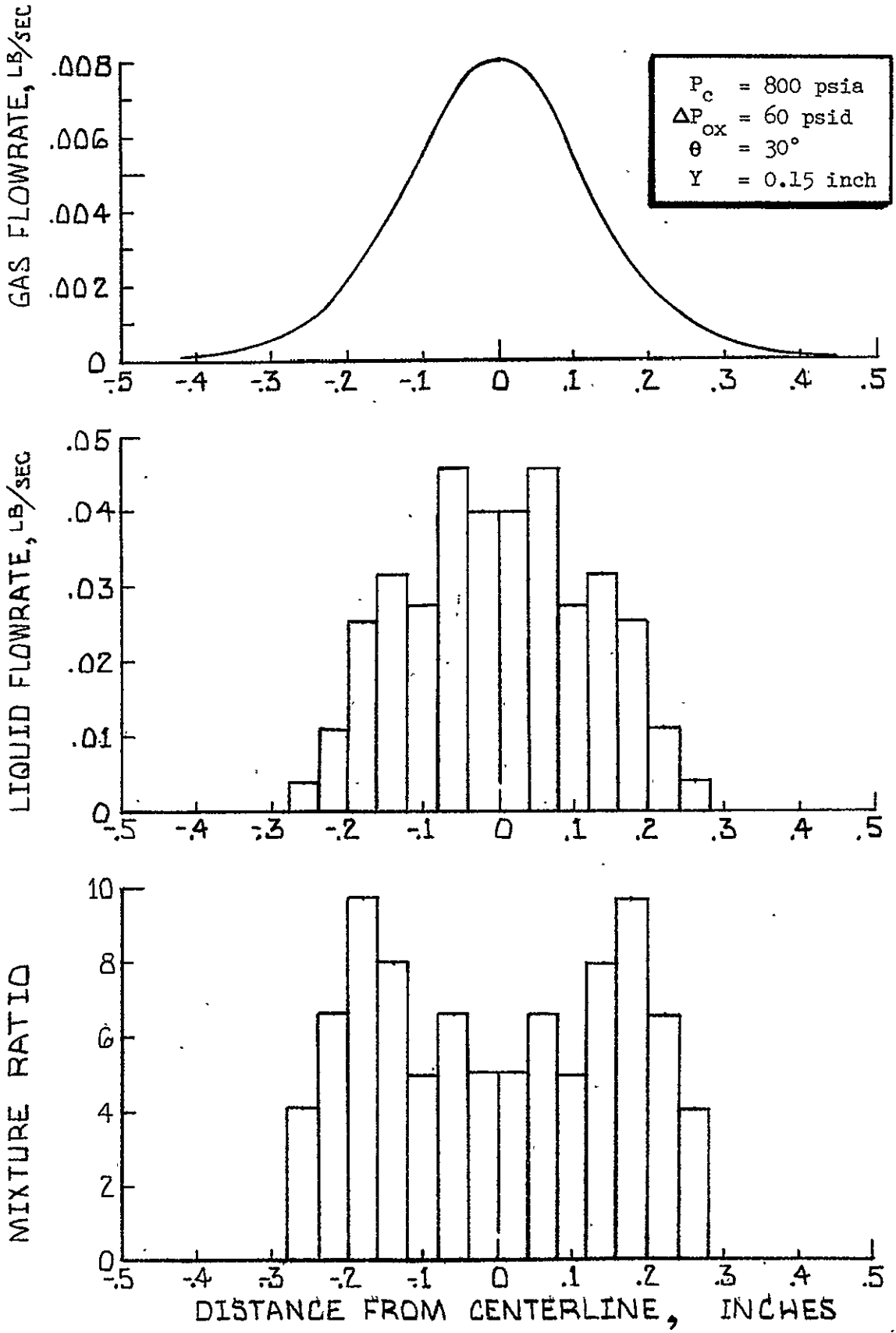

Figure 19. Gas Flow Rate, Liquid Flow Rate, and Mixture Ratio Profiles for the Spray Fan Triplet

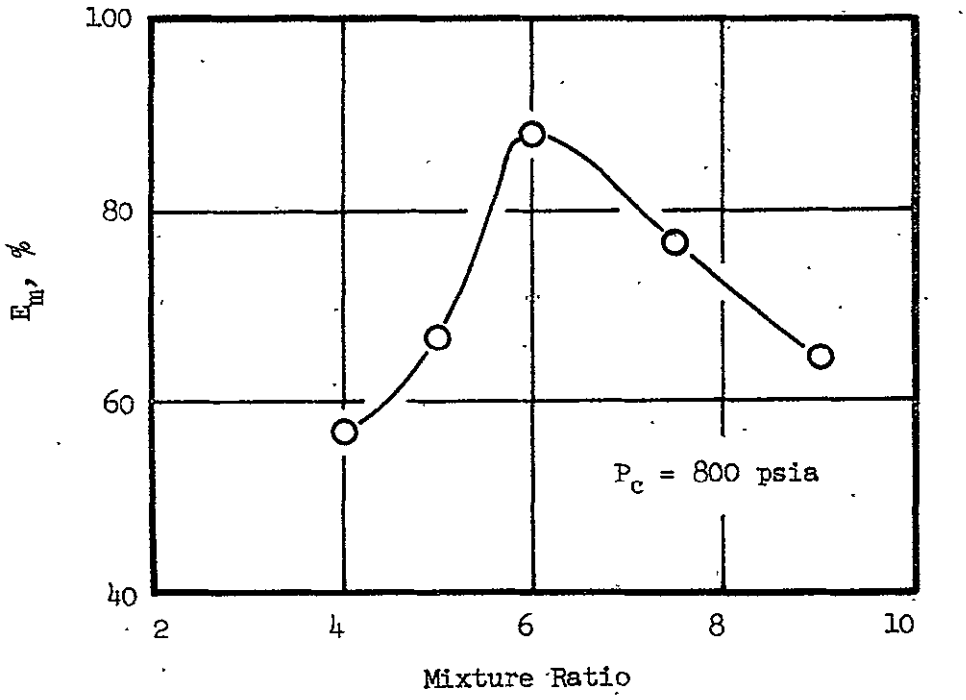

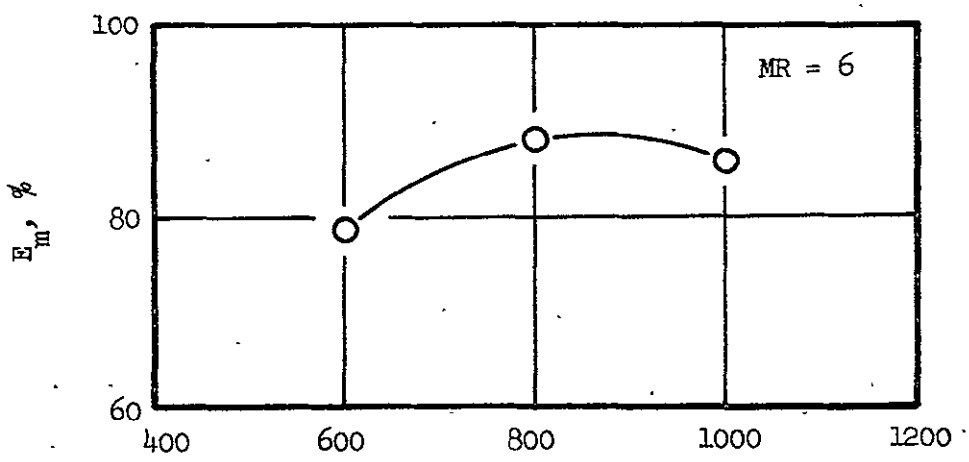

Figure 20. Mixing Uniformity, E_m, for the Spray Fan Triplet as a Function of Chamber Pressure and Mixture Ratio

3.2.3 Design of Impinging Jet Elements

Impinging jet element types considered in the design analysis study are shown in Table I. Only the unlike doublet and two versions of the four-on-one element were included as these were the circular element types for which gas/liquid mixing data were available at the time. The available data were obtained under Contract NAS3-12001, "Gas Augmented Injectors" for NASA, Lewis Research Center, Cleveland, Ohio (Ref. 3).

Mixing uniformity data for an unlike doublet and a four-on-one element are shown in Fig. 21. Here E_m is shown as a function of the penetration parameter defined in Eq. (40). Detailed analysis of these cold flow data and subsequent hot fire results suggested that X_p/S would be equal to 1.0 for unlike doublets and 0.8 for four-on-one elements. These values were selected for the design analysis of the present program.

The Unlike Doublet. The unlike doublet selected for design is composed of two rectangular orifices, one fuel and one oxidizer. For this design, the facing dimensions of the two orifices were assumed to be equal. A sketch of the element is shown in two views in Fig. 22, along with the nomenclature used in the various design equations.

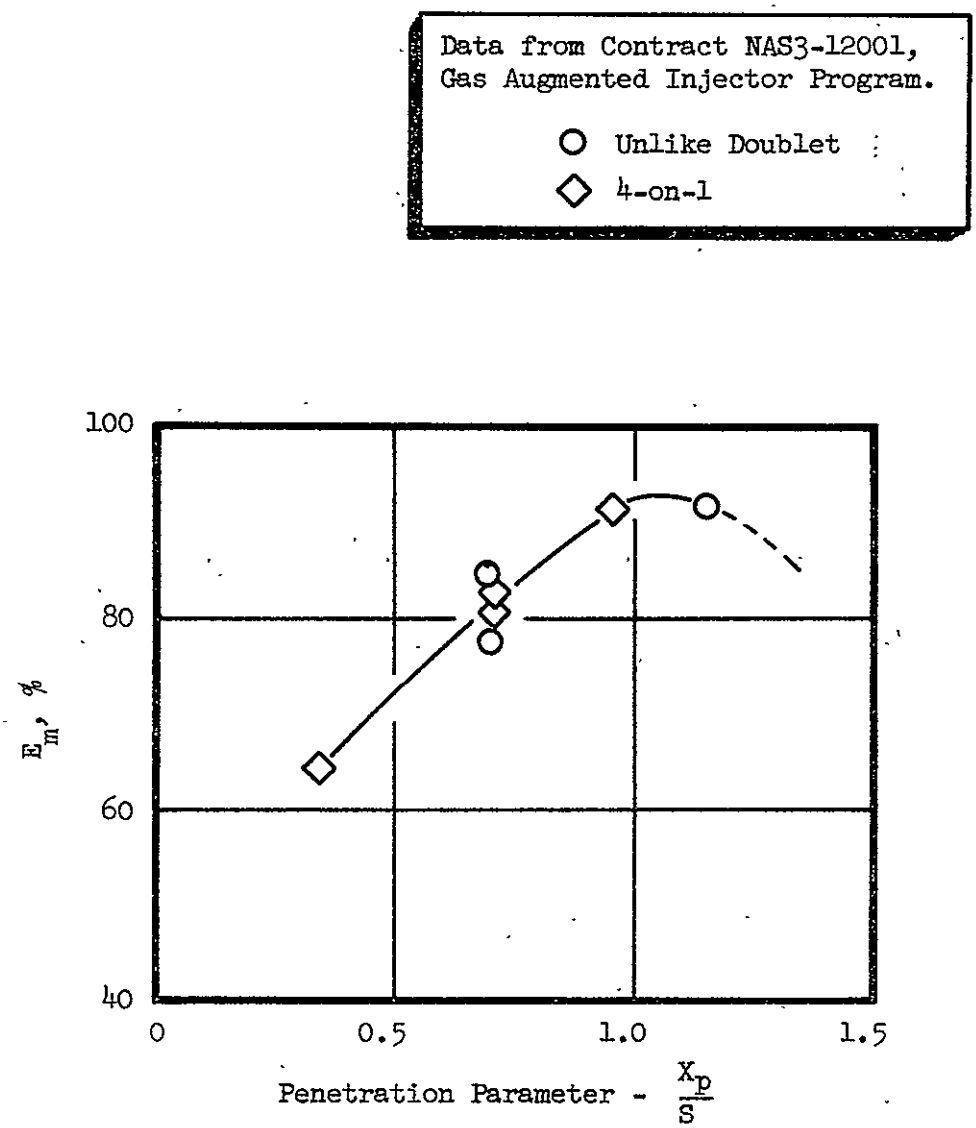

Figure 21. Mixing Uniformity, E_m, as a Function of the Penetration Parameter for an Unlike-Doublet Element and a 4-on-1 Element

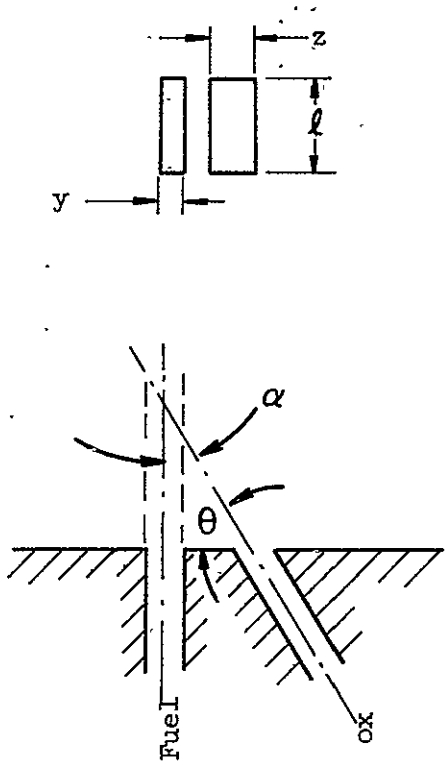

Figure 22. Geometry of the Noncircular Unlike Doublet

The design criterion used for this element is summarized in Eq. (50),

$$\frac{X_p}{y} = 1.0 \tag{50}$$

The design ground rules are those shown in Table VI. Those design variables which were independent and which were determined to define a specific design are: (1) the areas of the fuel and oxidizer orifices, (2) the aspect ratio of the fuel orifice (see Fig. 22), and (3) the impingement angle, θ. The aspect ratio of the oxidizer orifice was a dependent variable in this case due to the restriction that the facing dimensions of the two orifices be equal.

To begin the design, the penetration equation, Eq. (40), and the penetration criterion, Eq. (50) were combined. This step is shown below in Eq. (51) where y replaces dimensions in the original equation:

$$\frac{X_p}{y} = 1.0 = 2.5 \sqrt{\frac{\rho_L V_L^2}{\rho_g V_g^2}} \cos^2 \theta \tag{51}$$

Equation (51) was simplified in terms of the critical element dimensions, the element mixture ratio, and the density ratio of the propellants:

$$\frac{y}{z} = \frac{\sqrt{\frac{\rho_L}{\rho_g}}}{2.5 \text{ MR } \cos \theta} \tag{52}$$

where y, z = dimensions defined in Fig. 22

ρ_G = fuel or gas density

MR = $\dot{w}_{ox}/\dot{w}_{fuel}$

θ = impingement angle (Fig. 10).

ρ_L = oxidizer or liquid density

Substituting for the design conditions listed in Table VI, the following parametric values were defined:

$$\sqrt{\frac{\rho_L}{\rho_g}} = 15.27$$

$$MR = 6.0$$

Substitution of these parameters into Eq. (52) produced the desired design equation:

$$\frac{y}{z} = \frac{1.02}{\text{Cos } \theta} \tag{53}$$

Equation (53) defines the optimum area ratio of fuel to oxidizer required for any given impingement angle θ*.

At this point, in order to make the impinging jet element results comparable to the spray fan element result, the oxidizer pressure drop for this unlike doublet element was chosen to be equal to 60 psid.

With this assumption and the required element flow rate stated in Table VI, the area of the oxidizer was determined with the aid of the orifice flow equation:

$$\dot{w} = C_D \, A \sqrt{2_g \rho \, \Delta p} \tag{54}$$

* $\frac{y}{z} = \frac{y_\ell}{z_\ell} = \frac{A_{Fuel}}{A_{ox}}$

An orifice coefficient, C_D, equal to 0.70 was selected for the design. Solution of Eq. (54) in this case produced the following value for oxidizer orifice area

$$A_{ox} = 0.01223 = \ell z \tag{55}$$

Since, from Eq. (53):

$$\frac{y}{z} = \frac{\ell y}{\ell z} = \frac{1.02}{\text{Cos } \theta}$$

then, from Eq. (55),

$$\frac{\ell y}{0.01223} = \frac{1.02}{\text{Cos } \theta}$$

or:

$$\ell y = A_{fuel} = \frac{0.01247}{\text{Cos } \theta} \tag{56}$$

To insure the highest quality atomization, the velocity of the fuel was made as high as possible within the restrictions of the maximum allowable values of fuel Δp. The maximum allowable fuel pressure drop, from Table VI, is 130 psig. It was assumed that 50% of this Δp is converted into velocity head (i.e. $C_D \cong 0.7$), thus, with the assumption of incompressible flow

$$\frac{1}{2} \rho V_g^2 = C_D^2 \left(\Delta p_{fuel}\right)_{max} = (0.49)(130)$$

or

$$\frac{1}{2} \rho_g V_g^2 = 63.7 \text{ psi} \tag{57}$$

It was found from the solution of Eq. (57) that the maximum allowable gas velocity is V_g = 1400 ft/sec.

The area of the fuel orifice was determined from the continuity equation:

$$\ell y = A_{fuel} = \frac{\dot{w}_f}{\rho_f V_g} = \frac{0.0618}{0.3\ (1400)}\ (144) = 0.0212(\text{in.}^2) \qquad (58)$$

The impingement angle was determined from equating Eqs. (56) and (57):

$$0.0212 = \frac{0.01247}{\text{Cos } \theta}$$

or $\theta = 54°$ (59)

This is comparable to an included angle between the jets, α, equal to 36°.

Examination of Eqs. (53), (54), and (55) shows that there is no unique solution for the aspect ratio of the orifices (i.e., the specific relationship between the dimensions of the orifices) available from this theory. This is due to the fact that the relationship was derived from data obtained with circular orifices. Undoubtedly, the aspect ratios of the orifices will have an influence on the degree of mixing produced by the element. However, this effect could not be obtained from the analysis. Therefore, to complete the design and define the dimensions of the orifices, an aspect ratio of 4.0 was selected for the fuel orifice.

$$\frac{\ell}{y} = 4.0 \text{ assumed} \qquad (60)$$

A summary of the design variables for the unlike doublet element is presented in Table XII below.

TABLE XII
SUMMARY OF UNLIKE DOUBLET DESIGN DATA

Parameter	Value	Units
A_f	0.0212	Square inches
A_{ox}	0.01223	Square inches
ℓ	0.291	Inches
y	0.0728	Inches
z	0.042	Inches
V_g	1400	ft/sec
V_L	62.4	ft/sec
θ	54	Degrees
α	36	Degrees
ARF	4.0	--
$\dot{w}_{ox}$	0.371	lbm/sec
$\dot{w}_{fuel}$	0.0618	lbm/sec
Thrust/Element	200	lbf

Hopefully, with the added degree of freedom of aspect ratio, the noncircular unlike doublet could be optimized and made to outperform its circular counterpart. However, at this time, with no data available, it can only be assumed that the performance characteristics of the noncircular unlike doublet are at least as good as those shown in Fig. 21 for a circular doublet. In other words, the level of mixing uniformity that can be expected would be $E_m \geq 93\%$.

In the light of Eq. (50), an element of this form is desirable from the standpoint of design flexibility. The critical dimension for penetration is "y" in Eq. (50). With a noncircular orifice, this dimension can be varied independently with a fixed orifice area. This is not the case with a circular orifice whose penetration depth and area are directly related.

Droplet sizes for the unlike doublet were assumed to be smaller than 40 microns based upon the studies of Dickerson which were discussed previously. No formal calculation of dropsize was attempted.

Four-on-One Elements. In this preliminary design, two versions of the four-on-one element were investigated. Both incorporate a central fuel orifice in the form of a square. One element is composed of the fuel orifice surrounded by four oxidizer orifices in the form of equilateral triangles with sides equal in length to the side of the fuel orifice. The other element incorporates the same fuel orifice with rectangular oxidizer orifices with facing dimensions equal to the length of the sides of the fuel orifices. These elements are shown schematically in Fig. 23.

Triangular 4-on-1 Rectangular 4-on-1

Figure 23. Four-on-One Element Types

The design criterion which was used for the four-on-one elements is

$$\frac{X_p}{a} = 0.8 \tag{61}$$

where

a ≡ length of the sides of the fuel orifice.

Triangular Four-on-One. A sketch of the triangular, four-on-one element is shown below with appropriate nomenclature defined.

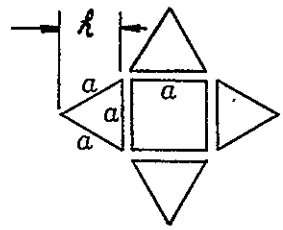

$$h = \sqrt{a^2 - a^2/4}$$

$$h = \frac{a}{2}\sqrt{3}$$

Figure 24. Triangular Four-on-One Element

The first step in the design was to combine the design criterion, Eq. (61) with the design Eq. (40).

$$\frac{X_p}{a} = 0.8 = 2.5 \sqrt{\frac{\rho_L V_L^2}{\rho_g V_g^2}} \quad \text{Cos}^2\ \theta \tag{62}$$

Equation (62) was simplified by the rearrangement of terms and is reproduced below in reduced form.

$$2.5\ (MR) \sqrt{\frac{\rho_G}{\rho_L}} \ \frac{\text{Cos}\ \theta}{\sqrt{3}} = 0.8 \tag{63}$$

It can be seen that Eq. (63) has only one solution and, thus, the angle θ is uniquely defined. Solution of Eq. (63) produced a value of 1.41 for the Cos θ. Unfortunately, this solution is not real and implies that no design of this configuration exists having the optimization constraints which were assigned. Physically, this means that even if the liquid jets were pointed directly normal to the gas jet, they would not have sufficient momentum to penetrate into the gas jet the distance required for optimum mixing. This configuration demonstrates the value of a preliminary analysis. The problem with the element is that the areas of the oxidizer orifices are dependent upon the area of the fuel orifice through purely geometrical limitations.

Rectangular Four-on-One. A four-on-one element configuration, which does not have the geometrical restrictions of the element discussed above, is pictured in Fig. 25.

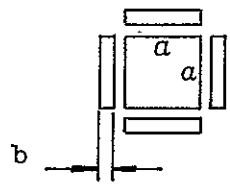

Figure 25. Rectangular Four-on-One

In this configuration, the oxidizer orifices are rectangular in shape with the length of their sides facing the fuel orifice equal to the length of the sides of the fuel orifice. With one side of the oxidizer orifices undefined, their area becomes geometrically independent.

The penetration equation, Eq. (40) was formulated for this element in the manner shown in Eq. (64):

$$\frac{X_p}{a} = 2.5\ MR \sqrt{\frac{\rho_g}{\rho_L}}\ \frac{A_g}{A_L}\ \cos\theta \tag{64}$$

where A_g = area of the fuel or gas orifice

A_L = total oxidizer or liquid area (4 orifices)

By the introduction of the geometrical relationships for areas and the penetration criterion, the following relationship was developed.

$$2.5\ MR\ \sqrt{\frac{\rho_g}{\rho_L}}\ \frac{ARO}{4}\ \cos\theta = 0.8 \tag{65}$$

where ARO = aspect ratio of an oxidizer orifice = a/b

Equation (65) was further reduced by substitution of the fixed operating parameters from Table VI:

$$\frac{a}{b} = ARO \cong \frac{2}{\cos\theta} \tag{66}$$

At this point, the restrictions placed upon the fuel velocity were introduced to size the fuel orifice. Once this was accomplished, the length of the sides "a" were determined. From Table VI, Δp_{fuel} = 130 psid. With an orifice discharge coefficient C_D = 0.7, this yields a maximum fuel velocity of 1400 ft/sec. Therefore, the area of the fuel orifice for this four-on-one element was the same as that of the unlike doublet element, see Table XII. With this area, 0.0212 $in.^2$ the lengths of the sides labeled "a" in Fig. 25 are equal to 0.1456 inch, and Eq. (66) becomes:

$$\text{Cos } \theta = 13.73\ b \tag{67}$$

To make this element comparable to the unlike-doublet element, the oxidizer Δp was assumed to be 60 psid. This, along with an oxidizer orifice coefficient of 0.7, made the total oxidizer area equal to that of the unlike doublet, 0.01223 $in.^2$. Therefore:

$$ab = 0.01223/4$$

$$\text{or} \qquad b = \frac{0.01223}{(4)\ 0.01456} = 0.021 \text{ inch}$$

and from Eq. (67)

$$\text{Cos } \theta = 0.289$$

$$\text{or} \qquad \theta = 73.2°$$

A summary of the rectangular, four-on-one design data is presented in Table XIII.

TABLE XIII
SUMMARY OF FOUR-ON-ONE ELEMENT DESIGN DATA

Parameter	Value	Units
A_f	0.0212	$in.^2$
A_{ox}	0.01223 ÷ 4	$in.^2$
a	0.1456	in.
b	0.021	in.
V_g	1400	ft/sec
V_L	62.4	ft/sec
θ	73.2	Degrees
α	16.8	Degrees
ARO	6.93	--
$\dot{w}_{ox}$	0.371	lbm/sec
$\dot{w}_{fuel}$	0.0618	lbm/sec
Thrust/Element	200	lb_f

As with the unlike-doublet element, the mixing uniformity parameter for this element should be $E_m \geq 93\%$ (see Fig. 21).

Parametric Study of the Unlike-Doublet Element. An estimate of the effect of engine throttling on the mixing uniformity of the unlike-doublet element was obtained through the analysis of the data shown in Fig. 21 with the penetration equation, Eq. (40).

$$\frac{X_p}{y} = 2.5 \cos\theta \frac{V_L}{V_g} \sqrt{\frac{\rho_L}{\rho_g}} \tag{40}$$

The optimum design for the unlike doublet was estimated by setting $\frac{X_p}{y}$ equal to 1.0. Values of $\frac{X_p}{y}$ at other pressures were estimated with Eq. (40) by describing the variation of the physical parameters in the equation with a simple engine model. The following functional relationships were assumed

$$\left.\begin{aligned} V_L &= K_1 P_c \\ V_g &= \text{const.} \\ \rho_L &= \text{const.} \\ \rho_g &= K_2 P_c \end{aligned}\right\} \text{ simplified engine model}$$

Equation (40) then becomes:

$$\frac{X_p}{y} = 2.5 \cos\theta \frac{K_1 P_c}{V_g} \sqrt{\frac{\rho_L}{K_2 P_c}} \tag{68}$$

The only variable on the right hand side of Eq. (68) is chamber pressure P_c. Therefore, Eq. (68) may be written:

$$\frac{X_p}{y} = K_3 \sqrt{P_c} \tag{69}$$

The constant, K_3 in Eq. (69) was obtained by recalling the boundary condition that $X_p/y = 1.0$ when $P_c = 800$. This condition yields:

$$K_3 = 0.0353 \text{ psi}^{-1/2} \tag{70}$$

Equation (69) then may be written:

$$\frac{X_p}{y} = 0.0353 \sqrt{P_c} \tag{71}$$

The mixing uniformity parameter, E_m, was estimated as a function of P_c by solving Eq. (71) for X_p/y and obtaining E_m as a function of X_p/y from Fig. 21. The results of this analysis are shown in Fig. 26.

A similar analysis was employed to determine the effect of mixture ratio variation on E_m at constant chamber pressure. The model equation for X_p/y in terms of mixture ratio is presented as Eq. (72).

$$\frac{X_p}{y} = \frac{MR}{6} \tag{72}$$

This relationship is presented graphically in Fig. 27. The mixing uniformity falls of rather steeply with mixture ratio above and below the maximum.

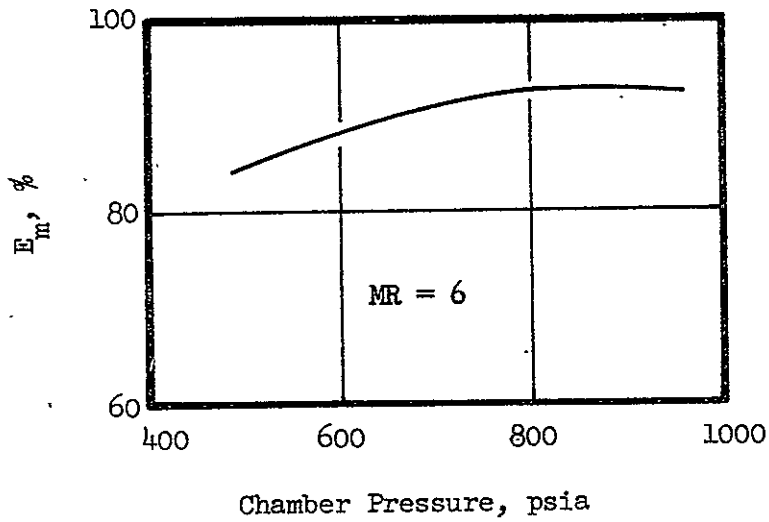

Figure 26. Estimated Mixing Uniformity, E_m, for the Unlike Doublet Element as a Function of Chamber Pressure

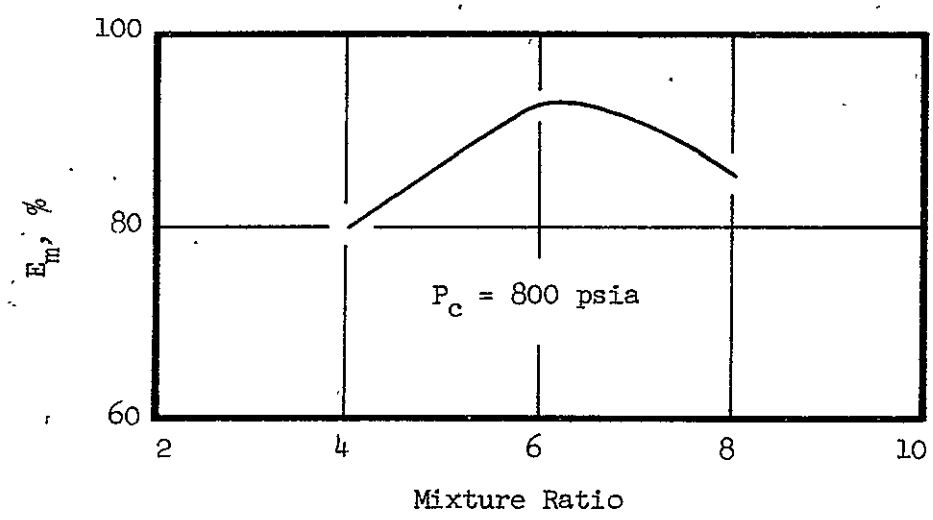

Figure 27. Estimated Mixing Uniformity, E_m, for the Unlike-Doublet Element as a Function of Mixture Ratio

A dropsize study was not included for the impinging jet elements as no droplet model was available to relate $\bar{D}$ to the operational parameters.

3.3 PRELIMINARY DESIGN SUMMARY AND EVALUATION

A summary of the design results for the elements studied thus far is presented in Table XIV and a summary of the estimated values of E_m for these elements is presented in Table XV. All elements were designed for the 200 lb_f thrust per element level with additional 130 lb_f thrust per element designs given for the concentric tube element types. For the self atomizing spray nozzles, the dimensions d_{ox}, given are equivalent diameters of circular orifices having the same Δp versus $\dot{w}$ characteristics.

TABLE XIV. PRELIMINARY DESIGN SUMMARY.

Thrust - 8000 lb_f $\quad \dot{w}_{ox} = 14.83$ lb/sec $\quad T_{ox} = 180°R \quad \rho_{ox} = 70$ lb/ft^3

P_c - 800 psia $\quad w_f = 2.47$ lb/sec $\quad T_f = 490°R \quad \rho_f = 0.3$ lb/ft^3

MR - 6.0

Element Type	Design Criterion	d_{ox}	ℓ_{ox}	A_{ox}	d_f	ℓ_f	A_f	α	T/E	ΔP_{ox}	ΔP_f	V_{ox}	V_f
Circular Concentric Tube	Maximum	.129		.0131	.2065		.0131	0	130	11.0	130	38	1500
	$\frac{4\ \Delta V}{d_{ox}\ MR}$	.160		.0201	.256		.0201	0	200	11.0	130	38	1500
Noncirc Concentric Tube	Maximum	.0466	.28	.0131	.1098	.343	.0131	0	130	11.0	130	38	1500
	$\frac{2(1+AR)\Delta V}{\ell_{ox}\ MR}$	.058	.346	.0201	.1365	.426	.0201	0	200	11.0	130	38	1500
Spray Fan Triplet	High E_m	.0791		.0049	.0396	.503	.0201	30	200	60.0	130	89	1500
Spray Fan Doublet	High E_m	.112		.0099	.0396	.503	.0201	30	200	60.0	130	89	1500
Spray Fan 4-on-1	High E_m	.059		.0027	.0324	.621	.0201	35	200	60.0	130	89	1500
Impinging Doublet	$\frac{X_p}{y} = 1.0$	.042	.291	.0122	.0728	.291	.0212	36	200	60.0	130	62.4	1400
4-on-1 Triangle ox	$\frac{X_p}{a} = .8$	NO OPTIMUM SOLUTION POSSIBLE											
4-on-1 Rectangle ox	$\frac{X_p}{a} = .8$	.021	.1456	.00306	.1456	.1456	.0212	16.8	200	60.0	130	62.4	1400

TABLE XV
ESTIMATED MIXING UNIFORMITY PARAMETERS
FOR PRELIMINARY ELEMENT DESIGNS

Element Type	Thrust per Element (lb_f)	E_m(%) (Estimated)	$\bar{D}$ (μ) (Estimated)
Circular Concentric	130	95.5 (calc.)*	37 (calc.)
Circular Concentric	200	91.8 (calc.)	45 (calc.)
Noncircular Concentric	130	99.3 (calc.)	13 (calc.)
Noncircular Concentric	200	98.3 (calc.)	16 (calc.)
Spray triplet	200	88.0 (calc.)	10 ~ 20 (est.)
Spray doublet	200	52.7 (calc.)	
Spray Four-on-One	200	86.0 (calc.)	
Jet Doublet	200	93.0 (est.)	< 40 (est.)
Jet Four-on-One	200	93.0 (est.)	

*(calc.) - Calculated from correlations or theoretical models.
(est.) - Estimated from data without direct correlation to noncircular configurations.

Results presented in Table XV suggested that the elements which offered the most promise were the noncircular concentric tube and the impinging jet-type elements. Of these candidates, the noncircular concentric tube appeared to offer the most advantages. In the first place, the level of mixing predicted was higher than that of the impinging types. Secondly, the throttling characteristics of the jet-type element shown in Fig. 26

showed the level of E_m to fall off with chamber pressure, while the performance factor for the concentric type elements (see Eq. (11)) was a very weak function of chamber pressure. Furthermore, the non-circular concentric tube predicted droplet sizes were comparable to those for the impinging type elements and smaller than those for the circular concentric tube element.

Based upon these conclusions, the noncircular concentric tube element was selected as the candidate element for experimental characterization in the remaining portion of the Phase II effort.

It must be stated that the conclusions drawn as to the throttling characteristics of the concentric tube elements were based upon data available at the time the preliminary analysis was conducted. Data obtained on other programs subsequent to the completion of this program suggest that gas density has a significant effect on mixing and that the value of E_m may depend on chamber pressure to a greater degree than predicted here.

4.0 COLD FLOW EXPERIMENTATION

4.1 DESIGN OF EXPERIMENTAL HARDWARE

The objective of the hardware design phase of this program was to design cold flow models of the circular and noncircular concentric tube element types with which the performance of each could be determined over ranges of the pertinent operational variables.

A primary ground rule for the design effort was that no one element type should receive an unfair advantage, a priori, due to the respective inherent quality of the design. This ground rule dictated the design restriction that the fuel and oxidizer areas of the two element types be equal in order to insure equality of propellant velocities at any given operating condition. At the outset of the program, it was generally held that the area of the elements which were most representative for calculation of the true velocities for interaction were the true physical area of the orifice in the oxidizer center post for the oxidizer and the annular area between the oxidizer area and the outer boundary of the element for the fuel, or the "diffused" area (not the area between the fuel boundary and the outside of the oxidizer post). The nomenclature is clarified in the sketch below for a circular concentric tube.

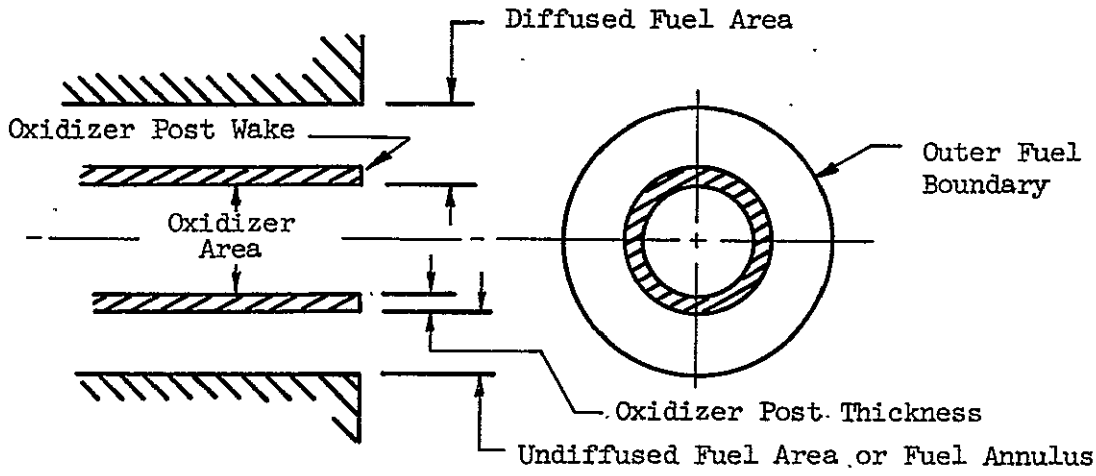

Figure 28. Concentric Tube Geometry Nomenclature

This fuel area was termed the "diffused" fuel area due to the fact that it was believed that the fuel would rapidly move over to the oxidizer jet upon leaving the fuel annulus and, thus, increase the fuel flow area by the area of the wake of the oxidizer post wall. For subsonic fuel velocities in the fuel annulus, this would constitute a deceleration of the gas, or a diffusion into this annular area.

Design of the two element types was predicated upon these assumptions and the oxidizer injection area, the "diffused" fuel injection areas and the oxidizer post thicknesses of the two elements were equated, respectively.

It should be noted at this point that subsequent experimental observation suggested that the representative fuel area is actually the fuel annulus area and not the "diffused" fuel area. The data were reduced and correlated

based upon these observations. Therefore, the noncircular concentric tube element produced "higher" fuel velocities at a given operating condition than the circular concentric tube. To overcome this inherent "advantage", the data were correlated based upon individual fuel and oxidizer velocities and performances were compared at equivalent velocities.

Selection of the actual magnitudes for the areas which have been discussed was based upon practical experimental considerations. It will be recalled that the preliminary design of element types was based upon ground rules supplied by the operational requirements of the conceptual Orbit Maneuvering Engine Injector (see Table VI). The designs that were developed for the concentric tube element types (see Tables XIV and XV) called for fuel velocities of 1500 ft/sec and produced estimated values of mixing uniformity in excess of 90% ($\eta_{c^*_{mix}} \cong 99\%$) at the 200 lb_f thrust per element level. This velocity was deemed to be too high for the purposes of this preliminary experimental effort for two reasons. In the first place, it was thought that the levels of mixing uniformity which would be produced at these operating conditions would be so high that comparison of the performance of the two element types would be difficult. Secondly, the gas which was to be used as a fuel simulant was nitrogen and due to the high molecular weight of this gas, 1500 ft/sec is a supersonic velocity. Helium could have been used, however, it is costly and requires operation of the test facility at elevated back pressures in order to match hot firing gas density. This was not feasible at the time.

To avoid these problem areas, the fuel areas of the elements were sized to provide subsonic fuel annulus velocities for the fuel simulant at the nominal levels of fuel flow rate. The nominal values for fuel and oxidizer flow rates were taken to be those listed in Table VI for a 40 element injector (i.e., 200 lb_f thrust per element). The oxidizer areas of the two element models were designed to be equal to those areas selected in the preliminary design or 0.0201 $in.^2$ (see Table VIII). A value of 560 ft/sec was selected for the diffused fuel velocity which dictated diffused fuel areas of 0.0529 $in.^2$ for both elements. An aspect ratio of 6.0 was selected for the oxidizer orifice of the noncircular concentric tube element based upon design and structure considerations as discussed briefly in the preliminary design section. To complete the design specifications, a wall thickness of 0.020 inch was selected for the oxidizer center posts of both element types. A summary of these design data is presented in Table XVI. Sketches of the elements are presented in Fig. 29 and photographs of the finished pieces are shown in Figs. 30 and 31.

TABLE XVI
SUMMARY OF DESIGN DATA FOR THE COLD FLOW MODEL HARDWARE

	Oxidizer area	Diffused fuel area	Fuel annulus area	Post wall thickness
Circular concentric tube	0.0201	0.0529	0.0426	0.020
Noncircular concentric tube	0.0201	0.0529	0.0352	0.020

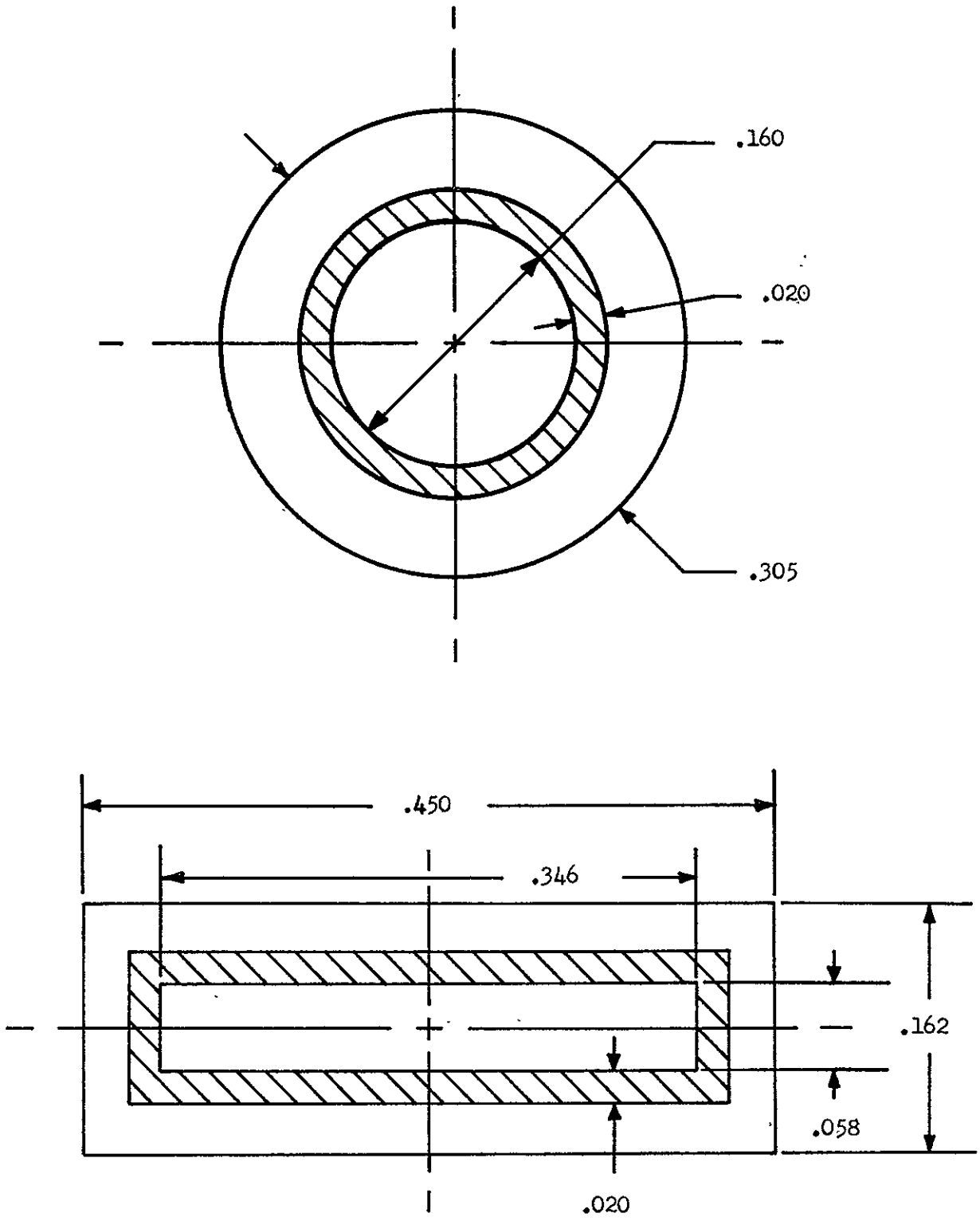

Figure 29. Sketches of Circular and Noncircular Concentric Tube Designs

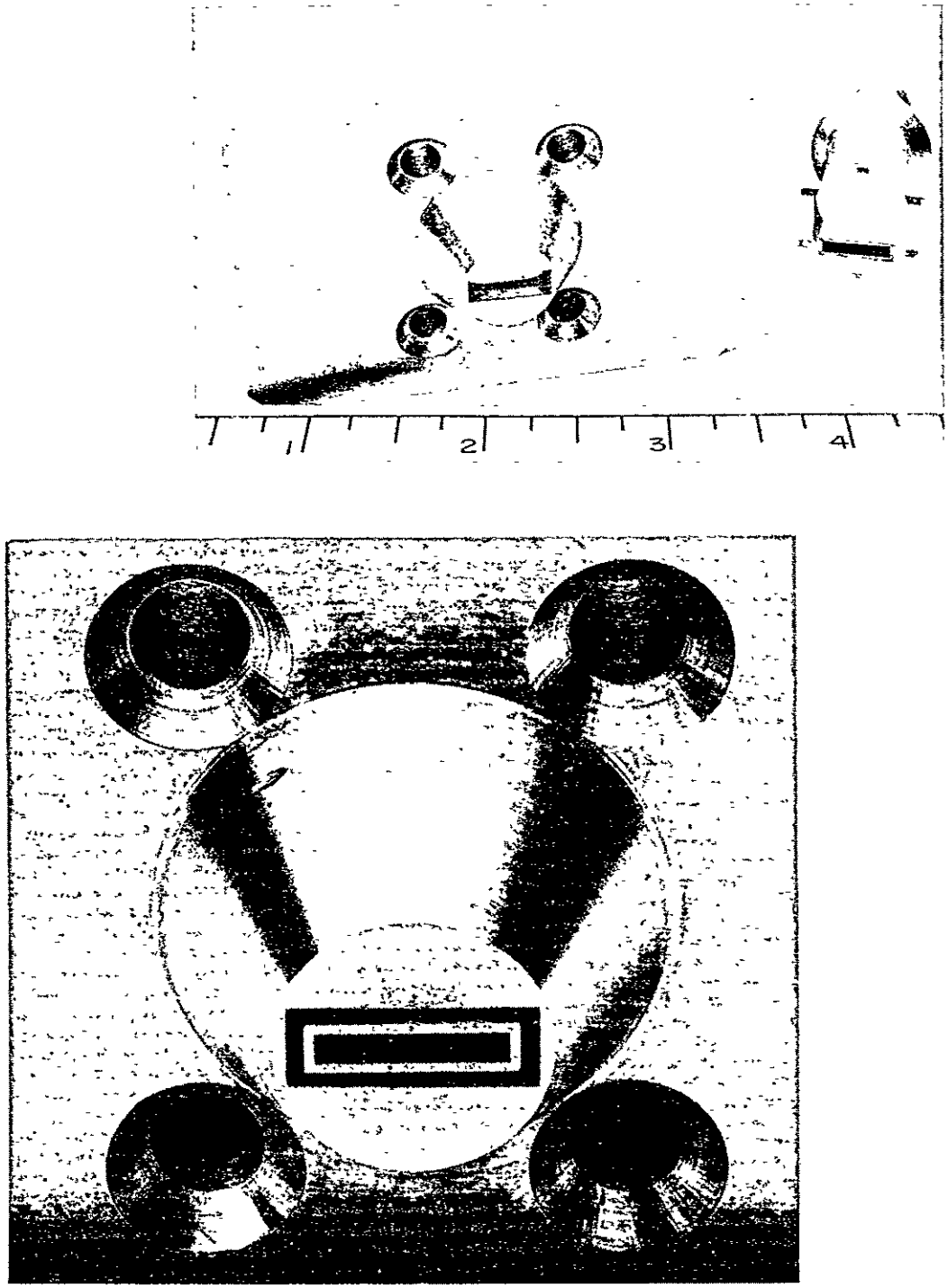

Figure 30. Noncircular Concentric Tube Element Hardware

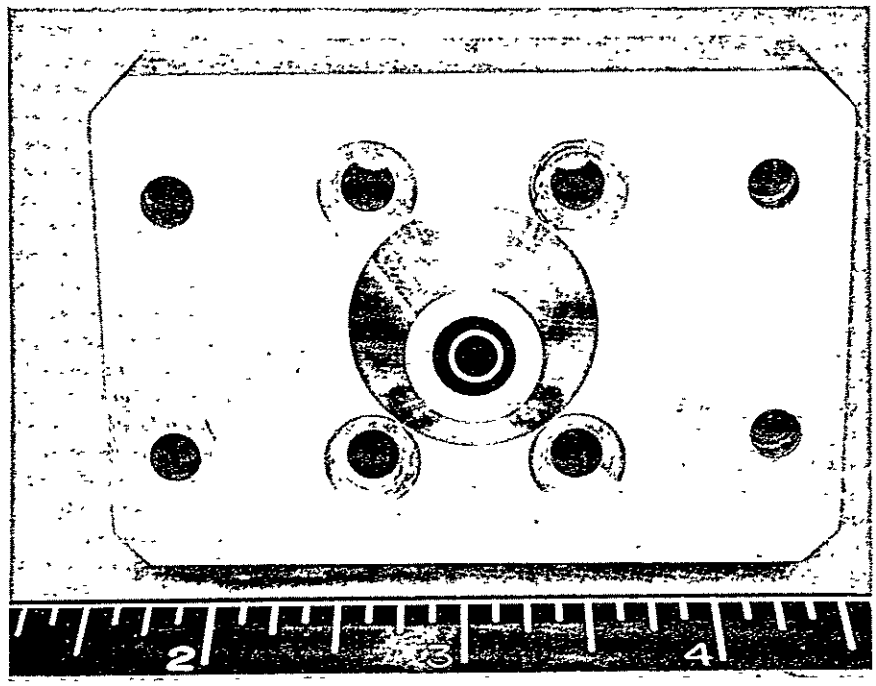

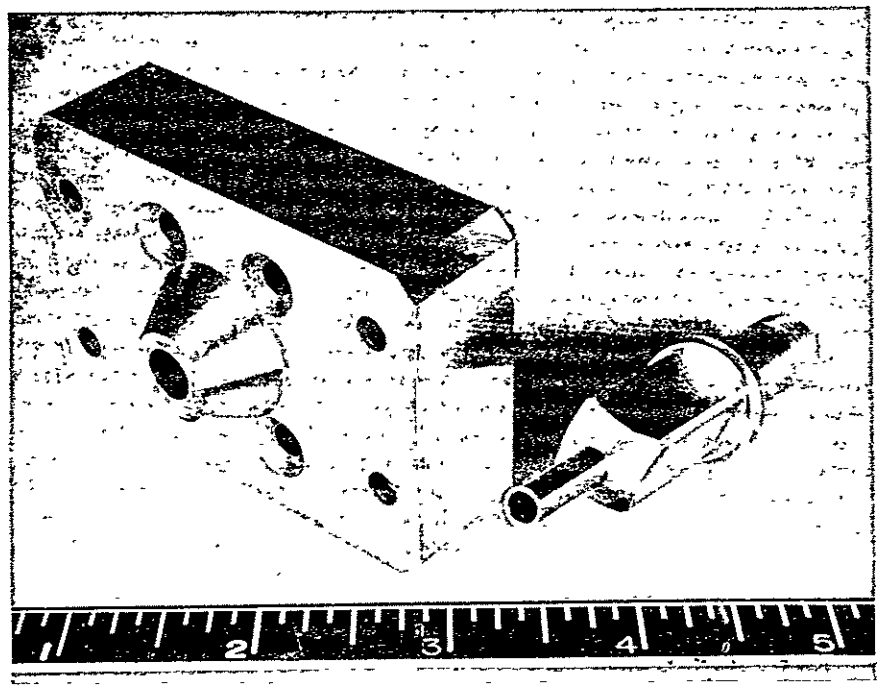

Figure 31. Circular Concentric Tube Element Hardware

A design variable of interest for concentric tube elements is the depth to which the oxidizer post is recessed beneath the injector face. The cold flow models were designed to accommodate post recess depths varying between zero recess (or flush post) and one oxidizer orifice diameter (or the smaller orifice inside dimension in the case of the noncircular element).

4.2 COLD FLOW TESTING

In the initial stages of the design of the experimental phase of this program, it was decided to test the models in the open atmosphere rather than under backpressure. This decision was prompted by two considerations. Rocketdyne's pressurized atomization facility had not been completed at the time and even though it would have been possible to run pressurized mixing tests, it would not have been possible to run pressurized atomization tests. It was, therefore, decided to run only atmospheric tests so that the mixing and atomization data would be taken under comparable conditions. Secondly, more mixing tests could be run within a given time period in the open air and thus a cost saving would be effected. This was attractive from the standpoint that these initial data were to be of a preliminary nature and a greater quantity of data would be more desirable than fewer data points at exact modeling conditions.

Operation of these elements at atmospheric pressure with gaseous nitrogen as a fuel simulant, modeled the operation of the elements at a chamber pressure of 200 psia with gaseous hydrogen based on injected gas density.

This level of operation was selected for the theoretical comparison of the performance values of the two element types.

Values of the various operating parameters which were employed in cold flow experimentation are summarized in Table XVII.

TABLE XVII
COLD FLOW TEST MATRIX (APPLICABLE TO BOTH MIXING AND ATOMIZATION TESTING)

Variable	Values or Ranges
Backpressure	13.8 psia
Mixture Ratio	3 and 6
Liquid Velocity	2.5 to 27 ft/sec
Gas Velocity	370 to 1100 ft/sec
Post Recess	0 and 1 liquid post diam.

Results which are to be presented in the following sections are displayed in graphical form for convenience, detailed test data may be found tabulated in Appendix A.

4.2.1 Atomization Results and Discussion

The mass median droplet diameter was employed to characterize the results of the atomization experiments. The data are presented in Fig. 32. Results for the elements at mixture ratios of 3 and 6 with post recess of zero and one liquid diameter are shown. Data for mixture ratio of

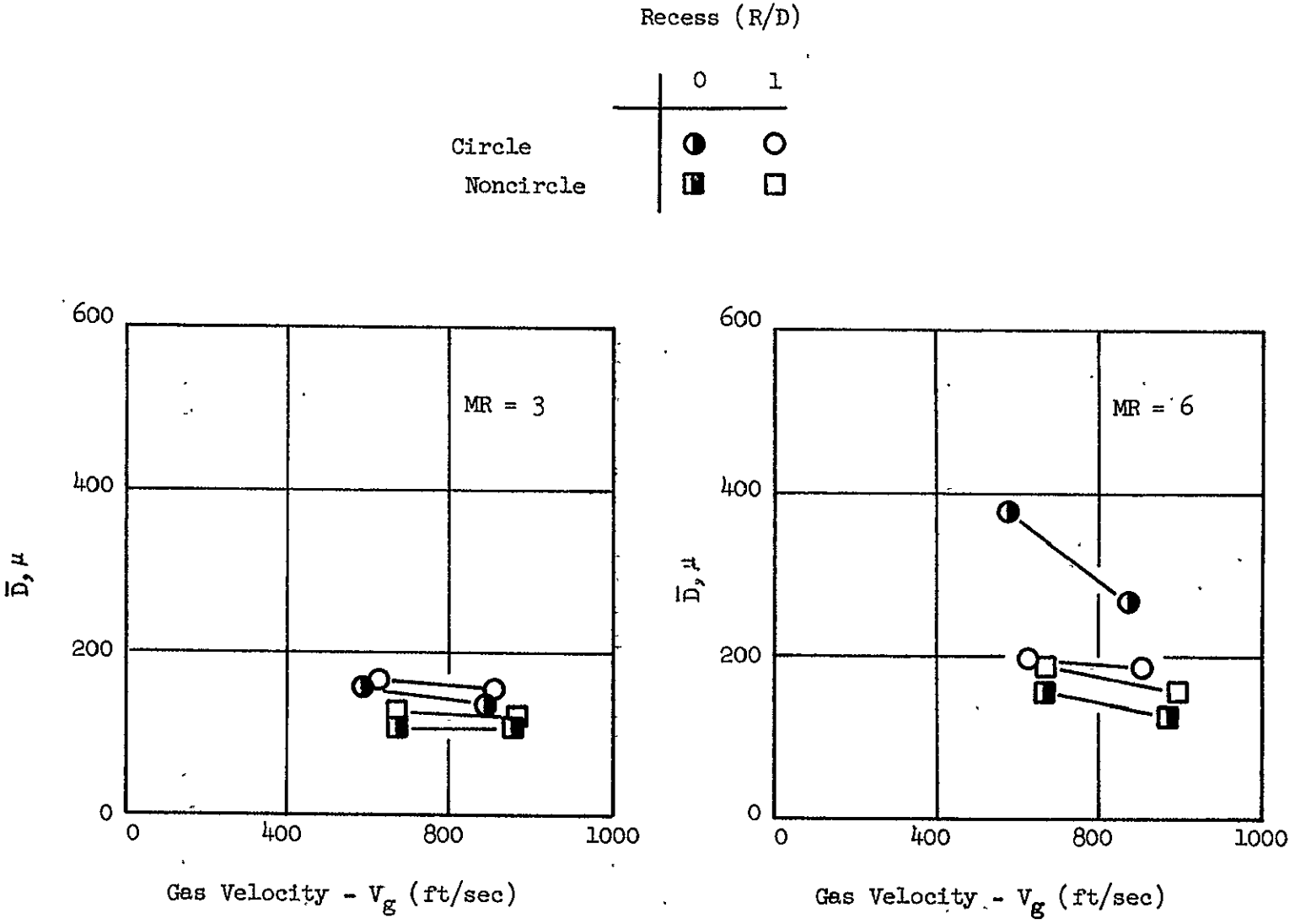

Figure 32. Atomization Test Results

3 are found in the left hand graph and data for mixture ratio of 6 are found in the right hand graph.

At a liquid to gas mixture ratio of 3, the atomization characteristics of the two elements are similar. The noncircular element produces droplets which are typically 20 to 50 microns smaller than those produced by the circular element. Differences of this magnitude are significant, however, when viewed in the light of the C* efficiency which can be achieved in a rocket combustor of given length. Comparisons of this nature will be made later in this document in the performance analysis section. The effect of oxidizer post recess on droplet diameters is slight at mixture ratio 3 for both elements. If anything, the droplets appear to get larger with recess. However, this conclusion is not substantiated by these data owing to the small percentage difference in the magnitude of the drop sizes. Differences of this magnitude can be attributable to basic experimental uncertainty.

Unlike the results at mixture ratio 3, the differences in droplet diameters for the two elements are quite pronounced at mixture ratio 6 for zero recess. The noncircular element produces droplets which are anywhere from 140 to 200 microns smaller than those of the circular element. Here, at mixture ratio 6, the effect of post recess is clear. Post recess greatly reduces the drop sizes of the circular element while producing a slight increase in size for the noncircular element. The droplet diameters for the two elements are similar with post recess of one diameter.

The general trend in the data is for drop size to decrease with increasing gas velocity. Another trend which is evident from the data is that median drop size increases with mixture ratio for both elements at all operating conditions at fixed values of post recess. At a mixture ratio of 6, post recess reduces the sensitivity of the circular element. With a post recess of one diameter, the droplet diameter is nearly constant over a wide range of gas velocity. In the flush post configuration, the non-circular element is less sensitive to gas velocity than the circular element. With the exception of the circular concentric tube element with flush center post, all droplet sizes produced by both elements fall between 100 and 200 microns.

Certain atomization tests which were conducted are not represented in the data shown in Fig. 32. There are two reasons for this. First, droplet samples taken with mixture ratios greater than 6 could not be analyzed due to the presence of "flakes" which were produced by large particles of molten wax striking the collecting surface. However, data from these tests would have been merely of academic interest due to the fact that the droplet sizes would have been much too large for consideration in practical rocket engines. Second, data from tests which were conducted with gas velocities close to the speed of sound were eliminated due to possible choking in the gas annulus.

The drop size data presented in Fig. 32 show that the noncircular concentric tube element has a distinct advantage over the circular element in the area of propellant atomization. This advantage is shown more

clearly in Fig. 33 wherein the drop sizes produced by the noncircular element are plotted versus those produced by the circular element at equivalent operating conditions. The data are for the zero post recess configurations. The lines which are drawn on the figure represent percentages by which the circular element droplet sizes exceed those of the noncircular element. Over the ranges of variables tested, the droplets produced by the circular element are 20% to 160% larger than the droplets from the noncircular element. The noncircular element appears to provide its greatest advantage at the higher mixture ratios.

The comparison presented in Fig. 33 shows the atomization characteristics of the two elements in the flush post or zero recess configuration. However, the characteristics of the two elements are quite similar when operating in the recessed configurations. In this recessed condition, the noncircular element still demonstrates a slight advantage in drop size. The selection of the recess depth for the noncircular element was based on the assumption that the characteristic dimension of the liquid orifice was it's minimum dimension, 0.058 inch in this case (see Fig. 29). The center post of this element was, therefore, recessed a distance equal to 0.058 inch, or one characteristic length. On the other hand, the characteristic length for the circular element was assumed to be the diameter of the circular liquid orifice, or 0.160 inch (see Fig. 29). The recess depth of one characteristic length for the circular element was, therefore, equal to 0.160 inch. Based upon these assumptions, the recess depth for the circular element was actually three times that of the noncircular

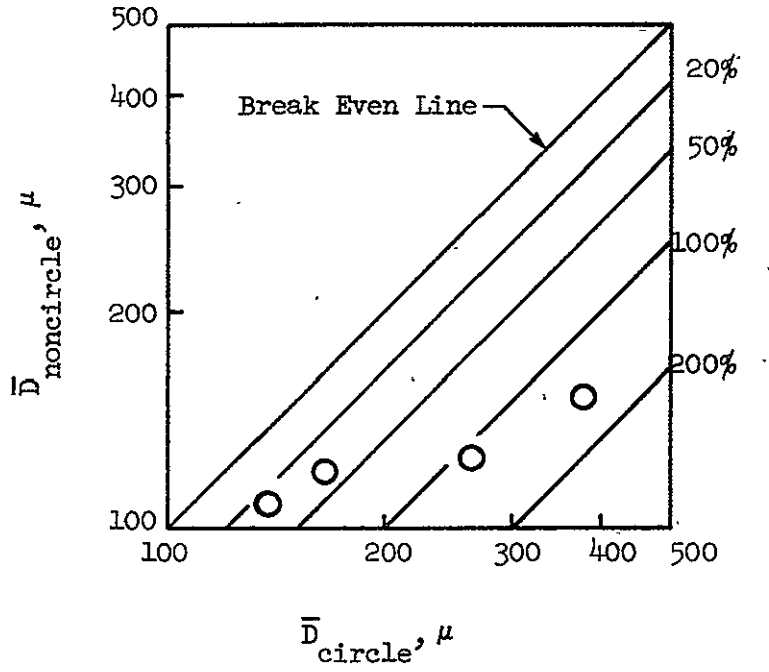

Figure 33. Comparison of Drop Sizes from Circular and Noncircular Concentric Tube Elements

element. As a result, the circular element may have received an unfair advantage in the comparison of performance in the recessed configuration.

4.2.2 Correlation of Atomization Results

Thus far, the atomization results have been presented in physical coordinates. It is appropriate now to compare these results with the original estimates of drop size which were made in the preliminary analysis section of this report in terms of correlating parameters.

The correlating parameters for dropsize which were employed in the preliminary analysis are $\bar{D}/D_L$ and $\Delta V/MR$. For the purposes of this analysis, functional relationships between these parameters were assumed for both the circular and noncircular concentric tube elements. These relationships are expressed in Eqs. (6) and (22).

Median droplet diameter data obtained with the circular concentric tube element are plotted in Fig. 34 along with the Ref. 3 data used to develop the correlations which were employed in the preliminary analysis. These data are presented in $\bar{D}/D_L$ versus $\Delta V/MR$ coordinates. The curves which appear in Fig. 34 are graphical representations of Eq. (6) for both zero and one post diameter recess.

It is evident from examination of Fig. 34 that the data from the current program do not fit the curves generated to extrapolate the Ref. 3 data to these operating conditions. However, the new data do graphically correlate satisfactorily with the Ref. 3 data in this coordinate system. The drop

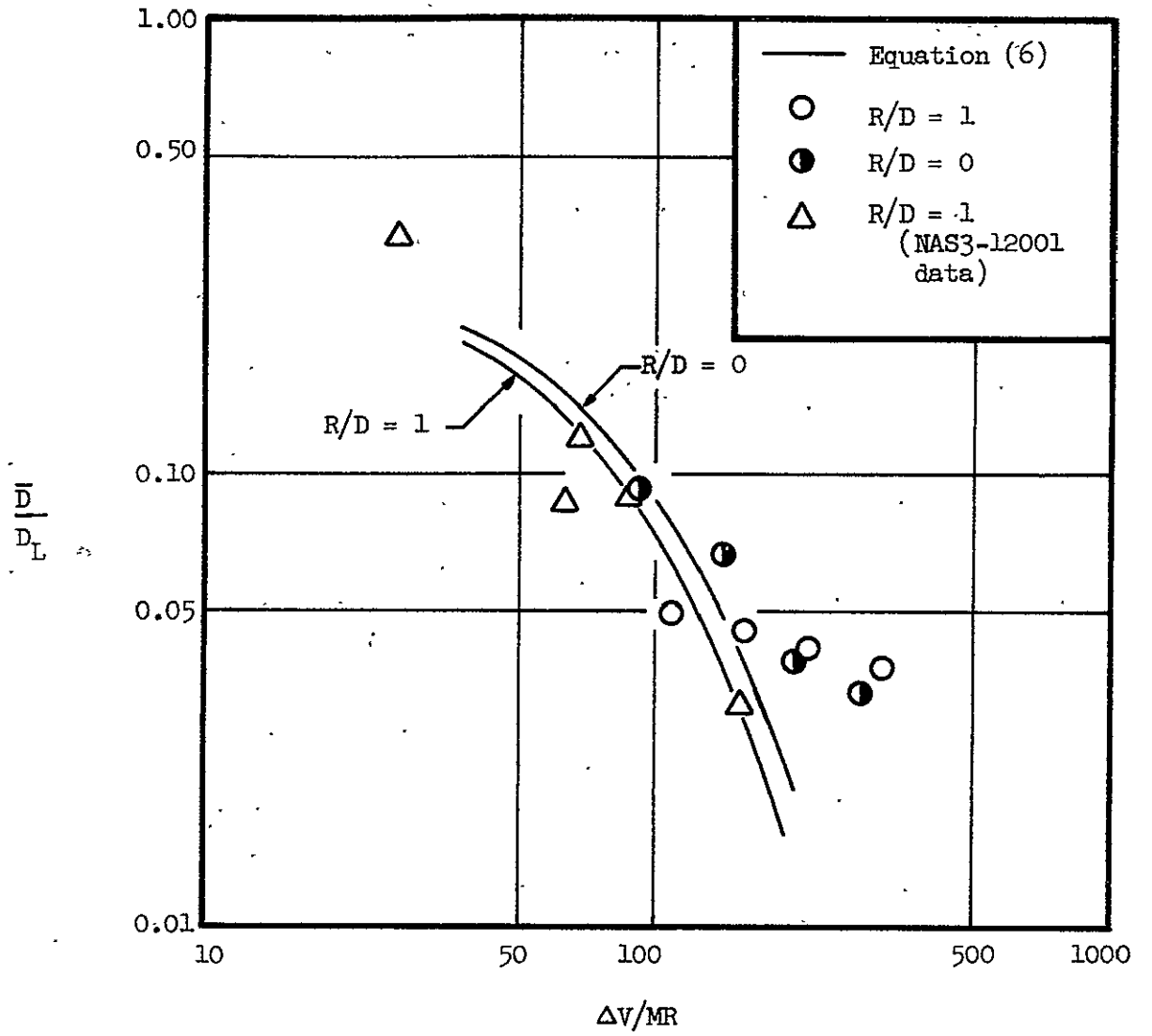

Figure 34. Correlation of Circular Concentric Tube Element Atomization Data

sizes for any one recess condition fall on curves which have the same general trends as the original functions. The decline in $\bar{D}/D_L$ with increasing $\Delta V/MR$ is simply slower than previously projected for $\Delta V/MR$ in excess of 100 ft/sec.

Droplet data obtained with the noncircular concentric tube element are shown in Fig. 35 in the same coordinates used for Fig. 34. However, in this case the droplet diameters are normalized with respect to the smaller dimension of the element liquid post, "b" (see Eq. 22). A curve generated by Eq. (22) is also shown in Fig. 35. Here again, as with the circular element results, the data do not follow the curve, yet the coordinates do provide an acceptable correlation.

For the noncircular element the droplet sizes are larger for the case with post recess. This trend was unexpected in the light of the preliminary analysis.

The model represented by Eq. 22 was developed with the assumption that the characteristic dimension of the noncircular element for atomization was the smaller dimension of the liquid port. However, the results shown in Fig. 35 show that the drop sizes obtained were substantially larger than predicted. This suggests that the true characteristic dimension for these elements is larger than that which was assumed.

The droplet data for the circular and noncircular elements are replotted and compared on the basis of absolute median drop size (i.e. not normalized

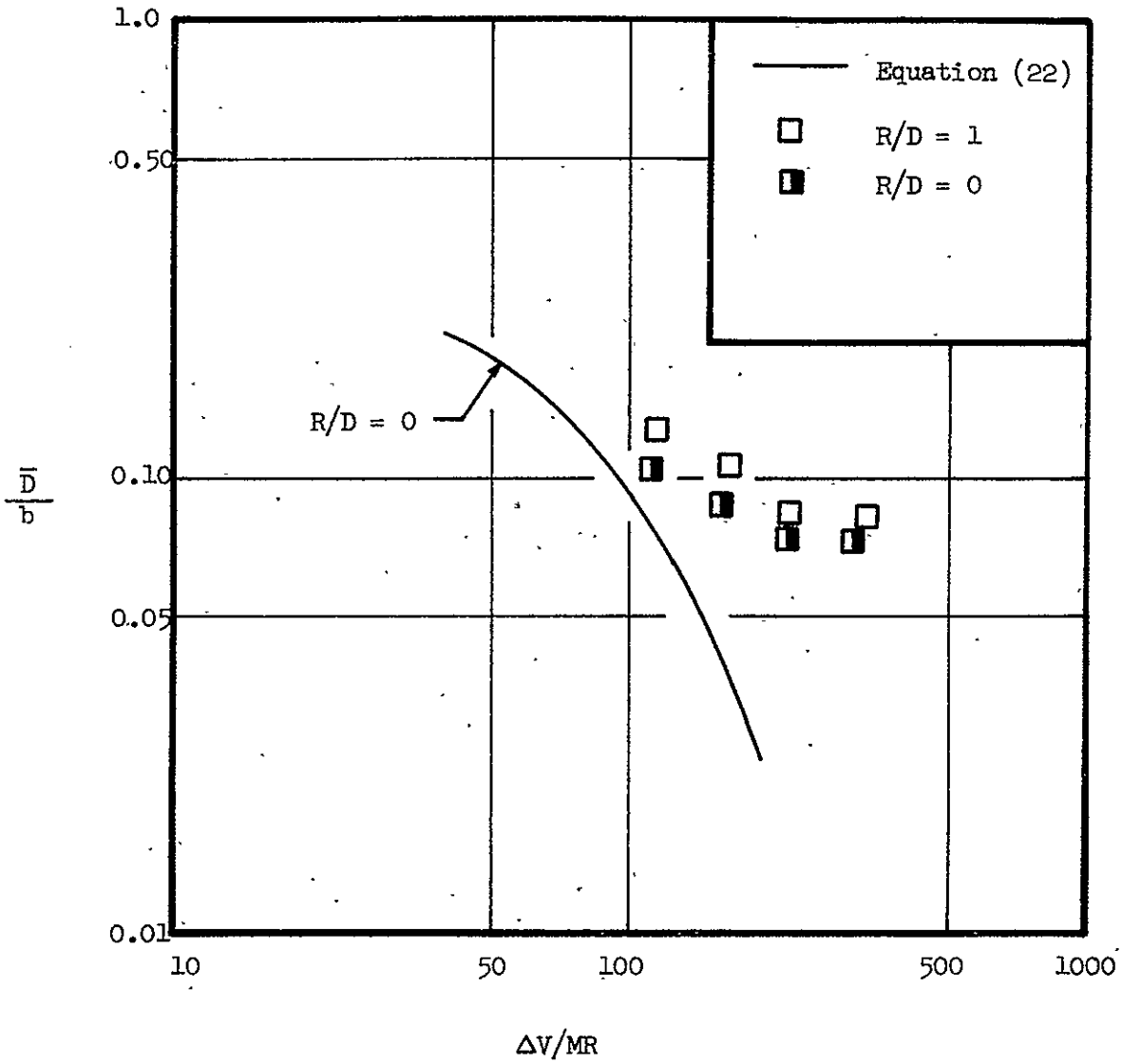

Figure 35. Correlation of Noncircular Concentric Tube Element Atomization Data

by D_L or b) as a function of the parameter $\Delta V/MR$ in Fig. 36. Two separate plots are presented, one for recessed and one for nonrecessed elements. It can be seen that the droplets from the noncircular element are smaller than those from the circular element in all cases.

It must be emphasized in conclusion that the correlations which have been presented were based upon data obtained at constant gas density. Current work in progress at Rocketdyne is suggesting that the density of the gas species plays a significant role in the determination of the drop sizes for a given element.

4.2.3 Mixing Results and Discussion

Results of mass and mixture ratio uniformity experiments are expressed in terms of the mixing uniformity paramete, E_m. Values of E_m obtained from experiments are shown in Fig. 37 for both the circular and the noncircular concentric elements. Data are presented for post recess of zero and one "liquid diameter"* and for mixture ratios of 3 and 6. Data obtained at a mixture ratio of 3 are shown in the left hand graph, while data obtained at a mixture ratio of 6 are shown in the right hand graph. Tests were conducted for each mixture ratio at each of several operating conditions. Most of the data were taken with the center posts of the elements flush with the injector face, i.e., R/D = 0. Recessed data was taken only at mixture ratio 6, where three tests were conducted with the circular element.

*No mixing data are shown for the noncircular element with post recess. One test was conducted for this condition, however the gas velocity in the annulus was equal to the speed of sound and the annular area was choked.

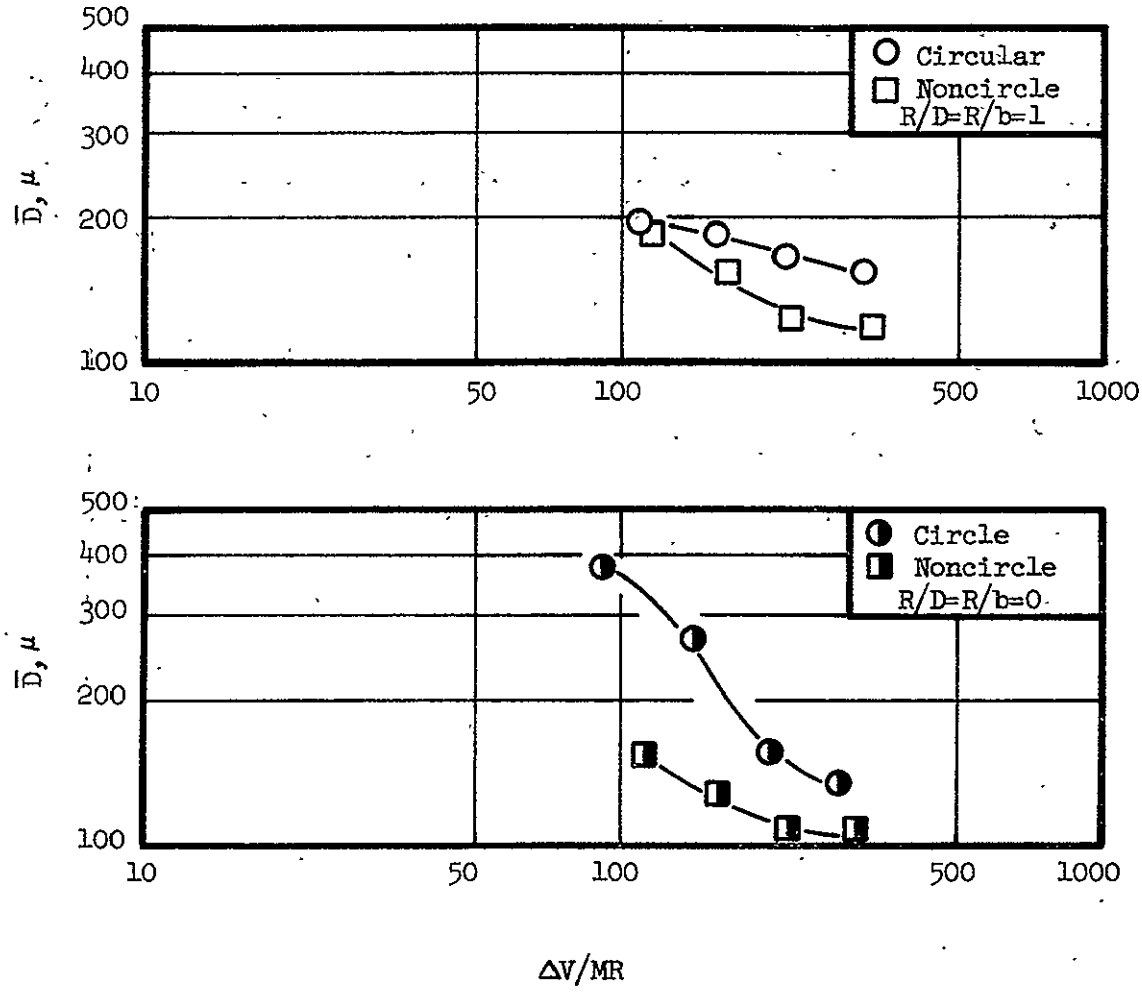

Figure 36. Comparison of Circular and Noncircular Concentric Tube Element Atomization Results

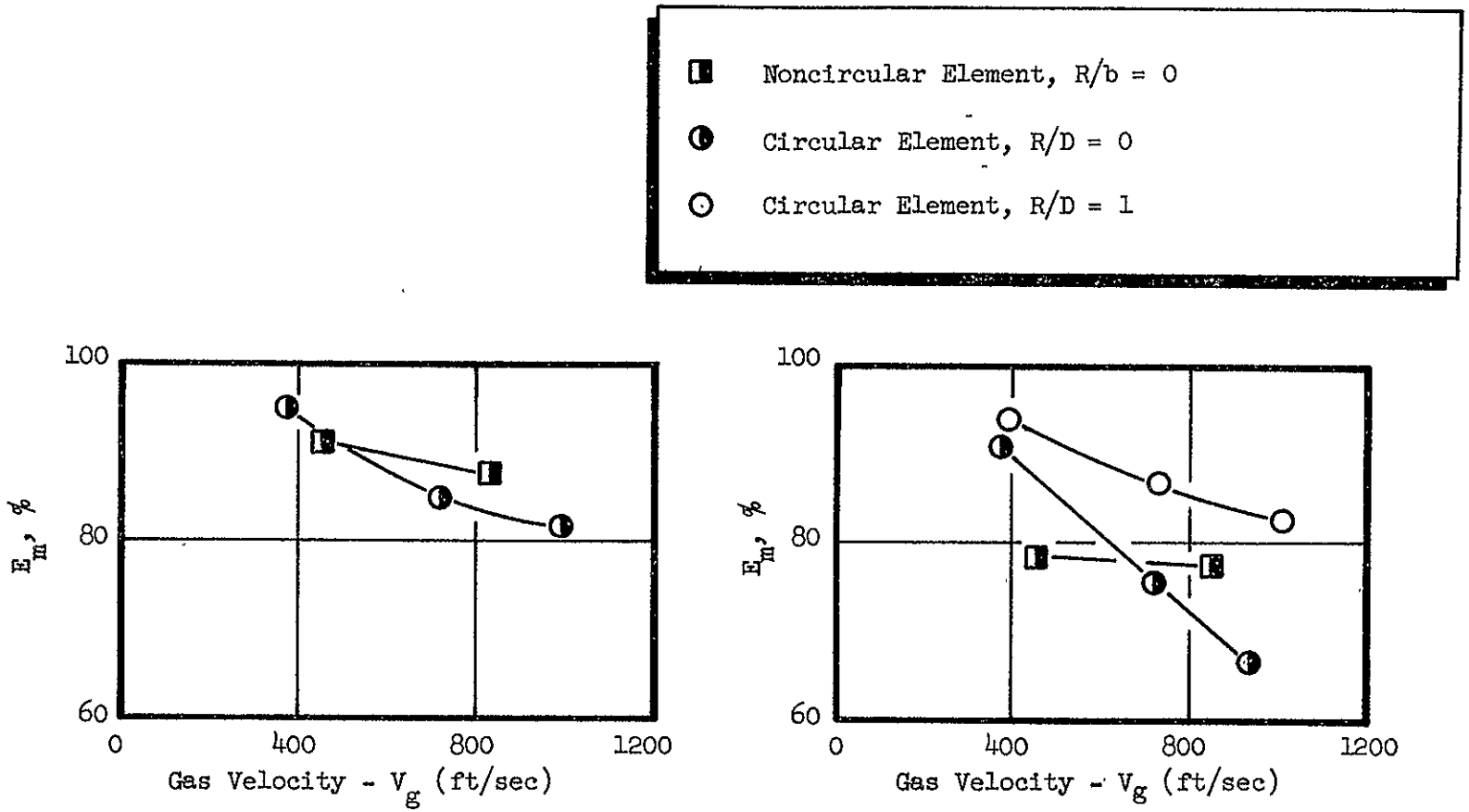

Figure 37. Mixing Uniformity Results for the Circular and Noncircular Concentric Tube Elements

At a mixture ratio of 3, the two elements exhibit mixing uniformity characteristics which are very similar. Both show E_m dropping off with increasing gas velocity, or total element flow rate, from a value of 95% at a velocity of 400 ft/sec to a value of 80% at a gas velocity of roughly 1100 ft/sec. These data were all taken at zero post recess.

At mixture ratio 6, the two element types appear to operate with different characteristics. They both exhibit a drop in performance with increasing gas velocity but with different slopes. The circular concentric tube element seems to be much more sensitive to changes in gas velocity or total element flow rate than does the noncircular element. For gas velocities below 550 ft/sec, the circular element outperforms its noncircular counterpart, whereas for gas velocities above 550 ft/sec, the reverse is true.

For fixed values of gas velocity, the mixing uniformity for both elements is higher at mixture ratio 3 than at mixture ratio 6 for all cases studied.

The effect of oxidizer post recess is shown in the right hand graph in Fig. 37. There is a marked improvement in the mixing of the circular element with recess. The improvement for the circular element is much more striking at high gas velocities or low efficiencies. At a gas velocity of 400 ft/sec, the increase in performance amounts to approximately 3.5 percentage points whereas at a gas velocity of 900 ft/sec, the improvement due to recess is 16.5 percentage points.

There are several interesting facets of the mixing uniformity results which cannot be appreciated from examination of the values of E_m alone. Certain of the conclusions which can be drawn from the mixing data are derived from study of the actual flow patterns which were produced by the elements. These patterns are composed of mass flux and mixture ratio distribution plots showing the physical location of these variables on a two dimensional plane.

Distribution plots for tests No. 4 and 10 are presented in Fig. 38. Test 4 was conducted with the circular concentric tube element and test 10 was conducted with the noncircular element. In Fig. 38 mixture ratio is plotted as a function of the distance from the respective element center lines. Mixture ratio is computed by dividing the mass flow rate of liquid propellant simulant by the mass flow rate of gaseous propellant simulant at a given point.

In Fig. 38, results for the circular element are shown along one diameter. This is sufficient to describe the entire flow field, due to its symmetry. Results for the noncircular element are shown along two different axes which are normal to each other. These data describe only the distributions along these axes and not the entire flow field.

The mixing uniformity parameter, E_m, is very nearly the same for the two elements under the test conditions presented. Reference to Appendix A will show that both tests were conducted at a mixture ratio of 6 and a

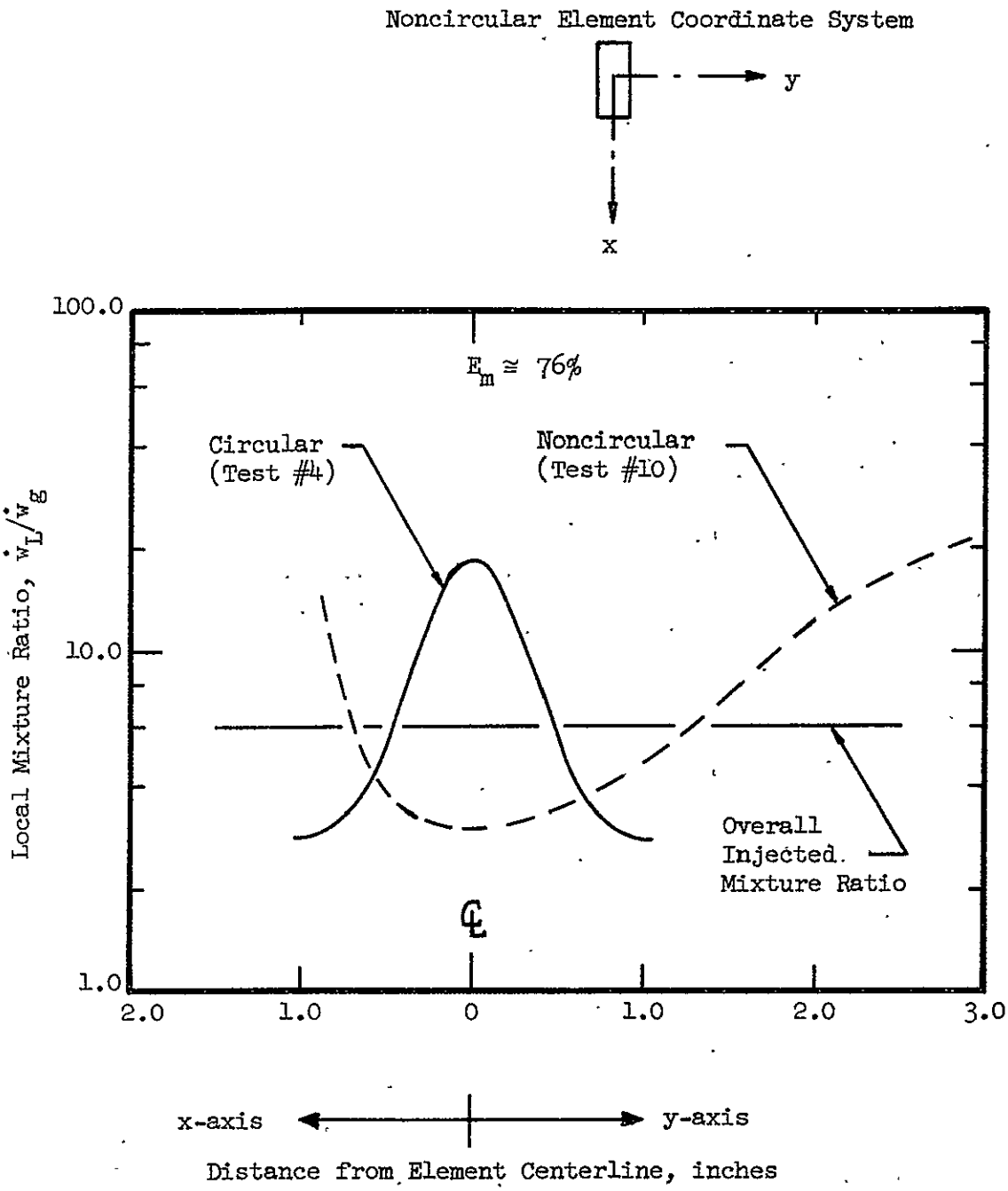

Figure 38. Mixture Ratio Profiles for the Circular and Noncircular Concentric Tube Elements

gas velocity of approximately 800 ft/sec. It is the qualitative difference in the distribution plots for the two elements which is of interest.

The maldistribution problem for the circular element is characterized by high mixture ratios in the center of the flow field with low mixture ratios in the outer zone. Since the liquid species is injected at the center of the element, it may be concluded that the mixing efficiency is low because the momentum of the annulus gas was not sufficient to strip away all of the liquid core and distribute it throughout the gas flow field.

In the case of the noncircular element, the maldistribution problem is just reversed from that of the circle. Here, the mixture ratios in the central regions are low, while relatively high mixture ratios are found in the outer regions of the flow field. Again, since the liquid was also injected at the center of this element, it must be concluded that the gas momentum (or more specifically, its rate of transfer to the liquid) was too high for optimum mixing as the liquid was stripped away and thrown outside the gas field. The injected gas momentum for the noncircular element was roughly the same as for the circular element under these conditions.

If the assumption is made that the circular element would have roughtly the same mixing characteristics as a noncircular element with an aspect ratio equal to 1.0, then these results suggest that a relatively high optimum mixing level can be achieved with noncircular elements with aspect ratios which fall between 1.0 and 6.0. This conclusion contradicts

the assumption used in the preliminary analysis which presumed that the performance of noncircular concentric tube elements would increase continually as their aspect ratio was increased. Now it appears as if there is an optimum aspect ratio. This could produce some interesting tradeoffs in performance between element mixing and atomization characteristics. It still appears, for example, that droplet size for a given operating condition should decrease monotonically with increasing aspect ratio. Therefore, an element would not have an optimum with respect to drop size, and would only be limited by manufacturing requirements as to its aspect ratio.

4.2.4 Correlation of Mixing Results

A performance factor, P_F, was developed in the preliminary analysis to correlate the experimental propellant mixing data. The performance factors for the circular and noncircular concentric tube elements are defined in Eqs. (2) and (11) respectively. Mixing data obtained by a previous program, NAS3-12001, were used to formulate the performance factor into a correlation model, Eq. (3).

Circular concentric tube mixing test results from NAS3-12001 and those results for the circular concentric tube element from this program are presented in Fig. 39 in E_m versus P_F coordinates. Two graphs are shown, one for recessed and one for nonrecessed results.

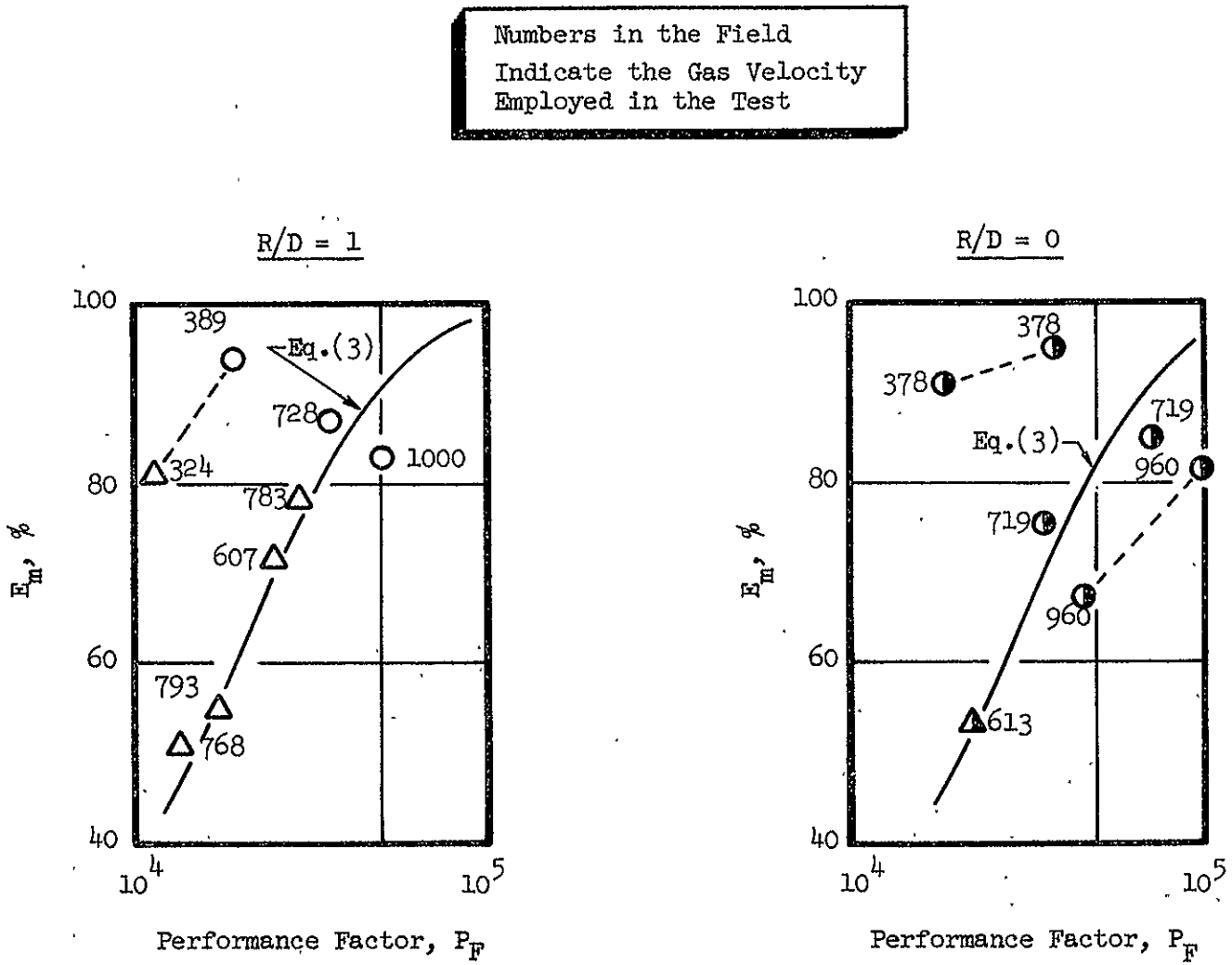

Figure 39. Correlation of Mixing Uniformity Results for the Circular Concentric Tube Element

When the results were first viewed in terms of the original correlations, there was seemingly no agreement between the values of E_m obtained during this program and the estimates results. Upon further investigation and review of the preliminary analysis, it was noted that the gas velocities for the several tests used to develop the correlations were all of the same magnitude, i.e., between 600 and 800 ft/sec (see Table II). It was then noted (see Fig. 39) that those data obtained with gas velocities between 600 and 800 ft/sec on this program did correlate with the original model. In addition, one data point from NAS3-12001, which had been thought to be a bad point, correlated quite well with data from this program as these points represented gas velocities between 300 and 400 ft/sec (see Fig. 39). These comparisons were made for recessed post configurations. Similar results were noted in Fig. 39 for elements with no recess.

It must be concluded from these observations that the correlating parameter, P_F, does not satisfactorily describe the total influence of gas velocity on the mixing process, but that families of lines, of constant velocity, do satisfactorily describe the results in E_m versus P_F coordinates.

It should also be noted that P_F does not consider the independent effect of gas density upon mixing. These effects could not be tested in the open atmosphere. Data currently being taken in a pressurized environment suggest the fact that gas density also plays a role in mixing.

The performance factor indicates that the data from NAS3-12001 and data from the present program are in agreement for comparable gas velocities. Additional data for variable gas velocity and gas density are required to define a more comprehensive correlating parameter.

5.0 PERFORMANCE ANALYSIS

The objective of the performance analysis is to employ the mixing and atomization cold flow data which have been presented along with analytical combustion models to predict actual C* efficiencies for the two elements under investigation and to compare the performance of these elements on the basis of predicted performance. Evaluation of the elements has much more meaning when viewed in terms of predicted C* efficiency rather than in terms of E_m and $\bar{D}$ alone.

5.1 APPROACH

The approach which was used to predict performance was to first predict mixing and vaporization limited C* efficiencies for a given element and then estimate the overall predicted performance by the first order approximation of the product of the two separate performance numbers. This technique is stated briefly in Eq. (73).

$$\eta_{c^*_{pred}} = \eta_{c^*_{dist.}} \cdot \eta_{c^*_{vap}} \tag{73}$$

Values of the mixing limited performance, $\eta_{c^*_{dist}}$ were computed with a multi-streamtube combustion model which generated a mass weighted C* efficiency from the mass and mixture ratio distribution data. Values of E_m are dependent functions of the same distributions used to compute predicted mixing limited C* efficiency and are only related to values of predicted performance for the specific flow field from which they were generated.

Values of vaporization rate limited C* efficiency, $\eta_{c^*_{vap}}$, were obtained as a result of analysis of cold flow droplet size distribution data by a droplet burning model. Both vaporization efficiency and mass median droplet diameter are dependent functions of the droplet distribution data.

A more detailed discussion of both mixing and vaporization limited combustion models may be found in Appendix C. The results of these models are presented in the following sections.

5.2 RESULTS OF THE PERFORMANCE ANALYSIS

5.2.1 Mixing Limited Performance

Mass and mixture ratio distribution data for the two cold flow elements were analyzed with Rocketdyne's mixing limited combustion model. Data in the form shown in Fig. 38 was required for this analysis. The results of the combustion model are presented in Fig. 40.* Mixing limited C* efficiency is shown as a function of E_m for the circular and noncircular concentric tube elements for mixture ratios of 3 and 6. These results were generated for the hydrogen/oxygen propellant combination.

5.2.2 Vaporization Rate Limited Performance

Vaporization limited efficiency predictions which were required for this study were computed on a parametric basis employing Rocketdyne's one

*See Appendix C for discussion of the computational technique.

	Injector	MR	R/D
———	Circle	6	0,1
- - - - - - - -	Circle	3	0
— .. — .. —	Noncircle	6	0
— · — · —	Noncircle	3	0

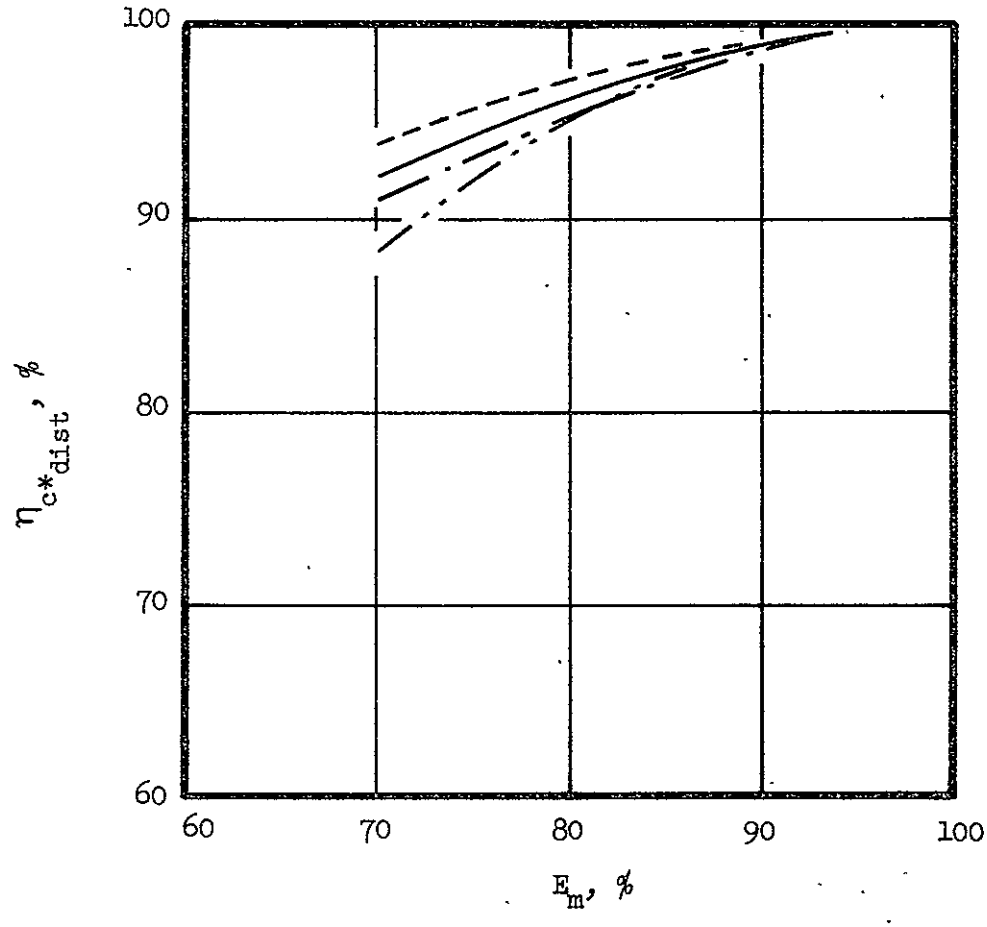

Figure 40. Predicted Mixing Limited C* Efficiency As a Function of E_m for Circular and Noncircular Elements

dimensional droplet burning model. Droplet distribution data in the form shown in Fig. 41 were first normalized with respect to the mass median droplet diameter and then stored in the memory of the computer. In this manner, actual experimental distribution functions could be generated for any given value of $\bar{D}$. The computer model was then used to generate several curves representing the relationship between vaporization rate limited C* efficiency and mass median droplet diameter, $\bar{D}$, for various operating conditions of interest. Those rocket engine operating parameters which were employed in the vaporization analysis are listed in Table XVIII.

TABLE XVIII
ENGINE OPERATING CONDITIONS EMPLOYED FOR ANALYSIS OF VAPORIZATION LIMITED COMBUSTION EFFICIENCY

Chamber pressure	200 psia
Contraction ratio	2.5 : 1
Propellant combination	hydrogen/oxygen
Chamber geometry	conical taper from injector to throat

For the calculations, the hydrogen was considered to have been injected as a gas so that the only propellant which required vaporization analysis was the oxidizer. Parametric curves were computed for mixture ratios of 3, 4.5, and 6, and for chamber lengths of 3, 6, and 9 inches. The results of the calculations are shown in Fig. 42, wherein vaporization efficiency, $\eta_{c^*_{vap}}$, is presented as a function of mass median droplet diameter, $\bar{D}$.

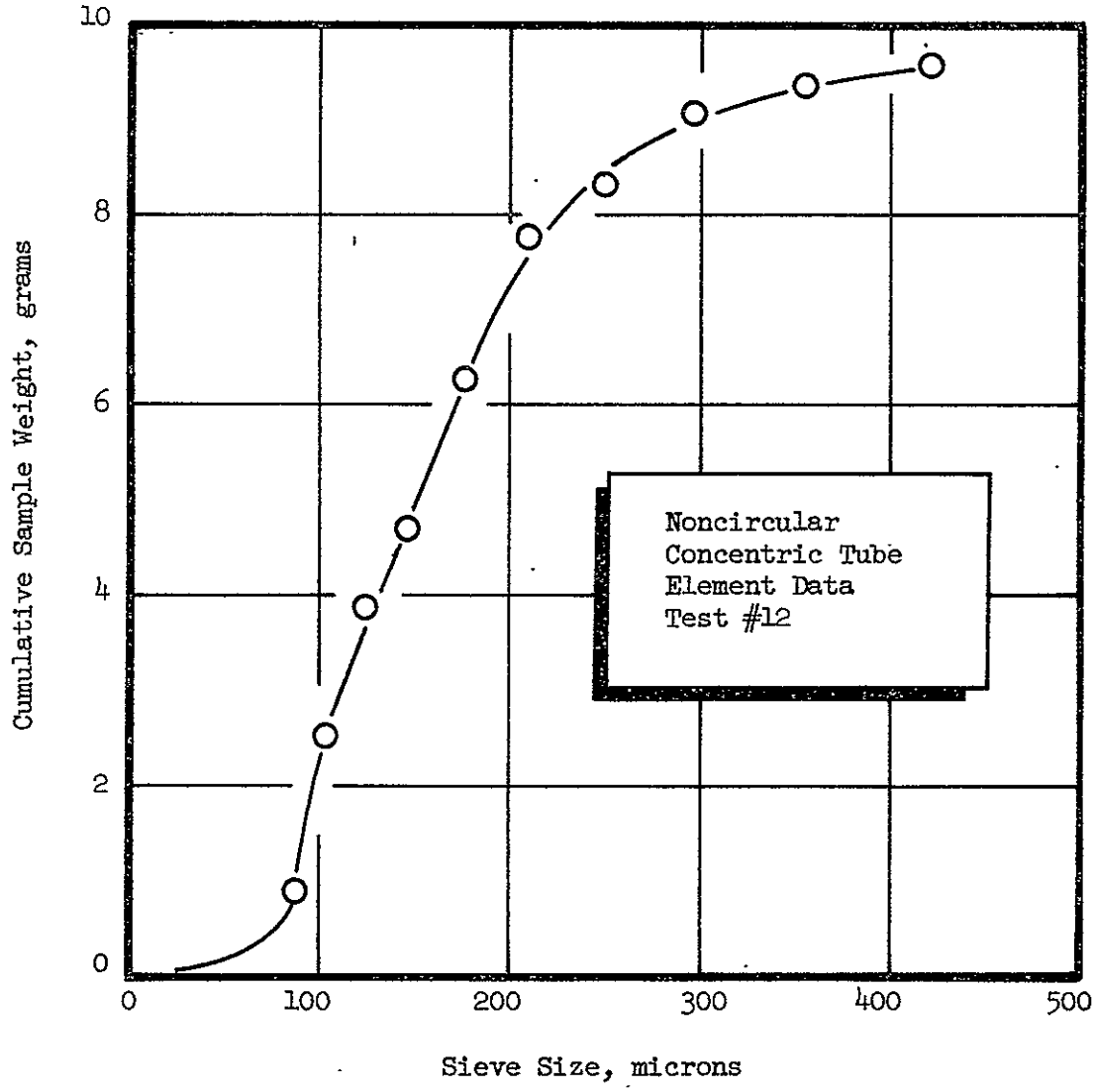

Figure 41. Dropsize Distribution Data from the Noncircular Concentric Tube Element

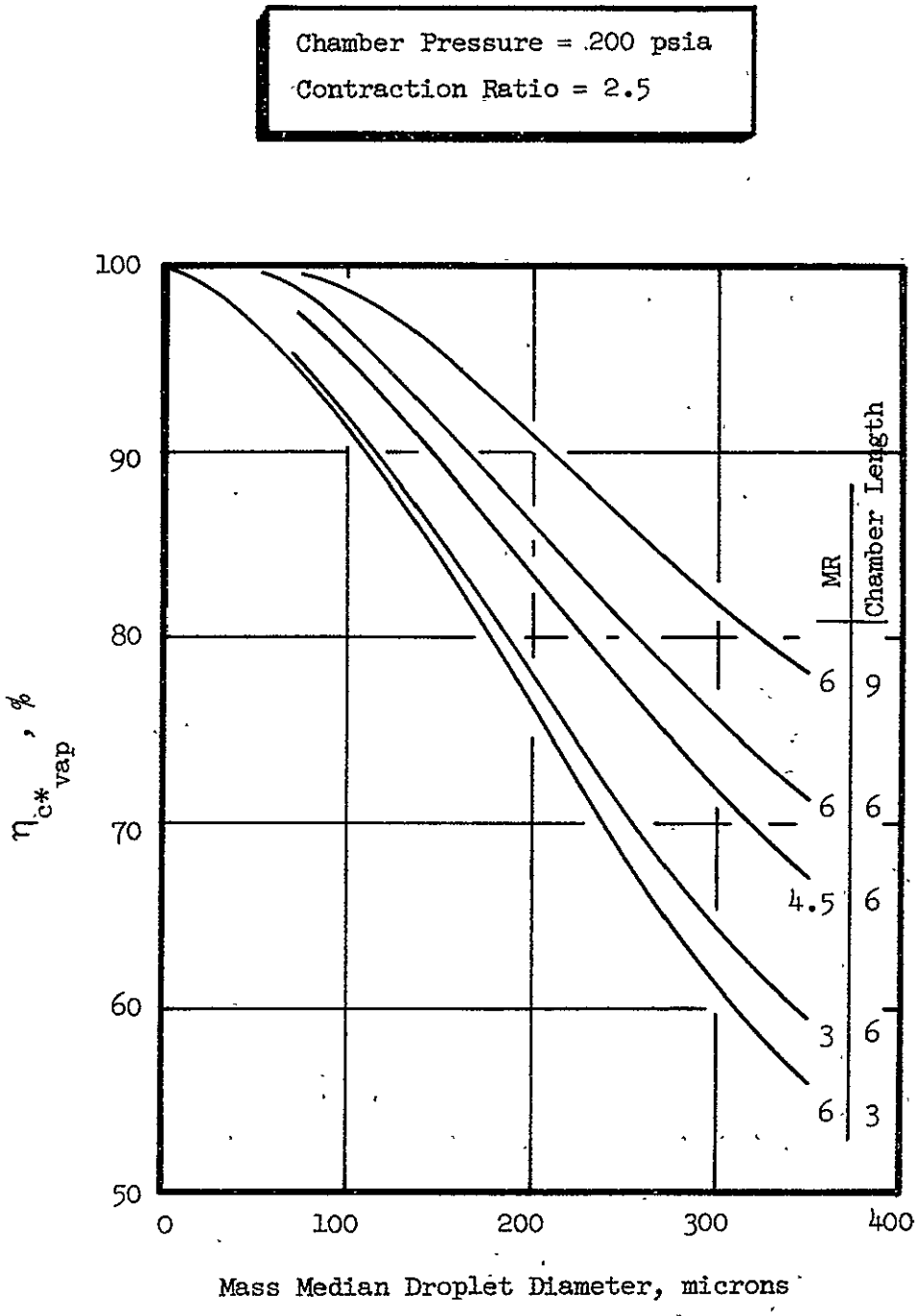

Figure 42. Predicted Vaporization Rate Limited C* Efficiency As a Function of Drop Size

5.3 COMPARISON OF CIRCULAR AND NONCIRCULAR ELEMENT PERFORMANCE

5.3.1 Engine Model and Modeling Approach

One final analysis was required before the performance of the circular and noncircular elements could be compared. Specific mixing and vaporization efficiencies were assigned to each element by relating these efficiency values to the physical operating parameters of the elements. The liquid and gas velocities were chosen as the primary modeling parameters. Mixing and atomization cold flow data were replotted as functions of liquid velocity along lines of constant gas velocity. Cross plots of these data were then constructed to show the E_m and $\bar{D}$ results as functions of gas velocity along lines of constant liquid velocity.

The next step in the analysis was to select an appropriate engine operating condition at which to compare the two elements. A chamber pressure of 200 psia was chosen for the model as the density of gaseous hydrogen at 200 psia is equal to that of gaseous nitrogen at atmospheric pressure. At this pressure, the density, mass flow rate and fuel velocity are modeled exactly. Furthermore, the density of water, which was employed as an oxidizer simulant, is quite close to the density of liquid oxygen, (e.g., 62.4 as compared to 70 lbm/ft^3). Thus, the flow rates, mixture ratios, densities, and injection velocities of both propellants were modeled.

A simplified engine model was run to estimate the propellant flow rates and velocities require for these elements to maintain a chamber pressure

of 200 psia with oxygen and hydrogen. The results of these calculations are presented in Table XIX for several values of mixture ratio.

TABLE XIX
MODEL ENGINE OPERATING CONDITIONS
(P_c = 200 psia)

Mixture Ratio $\dot{w}_{ox}/\dot{w}_f$	Oxidizer Velocity (ft/sec)	Fuel Velocity (ft/sec)
3	7.5	1200
4.5	8.5	906
6	9.3	750

Values of the various efficiencies were determined at these points by the following procedure. First, the values of E_m and $\bar{D}$ for each case were obtained from the working plots of these parameters as functions of liquid and gas velocity. Mixing limited efficiency was obtained from Fig. 40 as a function of E_m, and vaporization limited efficiency was obtained from Fig. 42 as a function of $\bar{D}$.

5.3.2 Predicted Element Performance

Results of the element performance calculations are summarized in Table XX. Values of mixing limited, vaporization rate limited, and overall predicted C* efficiency are presented. The chamber pressure is constant and equal to 200 psia and the contraction ratio is constant and equal to 2.5 for all cases listed in Table XX. Overall predicted C* efficiencies for the circular and noncircular elements are compared

TABLE XX

SUMMARY OF PREDICTED PERFORMANCE

P_c = 200; ϵ_c = 2.5; R/D = 0

Element Type	MR	L, Inches	V_L ft/sec	V_g ft/sec	E_m %	$\bar{D}$ microns	η_{dist}, %	η_{vap}, %	η_{pred}, %	$\Delta\eta$, %
Circular	6	6	9.3	750	77.0	255	95.0	80.2	76.2	
Noncircular	6	6	9.3	750	75.5	148	92.5	91.6	84.7	+8.5
Circular	3	6	7.5	1200	72.0	40	94.6	98.2	92.9	
Noncircular	3	6	7.5	1200	95.6	80	99.8	94.5	94.4	+1.5
Circular	4.5	6	8.5	906	75.2	148	95.1	89.7	85.4	
Noncircular	4.5	6	8.5	906	83.5	120	96.5	93.0	89.7	+4.3
Circular	6	3	9.3	750	77.0	255	95.5	67.5	64.1	
Noncircular	6	3	9.3	750	75.5	148	92.5	84.2	77.9	+13.8
Circular	6	9	9.3	750	77.0	255	95.0	86.0	81.7	
Noncircular	6	9	9.3	750	75.5	148	92.5	95.3	88.1	+6.4

in Fig. 43 as functions of element mixture ratio. The chamber length is constant at 6 inches for this comparison. The performance of both elements falls of sharply with mixture ratio, however, the noncircular element appears to be much less sensitive to mixture ratio variations. The differences between the two curves in Fig. 43 are plotted as functions of mixture ratio in Fig. 44. The performance advantage of the noncircle varies from 1.5 percent at mixture ratio 3 to 8.5 percent at mixture ratio 6.

Further comparison of the two elements is shown in Fig. 45. The predicted effect of chamber length on C* efficiency is depicted for both elements. These results suggest that a combustion chamber length for the circular element would have to be roughly twice that for the noncircle to produce the same level of efficiency.

The results presented in Figs. 43, 44, and 45 clearly demonstrate the performance advantages inherent in the noncircular concentric tube element concept. An area in which these advantages may be most beneficial is the overall reduction of chamber length.

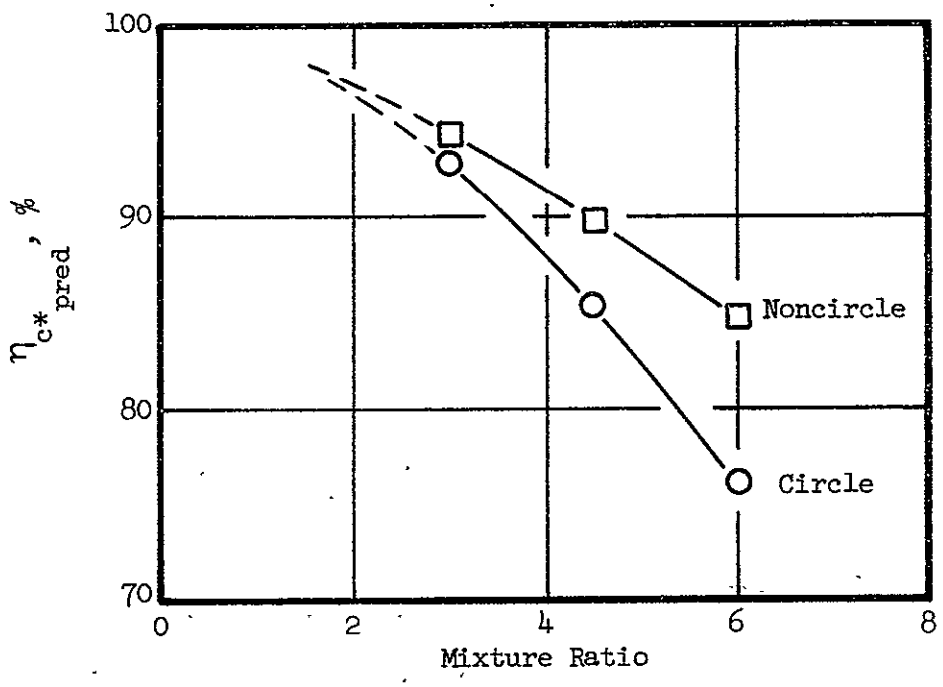

Figure 43. Predicted C* Efficiency (P_c = 200 psia, L = 6 inches)

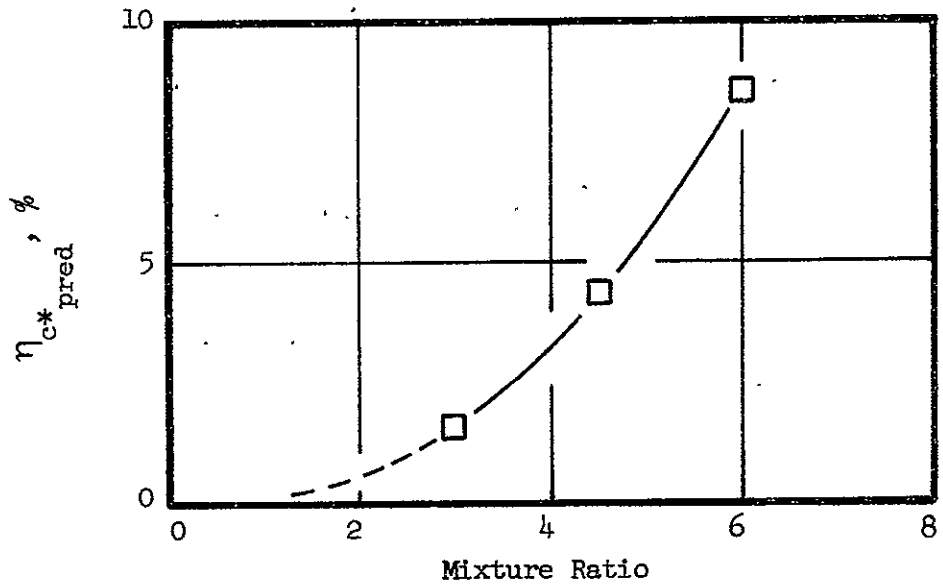

Figure 44. Difference Between Noncircular and Circular Concentric Tube Element Predicted Performance (P_c = 200 psia, L = 6 inches)

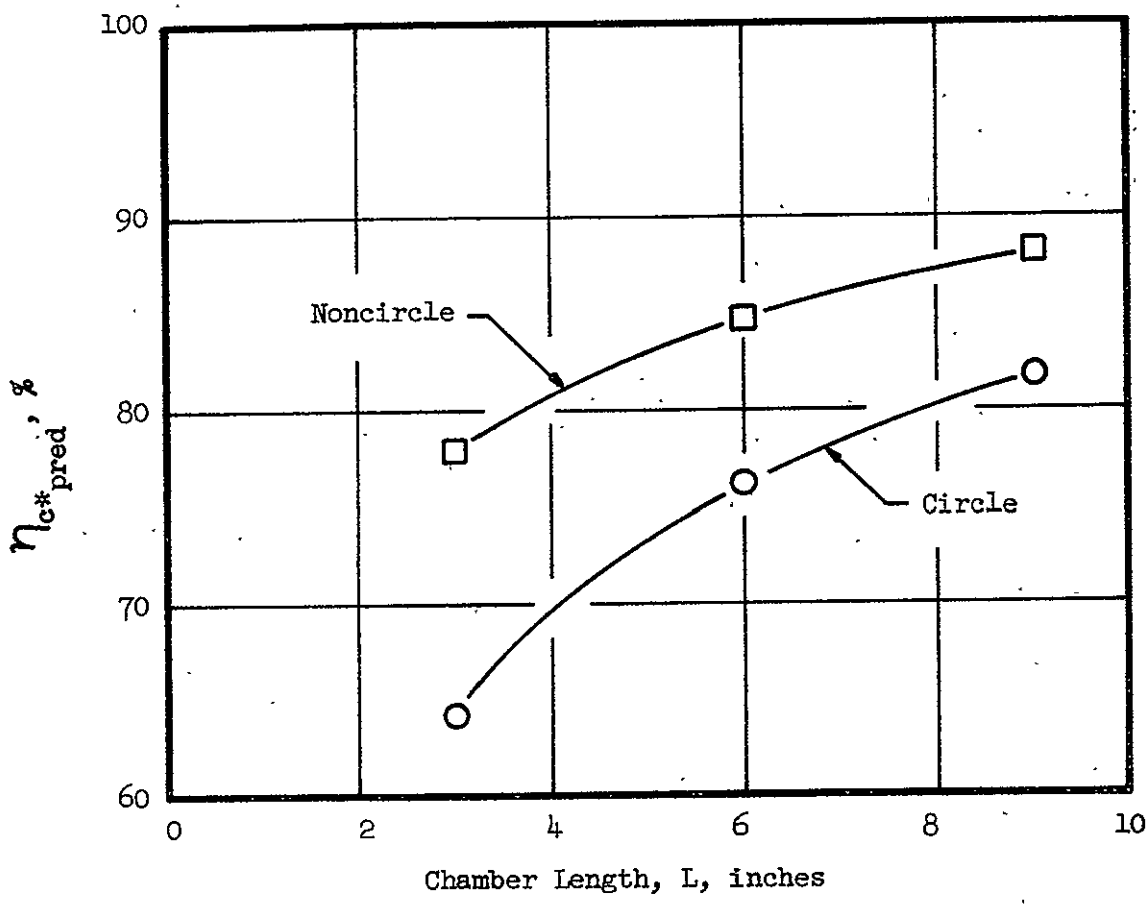

Figure 45. Predicted C* Efficiency as a Function of Chamber Length for the Circular and Noncircular Concentric Tube Elements (P_c = 200 psia, MR = 6)

6.0 CONCLUDING REMARKS

6.1 EVALUATION OF NONCIRCULAR ORIFICE GAS/LIQUID INJECTOR ELEMENT

The most significant conclusion which may be made concerning the results of this program is that the noncircular concentric tube element does possess inherent performance advantages for gas/liquid propellant applications. The noncircular element has demonstrated performance characteristics which are superior to those of a conventional circular concentric tube element for the same operating conditions. This is indeed an outstanding accomplishment in the light of the fact that the circular concentric tube element has a long established record as one of the best candidate element types for gas/liquid propellant combinations.

It is in the area of propellant atomization that the noncircular concentric tube element has demonstrated the greatest promise. Dropsizes produced by this element were considerably smaller than those produced by the circular concentric tube element.

Significant conclusions can also be reached concerning the mixing characteristics of the noncircular concentric tube element. At the outset of the program, it had been predicted that both the mixing and the atomization performance of the noncircle orifice concentric tube element were related directly to the aspect ratio of the element, and

that elements with higher and higher aspect ratios would be higher and higher performing. As far as atomization is concerned, this appears to be the case. However, the data which have been presented suggest that for mixing there may be an optimum aspect ratio. This conclusion was reached from the mass and mixture ratio distribution data which show clearly that the maldistribution evinced by the noncircular element was characterized by relatively high amounts of the liquid species in the outer zones. This suggests that the injected gas phase momentum was so effectively transferred through shear along the large gas/liquid contact periphery that the liquid phase was aspirated to a high degree and thrown to the outside of the flow field. On the other hand, the liquid phase remained near the center of the flow field for the circular concentric tube element with approximately the same level of gas species momentum. This high mixture ratio core is principally responsible for the incomplete mixing of these elements. It appears that the liquid was actually spread out somewhat too far with a rectangular concentric tube orifice aspect ratio of 6:1; in other words the problem of liquid "coring" was apparently over-corrected. It is thus probable that the distribution of liquid throughout the gas flow field could be made highly uniform with the proper selection of the aspect ratio for the noncircular element. This "optimum" aspect ratio would be expected to fall between 6:1 and 1:1. The selection of aspect ratio would have to be based on an optimization study which would include consideration of both mixing and atomization effects.

Aside from the performance aspects, the variable aspect ratio feature of the noncircular concentric tube element also provides a powerful new design capability for tailoring the character of the flow distribution pattern produced by the elements. This feature should be quite valuable from the standpoint of enhancing injector/chamber compatibility and controlling chamber heat flux.

Further investigation of the characteristics of the noncircular concentric tube element is more than warranted by the results of this program. In an optimized configuration, this element can provide significant contributions in the field of gas/liquid injector technology.

6.2 TECHNICAL APPROACH

The objective of this program has been to study and characterize, on a preliminary basis, a new and somewhat revolutionary injector element configuration. The approach which was adopted to accomplish this objective embodied the favorable aspects of both the "scientific method" and the practical realities of research and development in a highly cost conscious market place.

The study of a noncircular concentric tube element was initiated with a preliminary analysis followed by cold flow experimentation, on a single element scale, to characterize the individual contributions of both propellant mixing and atomization to the overall performance of the element.

It is already apparent that this approach has yielded insight into the characteristics and advantages of noncircular orifice gas/liquid injectors which would not have been obtained by a traditional cut-and-try hot firing approach.

To illustrate this, consider what information would have been available had this program been structured such that the method for element characterization was hot fire experimentation. What would the conclusions be at this point in time?

Essentially, it would be known at best that the noncircular concentric tube element provided a higher C* efficiency than its circular counterpart for a fixed set of operating conditions. However, there would be no indication of why the performance had improved and no guidance as to the inherent advantages and limitations of the noncircular orifice element.

It would be interesting to speculate as to the direction in which the investigation would proceed in a follow-up effort with only the information available from the hot fire program and contrast this direction with that which is recommended based on the background available from the actual program which was conducted.

Following the hypothetical hot fire program, the indications would be that the noncircular element does have performance advantages. This would be in agreement with estimates arrived at in the preliminary analysis (if one had been conducted). The fact that the element did outperform

the circular concentric tube element may have been construed to imply that aspect ratio alone was the valuable feature of the element and that the next element which should be hot fired should incorporate an even larger aspect ratio to further increase performance (also in keeping with the preliminary analysis assumptions). Other than these sketchy conclusions, nothing further would be known of exactly why the noncircular element performed higher. Was it a better mixer? Did it produce better atomization? Or were both mixing and atomization superior? None of the trade-offs between mixing and atomization would be known.

In line with these conclusions, an additional element would be fabricated incorporating a high aspect ratio orifice (i.e., > 6:1). Hot fire tests conducted with this element would probably yield performance results which are lower than those obtained with the original element, but with no indication as to why this happened.

The traditional cut-and-try hot firing approach would probably also have led to erroneous conclusions regarding injector/chamber compatibility. For example, one salient observation from the flow mixing studies of the rectangular coaxial element was that the long axis of the elliptical spray fan is oriented 90° from the long axis of the orifice slot. It is likely that an initial design would have erroneously placed the rectangular orifices parallel with adjacent chamber walls and that, as a result, high heat flux or local erosion would have been seen in the chamber near the injector. In an attempt to lower heat flux, the common "fix" of adding dump fuel coolant on

the wall would have been considered. If this had been attempted, the heat flux would have increased even more, creating confusion as to the mechanisms involved in the process.

At this point, the program would probably have been abandoned and the concept of a rectangular concentric tube element would be labeled as unsatisfactory for rocket engine injector application.

These program pitfalls have been avoided with the approach which was actually selected for this program. The results available from this program indicate that the noncircular concentric tube element should out-perform a circular configuration on an overall basis. Furthermore, the results suggest why this is true and in what areas the element can be improved to achieve even higher performance. It is also known that the aspect ratio of 6:1 is probably too large and that superior results can be achieved with smaller, not larger, aspect ratios.

Additionally, the degree to which mixing and atomization contribute individually to overall performance is known and the relationships between these contributions and the operational parameters (i.e., flow rate per element and mixture ratio) are known.

The next step in the characterization of the noncircular concentric tube which is recommended based on these results would consist of further cold flow studies of modified configurations to establish optimization

design criteria for these elements. Variables such as aspect ratio, velocity ratio, and post recess should be investigated. Finally, an optimum configuration based on cold flow results should be designed and fabricated and hot fire experiments should be conducted in a variable length chamber to confirm the conclusions drawn in cold flow. (Mixing-limited performance estimates could be verified by hot fire tests in long chambers which can insure complete vaporization.)

It must be concluded that the adoption of the approach which has been taken has provided extensive savings in cost and frustration, while providing the maximum amount of information for element characterization.

7.0 REFERENCES

1. Nurick, W. H., and McHale, R. M., Noncircular Orifice Holes and Advanced Fabrication Techniques for Liquid Rocket Injectors, Phase I Final Report, NASA CR-108570, R-8224, Rocketdyne, a Division of North American Rockwell Corporation, Canoga Park, California, 1970.

2. Rupe, J. H., A Correlation Between the Dynamic Properties of a Pair of Impinging Streams and the Uniformity of Mixture-Ratio Distribution in the Resulting Spray, Progress Report No. 20-209, Jet Propulsion Laboratory, Pasadena, California, 28 March 1956.

3. Mehegan, R. F., Campbell, D. T., and Scheuerman, C. H., Investigation of Gas-Augmented Injectors, Final Report, submitted to NASA for approval as R-8361, Rocketdyne, a Division of North American Rockwell Corporation, Canoga Park, California, September 1970.

4. Schlichting, H., Boundary Layer Theory, 4th Ed., McGraw-Hill Book Co. Inc., New York, 1960.

5. Arbit, H. A., Dickerson, R. A., Clapp, S. D., and Nagai, C. K., Lithium-Fluorine-Hydrogen Propellant Study, NASA CR-72325, Rocketdyne, a Division of North American Rockwell Corporation, Canoga Park, California, 22 Feb. 1968.

6. Wolfe, H. E., and Andersen, W. H., Kinetics, Mechanisms, and Resultant Droplet Sizes of the Aerodynamic Breakup of Liquid Drops, Report No. 0395-04(18) SP, Aerojet-General Corp., Downey, California, April 1964.

7. Abramovich, G. N., The Theory of Turbulent Jets, The MIT Press, MIT, Cambridge, Mass., 1963.

8. Dussourd, J. L., and Shapiro, A. H., "A Deceleration Probe for Measuring Stagnation Pressure and Velocity of a Particle-Laden Gas Stream," presented at the Heat Transfer and Fluid Mechanics Institute, University of California, Berkeley, California, June 1955.

9. Elverum, G. W., and Morey, T., Criteria for Optimum Mixture Ratio Distribution Using Several Types of Impinging Stream Injector Elements, Memorandum No. 30-5, Jet Propulsion Laboratory, Pasadena, California, 25 February 1959.

10. Pieper, J. L., Dean, L. E., and Valentine, R. S.: "Mixture Ratio Distribution--Its Impact on Rocket Thrust Chamber Performance," J. Spacecraft and Rockets, Vol. 5, No. 6, June 1967, p 786-789.

11. AFRPL-TR-68-147, Correlation of Spray Injector Parameters with Rocket Engine Performance, R. Dickerson, K. Tate, and N. Barsic, Rocketdyne, a Division of North American Rockwell Corporation, Canoga Park, California, June 1968.

12. Wrubel, J. R., "Some Effects of Gas Stratification on Choked Nozzle Flows," AIAA Paper 64-266, 1964.

8.0 APPENDIX A

TABLES OF EXPERIMENTAL RESULTS

Tables of experimental data and test results are presented in this section. Results of the mixing uniformity tests are shown in Table A-1. Results of the atomization tests are presented in Table A-2. The density of the wax which was employed in the atomization experiments is approximately 47.7 lbm/ft^3. The injection temperatures of the gaseous nitrogen were 70°F for the mixing tests and approximately 200°F for the atomization experiments. Droplet mean diameters in Table A-2 are expressed in microns. One micron is equal to 10^{-6} meters.

TABLE A-1. MIXING UNIFORMITY TEST RESULTS

Test No.	Element*	Recess R/D	$\dot{w}_{H_2O}$ lbm/sec	$\dot{w}_{GN_2}$ lbm/sec	MR	E_m	Remarks
1	C	0					Checkout
2	C	0					Checkout
3	C	0					Checkout
4	C	0	0.090	0.015	6.00	75.5	
5	C	0	0.045	0.015	3.00	85.0	
6	C	0	0.045	0.0075	6.00	90.7	
7	C	0	0.135	0.0225	6.00	66.9	
8	C	0	0.023	0.0075	3.00	94.7	
9	C	0	0.068	0.0225	3.00	81.7	
10	NC	0	0.090	0.0150	6.00	77.2	
11	NC	0	0.045	0.0150	2.99	87.1	
12	NC	0	0.135	0.0225	6.00	71.3	X**
13	NC	0	0.068	0.0225	3.00	79.4	X
14	NC	0	0.045	0.0075	6.00	78.3	
15	NC	0	0.023	0.0075	3.00	90.9	
16	C	1	0.045	0.0075	6.00	93.9	
17	C	1	0.090	0.0150	6.00	86.8	
18	C	1	0.135	0.0225	6.00	82.5	
19	NC	1	0.135	0.0225	6.00	71.8	X

* C - Circular
NC - Noncircular

**X - Indicates that test was invalidated due to high Mach No. (i.e., near or equal to 1.0)

TABLE A-2. ATOMIZATION TEST RESULTS

Test No.	Element*	Recess R/D	$\dot{w}_{max}$ lbm/sec	$\dot{w}_{GN_2}$ lbm/sec	MR	$\bar{D}$ microns	Remarks
1	C	0	0.0285	0.0099	2.88	157	
2	C	0	0.0615	0.0099	6.21	374	
3	C	0	0.120	0.0099	12.1		Flakes
4	C	0	0.045	0.0149	3.02	133	
5	C	0	0.0915	0.0149	6.14	268	
6	C	0	0.174	0.0149	11.7		Flakes
7	C	0	0.238	0.0200	11.9		Flakes
8	C	0	0.119	0.0200	5.95	297	X**
9	C	0	0.0605	0.0202	3.00	166	X
10	C	0	0.133	0.0201	6.62	393	X
11	NC	0	0.030	0.0099	3.03	108	
12	NC	0	0.058	0.0099	5.86	151	
13	NC	0	0.046	0.0149	3.09	107	
14	NC	0	0.0905	0.0149	6.07	126	
15	NC	0	0.058	0.0198	2.93	120	X
16	NC	0	0.116	0.0198	5.86	156	X
17	NC	0	0.116	0.0105	11.05		Flakes
18	C	1	0.030	0.0105	2.86	167	
19	C	1	0.060	0.0105	5.69	197	
20	C	1	0.045	0.0158	2.85	152	
21	C	1	0.089	0.0155	5.74	183	
22	C	1	0.060	0.0208	2.88	134	X
23	C	1	0.120	0.0200	6.00	188	X
24	C	1	---------- Test No. not used				
25	NC	1	0.030	0.010	3.0	123	
26	NC	1	0.0585	0.010	5.85	186	
27	NC	1	0.0440	0.015	2.93	119	
28	NC	1	0.0900	0.015	6.00	152	
29	NC	1	0.0610	0.020	3.05	124	X
30	NC	1	0.1195	0.020	5.98		Flakes

* C - Circular
NC - Noncircular

**Data invalidated due to high Mach No.

9.0 APPENDIX B

MIXING UNIFORMITY TEST APPARATUS AND PROCEDURES

A description of the experimental apparatus and procedures for atomization tests is presented in detail in the final report which covers the first portion of this program (Ref. 1). However, the apparatus and procedures described in that report for mixing uniformity experimentation are not applicable to this phase of the program. This is due to the fact that the injectors which were investigated in the original program were of the liquid/liquid type. Thus the mixing uniformity of these injectors could be measured simply by flowing the elements over an open, multi-tube matrix and collecting the spray. Mass and mixture ratios at each point in the flow field could then be determined from an analysis of the two immiscible simulants collected at each point in the matrix. This technique was not suitable for gas/liquid flow fields. A detailed discussion of experimental techniques for gas/liquid flow field measurements is presented in Ref. 3. A brief discussion will be presented here for completeness.

In order to calculate E_m and mixing limited C* performance for a given element, the mass fraction of the total fuel and oxidizer present at each point in the flow field must be determined. A specially designed, two-phase impact probe is employed to accomplish this task. A schematic of such a probe is presented in Fig. B-1. The theory of the two phase impact probed was first published by Dussourd and Shapiro (Ref. 8). Basically, the probe serves the function of stagnating the gas component

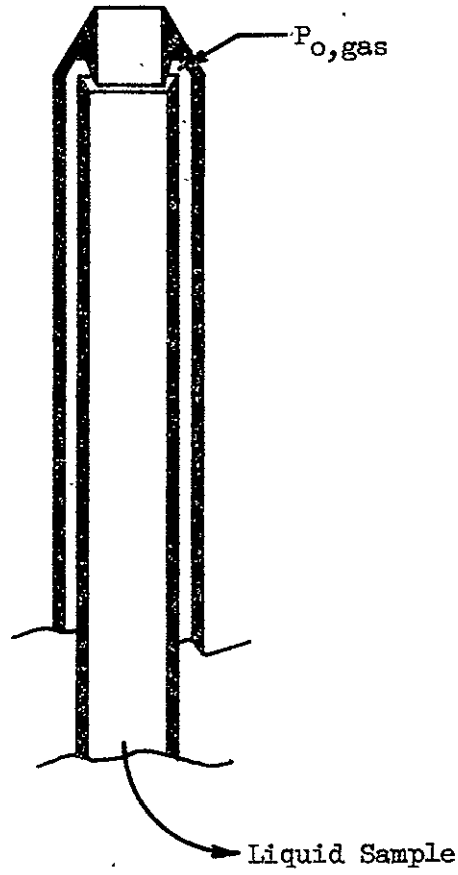

Figure B-1. Schematic of Concentric Tube Two-Phase Impact Probe

at the probe tip while allowing the liquid droplets to proceed down the length of the probe. The principles of operation are outlined in schematic form in Fig. B-2. At a distance "x" from the probe tip, an annular opening is provided by a concentric tube marked "A" in Fig. B-2. Theoretically, at this point, the gas species is stagnant while the liquid species is still travelling with most of it's original momentum. Thus, the true component of the total pressure of the flow field attributable to the gas species may be measured as the static pressure in the annulus between tube A and tube B, (see Fig. B-2). In practice, however, this is only an approximation and certain corrections must be applied to the data to determine the true gas stagnation pressure. With a knowledge of the gas density and the area of the probe tip, the gas velocity and mass flow rate can be determined from the stagnation pressure data. The liquid species flow rate can be easily measured at the same point by merely collecting liquid in the probe for a known time interval and then weighing the sample. Thus, both gas and liquid flow rates can be determined at each point.

There is one additional problem associated with the determination of the gas species flow rate. As the gas/liquid flow field moves through the surrounding environment on its way from the injector to the probe location, much of the gas in the environment is ingested into the flow field. Therefore, the gas flow rate measured at the probe is composed of gas which was injected and gas which was ingested. These two components must be segregated to determine the injected portion. To accomplish this, for open air testing, pure nitrogen is injected through the element as a fuel simulant. The gas

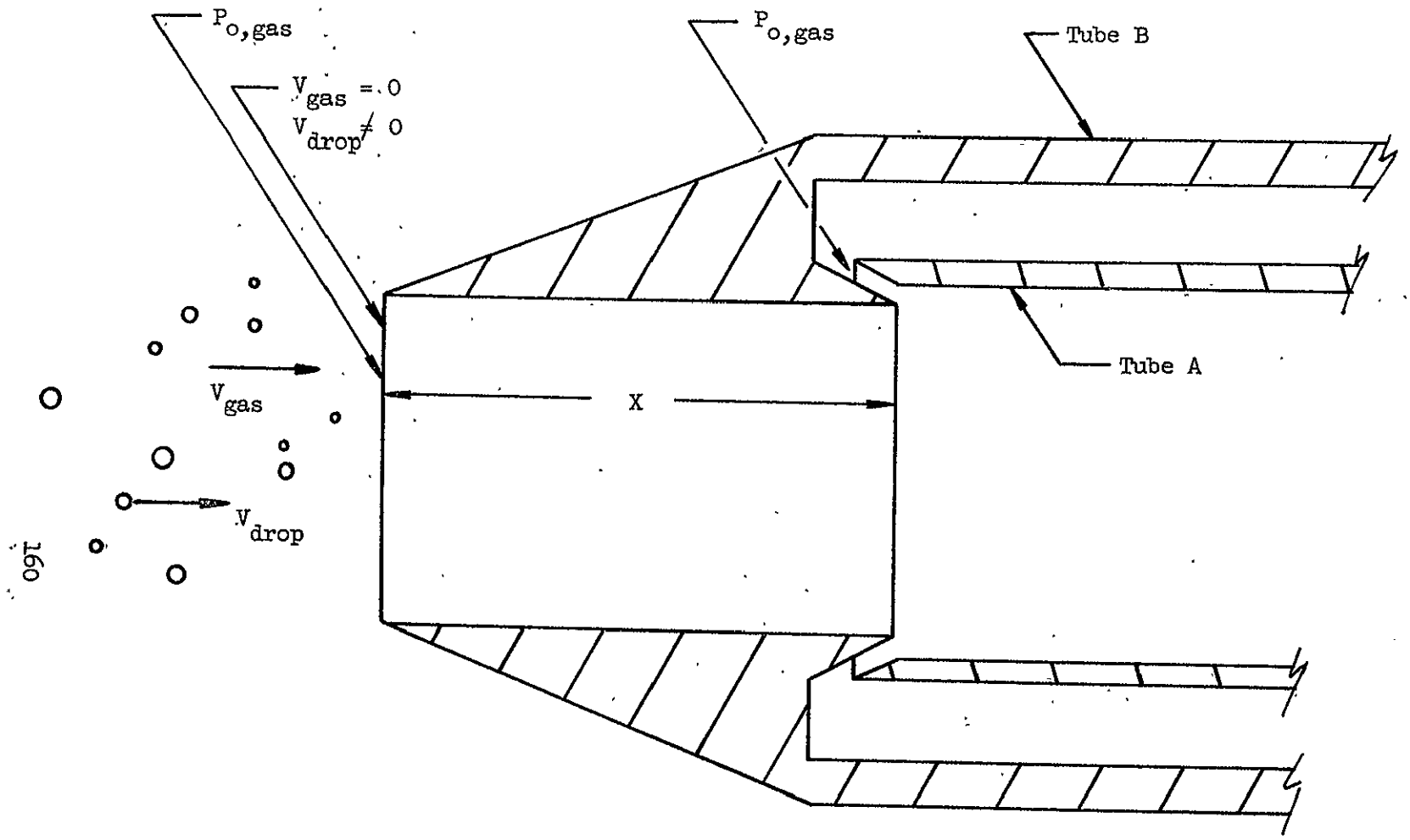

Figure B-2. Two-Phase Impact Probe

sample which arrives at the probe is processed through an oxygen sampler. The concentration of oxygen in the sample can then be used to determine the concentration of the original injectant, (e.g., the concentration of oxygen in the environment is approximately 20%).

A schematic of the overall system is shown in Fig. B-3. For operation in the open air, the section labeled "pressure chamber" is removed. This apparatus is also capable of performing mixing uniformity measurements under backpressure.

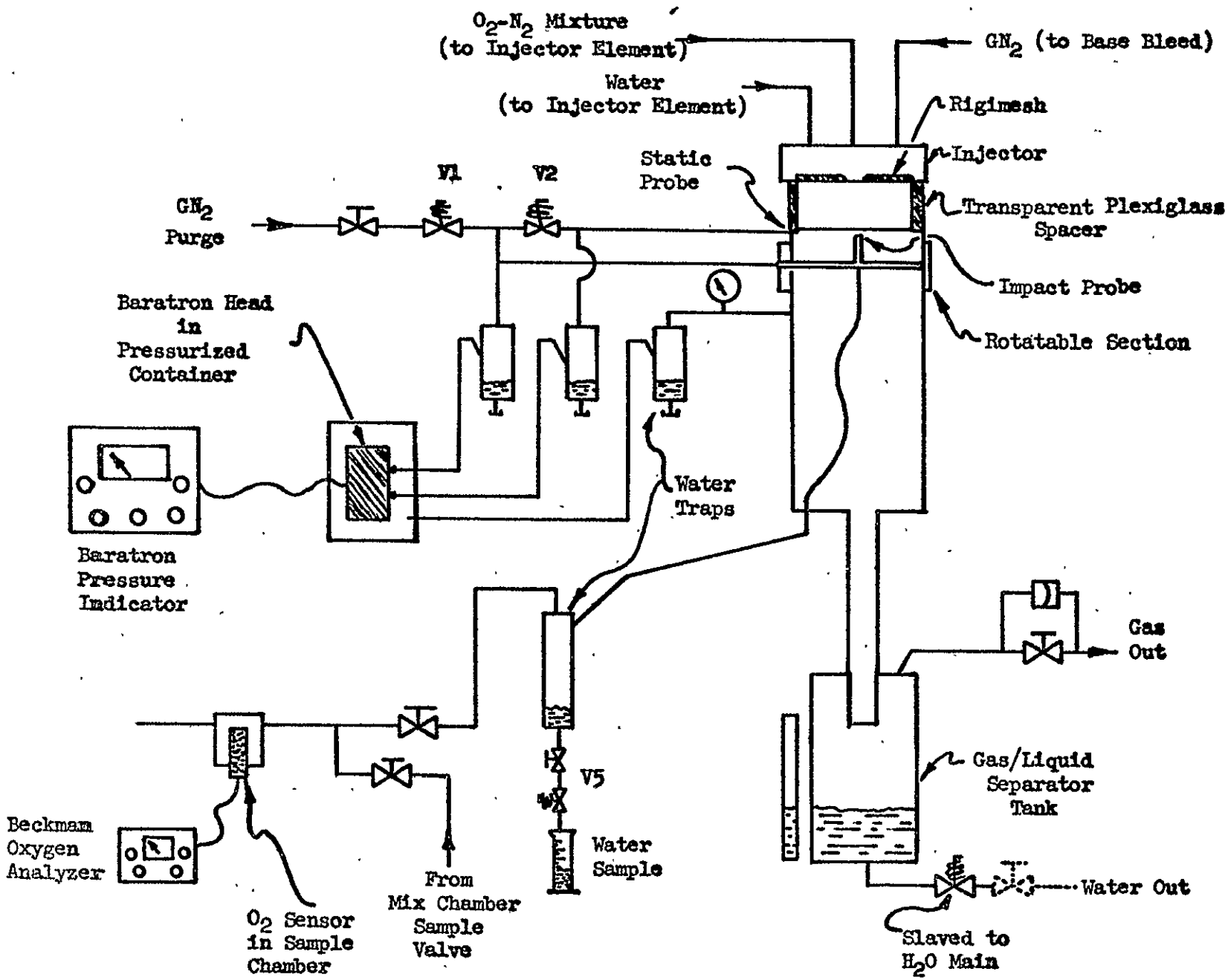

Figure B-3. Gas/Liquid Mixing Facility Schematic

10.0 APPENDIX C

COMBUSTION MODELS

10.1 VAPORIZATION LIMITED COMBUSTION

The vaporization limited combustion model formulation is based on the development of mathematical expressions for the various physical processes involved in the combustion of liquid droplet sprays in a bipropellant liquid rocket engine. The model considers propellants to be injected as sprays containing ranges of discrete droplet size groups, each possessing a given average diameter. The total spray mass is distributed among the various groups according to an experimental mass distribution function.

Of central importance in the model is the solution of the individual droplet burning rates, which are assumed to be limited by diffusion. Analysis of the dynamic behavior of single droplets is justified on the basis that the volumetric flow rate of liquid propellants into the downstream region is only about 1 to 2 percent of that of the combustion gases and, therefore, that the likelihood of droplet collisions or interference with one another is negligibly small. Under rocket conditions, in the uniform mixing zone, droplets are spaced on the order of 2 to 3 diameters apart, while the vapor film thickness is on the order of 5 to 15 percent of the droplet diameters. As a result, each droplet is considered to be immersed in an infinite combustion gas medium.

The calculation of single droplet evaporation is based on a spherically symmetric model of simultaneous heat transfer to, and mass transfer from a liquid sphere.

The liquid droplet temperature is assumed to vary with time, but to be uniform through the drop. Forced convection and resultant nonspherical transfer processes are accounted for through empirical Nusselt number correlations for both heat and mass transfer.

In evaluating the convective contribution, relative gas-to-droplet velocity is required. Droplet velocities are obtained from a drag relationship for evaporating spheres. A composite form of the drag coefficient for accelerating spheres which accounts for droplet flattening is employed.

Compressible gas dynamics are accounted for with area changes corresponding to chamber geometry. The droplets are treated as point sources (or sinks) of fuel (mass), oxidizer (mass), momentum, and energy with local transport rates obtained by summing the contributions of all droplets at any given location in the chamber.

The gas-phase energy equation is simplified normally by the assumption that the composition and stagnation temperature are the equilibrium values for the gas-phase oxidizer, fuel mixture ratio, and the chamber pressure. Other gas properties (static temperature, density, etc.) are evaluated from

the respective stagnation values by applying the local Mach number to the frozen isentropic expansion equations.

The model is solved in numerical form by high-speed digital computers. It requires input of the "upstream boundary condition," which completely describes the initial conditions of spray (drop size distribution, drop velocities, and temperature) and gas (composition, flowrate, and pressure) at the location where computation is started. Chamber geometry must also be specified.

Solution proceeds in a stepwise manner moving downstream to the nozzle throat. At each step, interphase transport of mass, momentum, and energy is evaluated from the transport equations previously described with subsequent solution of gas-phase equation of state and continuity, momentum, and energy balances. This results in a description of droplet group diameters, velocities, and temperatures as well as gas composition, velocity, and pressure at the new location.

This "marching technique" proceeds into the nozzle up to the geometric throat, where it is necessary to satisfy the downstream boundary condition of sonic gas velocity. If the throat Mach number deviates from unity by more than a pre-selected tolerance, iteration is required whereby either the injector-end chamber pressure or propellant flowrates are adjusted and the entire calculation repeated. In practice, convergence of this iteration is rapid and a solution is readily obtained. The general validity of the analytical results is determined to a major

extent by the accuracy of the input spray description. Vaporization rate limited C* efficiency is computed from the following equation.

$$\eta_{c^*,vap} = \left[\frac{\dot{w}_B}{\dot{w}_I}\right]\left[\frac{c^*_B}{c^*_I}\right] \qquad \text{(C-1)}$$

where

$\dot{w}_B$ = flowrate of burned gas at the geometric throat

$\dot{w}_I$ = injection flow rate of fuel plus oxidizer

c^*_B = theoretical c* corresponding to the composition of the burned gas at the geometric throat

c^*_I = theoretical c* corresponding to the injection mixture ratio of liquid fuel and oxidizer

10.2 MIXING LIMITED COMBUSTION

Over the past 15 years, mass and mixture ratio distribution uniformity ("mixing") has been extensively studied both analytically and experimentally. The most notable efforts in this area are those by Rupe (Ref. 2), Elverum and Morey (Ref. 9), Pieper, et al. (Ref. 10), and an Air Force-sponsored Rocketdyne program (Ref. 11). Experimental/analytical correlations performed in these programs demonstrate quantitatively that high combustion efficiency in rocket engine thrust chambers occurs only when the initial local mixture ratio distribution is at, or near, the target chamber mixture ratio. This implies that the injector should provide a spray field having a uniform mixture ratio over the entire flow cross section.

The sketch below illustrates a typical curve of theoretical equilibrium c* as a function of propellant mixture ratio (oxidizer/fuel).

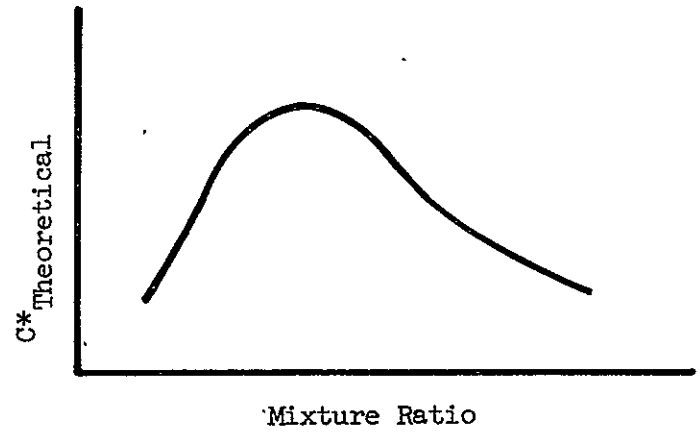

Normally the design operating point of overall injected mixture ratio falls close to the peak, and any maldistribution of propellant mixture ratio results in a loss in overall c*. An analytical model has been developed at Rocketdyne to relate these maldistributions to an attendant loss in c* efficiency. The development of this model is outlined in the following paragraphs.

Wrubel (Ref. 12) describes an analysis of mixing losses whereby the flow is hypothetically subdivided into "i" stream tubes, each containing propellant at some mixture ratio which is uniform within that stream tube. No mass or energy is considered to cross stream boundaries. Propellant vaporization, mixing, and combustion are treated as being complete upstream of the start of nozzle convergence. Within the nozzle the flow is handled as being one-dimensional and isentropic. At each axial station the static pressure is considered uniform for all stream tubes. In

addition, boundary layer effects are neglected. The resulting equation relating the mixing limited c* efficiency to the local mass and mixture ratio distribution is:

$$\eta_{mix} = \sum_i \left(\frac{\dot{w}_i}{\dot{w}_T} \frac{c^*_i}{c^*_{theo}} \frac{A_{t,i}}{A^*_i} \right) \tag{C-2}$$

Here $A_{t,i}/A^*_i$ is the ratio of the cross-sectional area of the ith stream tube at the minimum chamber area to its area at the point it becomes sonic. For most cases of interest the specific heat ratios γ_i, are all of similar value so the shifts in location of the sonic condition from the geometric throat will be small and the preceding equation is closely approximated by:

$$\eta_{mix} = \sum_i \frac{\dot{w}_i}{\dot{w}_T} \frac{c^*_i}{c^*_{theo}} \tag{C-3}$$

where the effective c* is simply a weighted average of the local c* for the individual stream tubes. For any given propellant mixture ratio distribution, Eq. (C-3) provides a simple means of determining c* efficiency loss due to "mixing".

Most investigators agree that distributions developed by spray mixing near the injector will not be appreciably changed downstream by turbulent mixing of the gases. As a consequence, if the initial spray distribution formed by an injector can be experimentally determined, $(\eta_{c^*})_{mix}$ can be computed by using Eq. (C-3).

Rupe (Ref. 2) introduced a term, commonly known as E_m, which is an index of mixing uniformity:

$$E_m = 1 - \sum_{i}^{N} \frac{\dot{w}_i}{\dot{w}_T} \frac{(R - r_i)}{R} - \sum_{i}^{N} \frac{\dot{w}_i}{\dot{w}_T} \frac{(R - \bar{r}_i)}{R - 1} \qquad (C\text{-}4)$$

where

E_m = mixing index

$\dot{w}_i/\dot{w}_T$ = mass fraction in the stream tube

R = ratio of total oxidizer mass to total oxidizer and fuel mass

r_i = ratio of oxidizer mass to total oxidizer and fuel mass in an individual stream tube for $r_i < R$

$\bar{r}_i$ = ratio of oxidizer mass to total oxidizer and fuel mass in an individual stream tube for $r_i > R$

The factor E_m, is not uniquely defined by $(\eta_{c*})_{mix}$. The correspondence is strongly affected by the propellant combination and the nominal mixture ratio. This term is employed to describe the average mixing uniformity of a given spray field.

14 KEY WORDS	LINK A		LINK B		LINK C	
	ROLE	WT	ROLE	WT	ROLE	WT
Injectors						
Drop Size						
Mixing						
Noncircular Orifices						
Gas/Liquid Propellants						

UNCLASSIFIED

Security Classification

DOCUMENT CONTROL DATA - R & D

(Security classification of title, body of abstract and indexing annotation must be entered when the overall report is classified)

1. ORIGINATING ACTIVITY (Corporate author)	2a. REPORT SECURITY CLASSIFICATION
ROCKETDYNE a division of North American Rockwell Corporation 6633 Canoga Avenue, Canoga Park, California 91304	Unclassified
	2b. GROUP

3. REPORT TITLE

FINAL REPORT--NONCIRCULAR ORIFICE HOLES AND ADVANCED FABRICATION TECHNIQUES FOR LIQUID ROCKET INJECTORS (PHASE II: ANALYTICAL AND EXPERIMENTAL STUDY OF NONCIRCULAR INJECOTR ORIFICES, AND ELEMENTS FOR GAS/LIQUID INJECTORS)

4 DESCRIPTIVE NOTES (Type of report and inclusive dates)

Final Report

5 AUTHOR(S) (First name, middle initial, last name)

R. M. McHale

6. REPORT DATE	7a. TOTAL NO. OF PAGES	7b. NO OF REFS
22 February 1971	169 & xiv	12

8a. CONTRACT OR GRANT NO	9a. ORIGINATOR'S REPORT NUMBER(S)
NAS9-9528 b. PROJECT NO.	R-8411
c.	9b. OTHER REPORT NO(S) (Any other numbers that may be assigned this report)
d	NASA CR-108571

10. DISTRIBUTION STATEMENT

11 SUPPLEMENTARY NOTES	12. SPONSORING MILITARY ACTIVITY
	NASA Manned Spacecraft Center

13 ABSTRACT

This report contains the results of the Phase II effort of the subject program, Noncircular Orifice Holes and Advanced Fabrication Techniques for Liquid Rocket Injectors. The Phase II portion of the program was comprised of an analytical and experimental study of injector elements incorporating noncircular orifices for application with gas/liquid propellant combinations. Based upon the results of a preliminary analysis and evaluation of several candidate injector elements, a rectangular concentric tube element was selected for further evaluation. Cold flow tests and subsequent analytical combistion modeling conducted with this element, and a standard, circular concentric tube demonstrated that the rectangular concentric tube element concept was superior, in many ways, to conventional injector concepts, especially in the area of propellant atomization.

DD FORM 1 NOV 65 1473

UNCLASSIFIED

Security Classification